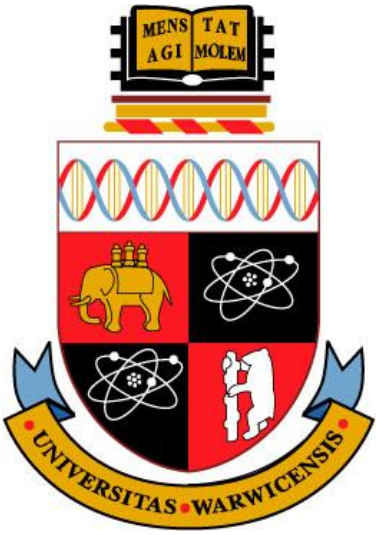

NUMERICAL MODELLING OF DRAWBEADS FOR FORMING OF ALUMINIUM ALLOYS

By

Yogendra Kamalakar Joshi

An innovation report submitted in partial fulfilment of the requirements for the degree of Engineering Doctorate

Warwick Manufacturing Group, University of Warwick,
Coventry, United Kingdom

March 2017

Abstract

Drawbeads control the flow of material into the die cavity during pressing operations. The tribological and forming properties of aluminium necessitate specific frictional and drawbead geometry requirements that are different from those established over many years for steels. Academic research on this topic is limited, requiring industry to rely on trial and error methods to determine the coefficient of friction and drawbead geometry.

This research project focused on developing an innovative, scientific and holistic methodology to determine the optimum drawbead geometry and an appropriate coefficient of friction value to be used in forming feasibility simulations for aluminium panels. Special attention was given to the ease with which this research could be implemented in an industrial environment. Hence, extensive experiments to gather material properties such as plane strain and pure shear tests, complex material models, or optimisation models based on artificial neural networks (ANN), and non-linear friction models were avoided.

Three approaches identified in the literature for designing drawbeads, namely, experimental, analytical and numerical modelling were investigated to test the underlying assumptions, strengths and limits of each. For example, analytical models assumed symmetric material flow passing over the drawbeads, which in reality does not occur. Based on these findings a systematic, hybrid approach has been developed which uses a combination of physical drawbead tests and numerical modelling, to determine the coefficient of friction which is then used to obtain the drawbead restraining force. Using a novel criterion, different drawbead geometry conditions have been ranked to aid selection of an optimised drawbead geometry.

The optimised drawbead geometry obtained from the hybrid approach was validated by stamping of rectangular pans. The rectangular pan, when stamped using the optimised geometry obtained from the hybrid approach, did not show defects such as severe thinning and wrinkles. The numerical stamping model with geometric drawbead predicted the punch force with a 4.5% error, thinning with a 5% error and draw-in with an 8% error.

An innovative hybrid approach has been proposed which is capable of accurately predicting the coefficient of friction, the drawbead restraining force and the drawbead geometry. The same coefficient of friction and the drawbead geometry when used in the forming simulation accurately predicted the punch force, thinning and draw-in. As a direct application of innovation, Jaguar Land Rover can use the novel criteria for selecting the drawbead geometry to use effectively the drawbead geometry generation feature in the commercial sheet metal forming software package during forming feasibility simulations. The hybrid approach can potentially save 34% of the die tryout time and provide average cost savings of £34,400 per die set per tryout attempt.

Declaration

I have undertaken all the work presented in this Engineering Doctorate programme unless otherwise acknowledged and has not been previously submitted for any other award.

March 2017

WMG, University of Warwick

Acknowledgements

I am greatly thankful to Prof Dr Richard Dashwood, Dr Darren Hughes and Dr Iain Masters for all their support over the course of my Engineering Doctorate. I am also grateful to Mr Martin Allen and his team from Jaguar Land Rover for providing industrial knowledge, test material and funding.

I want to express my deepest gratitude to Prof Dr Niels Bay and Dr Peter Christiansen from the Technical University of Denmark for their invaluable guidance and for allowing me to be a part of their research group during my placement. Sincere thanks to Mr Luis Matos from Jaguar Land Rover for assisting me in all the industrial matters.

Special thanks to Mr Sebastian Ballard, Mr Zack Parkinson and Mr Lewis Curry from the WMG workshop team and Dr Evans Mogire from Buehler for their prompt assistance in the lab work.

Finally, I would like to thank sincerely Dr Vivek Hajarnavis, Dr Abhishek Das, Chetan Shrouti and Gaurav Nanajkar for all the support, advice and good humour.

Table of Contents

List of Figures

List of Tables

List of Abbreviations and Symbols

ANOVA	Analysis of variance
ANN	Artificial Neural Network
R_b	Bead radius
BHF	Blankholder force
BHF_f	Blankholder force from fixed drawbead set-up
BHF_r	Blankholder force from roller drawbead set-up
μ	Coefficient of friction
π	Contact angle in radians
DoE	Design of experiments
d	Drawbead depth
DBRF	Drawbead restraining force
$DBRF_f$	Drawbead restraining force from fixed drawbead set-up
$DBRF_r$	Drawbead restraining force from roller drawbead set-up
EngD	Engineering Doctorate
FE	Finite element
FEM	Finite element method
FLC	Forming limit curve
GEP	Geometry effectiveness parameter
R_g	Groove radius
JLR	Jaguar Land Rover
ε_1	Major strain
ε_2	Minor strain
r/t	Ratio of bend radius to strip thickness
R_{ff}	Restraining force factor
n	Strain hardening exponent
m	Strain rate hardening exponent
σ_{xx}	Theoretical Yield Stress in X-direction
σ_{yy}	Theoretical Yield Stress in Y-direction
t	Thickness
ε_t	Through thickness plastic strain
UTS	Ultimate Tensile Strength
YS	Yield Strength
σ	Yield Stress obtained from uniaxial tensile test

1 Introduction

This section begins with the project background followed by objectives, scope and a brief description of the research methodology and deliverables to the industrial sponsor. The structure of the innovation report follows the research methodology.

1.1 Background

Jaguar Land Rover (JLR) is a premium British vehicle manufacturer well-known for the development of aluminium intensive vehicles across the product range, starting with the introduction of the Jaguar XJ in 2003 and now extended to other vehicle models as shown in **Figure 1.1**. Forming of aluminium alloys, unlike cold forming steel grades is a challenging task. The process to design dies for use with aluminium relies on trial and error methods that typically work 80% of the time but which may take between 6 and 24 months to complete. However, a widening product range, increasing sales volumes and more challenging product launch deadlines (Jaguar Land Rover, 2013) have increased the significance of having a proven and standardised die design method to reduce development time and scrap costs.

Figure 1.1: Aluminium intensive cars (Jaguar Land Rover, 2016)

Forming feasibility simulations are performed to verify virtually that the parts formed using a die will not suffer from defects such as wrinkles and splits. The key inputs to the simulation are the material model, contact conditions, and the drawbead geometry (Xu *et al.*, 1997). Drawbeads are locally situated, rib-like protrusions on the blankholder surface, which control the material flow into the die cavity. The material supplier usually provides the material model information. However, the contact conditions, represented by the coefficient of friction, and the drawbead geometry, represented by the drawbead restraining force (DBRF) must be adjusted in the simulations until the occurrence of wrinkles and splits are eliminated. The accuracy of the simulations depends upon the appropriate representation of these inputs in the feasibility studies, which is helpful in eliminating part defects.

1.2 Objectives

Based on the project background provided by JLR, the following research objectives were established:

1. Understanding the difference between steel and aluminium in terms of forming behaviour.
2. Establish the key steps in the automotive die design and tryout process.
3. Understanding and comparing state of the art drawbead design methods and studying the actual flow of the material over drawbeads.
4. Develop and prove a scientific method to derive an optimised drawbead geometry along with a coefficient of friction.
5. Propose an implementation strategy for JLR.

This EngD project will aim to "*Numerically determine, evaluate and derive the optimised drawbead geometries for stamping of aluminium alloys"*.

1.3 Scope

It was important to frame the scope of the project at the earliest stage to enable focused efforts in meeting the aim and objectives of the EngD project whilst simultaneously maintaining the academic rigour and industrial relevance. The scope of the project was as follows:

- Determining an accurate coefficient of friction to be used in numerical modelling of sheet metal flow over drawbeads:

  Drawbead tests to evaluate different metal forming lubricants and to determine minimum quantity of lubricant on the test samples was out of scope as the project was more focused drawbead geometry determination.

- Only aluminium alloys were used in testing and simulations:

  The focus on aluminium aligned with the strategic direction of Jaguar Land Rover in becoming world-class lightweight aluminium vehicle manufacturer.

- Validation of experimental and simulation trials with results from the literature was not conducted in this study because:

  a) Test set-ups and test materials were not adequately described in the literature and

  b) Simulations in the literature used the coefficient of friction as a "fitting factor" making it difficult to replicate the results.

- Analytical drawbead models studied and applied in this work were used in their original formulation:

  Attempting to improve the mathematical formulation or creating a new analytical model for better predicting the drawbead restraining force or drawbead geometry did not fit into the scope of an EngD programme.

1.4 Research methodology

The structure of the innovation report reflects the purpose of the Engineering Doctorate programme namely, to solve an industrial problem by application of knowledge, scientific tools and methods. The proposed solution is expected to be easy to implement and bring tangible benefits to the industrial sponsor.

The innovation report is designed to follow the development of the Engineering Doctorate as illustrated in **Figure 1.2**. There was a need to understand the underlying assumptions in the drawbead design approaches used in academia and industry for forming of aluminium alloys. This was done using data sources such as books, peer-reviewed journal articles and publications on Society of Automotive Engineers' (SAE) international repository. Press shop visits at Jaguar Land Rover and Tier-1 suppliers such as Covpress and Stadco were invaluable sources of practical knowledge, considering the shortage of published data on industrial drawbead design practices. This blend of academic and industrial source material led to the identification of knowledge gaps, which are documented in Chapter 2. An investigation of assumptions and knowledge gaps in academic and industrial practices was conducted by primary experimentation and simulation and is described in detail in Chapter 3.

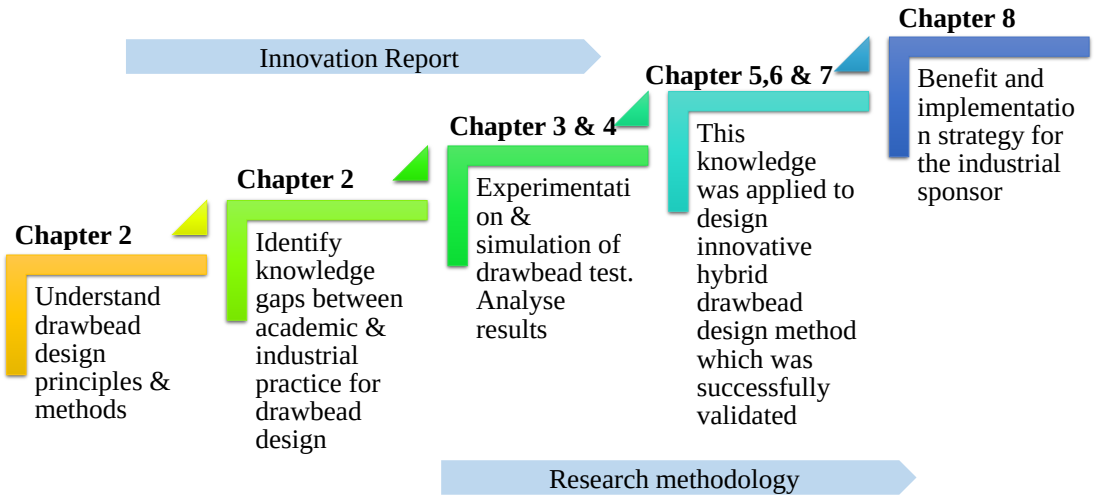

Figure 1.2: Research methodology applied in this Engineering Doctorate project

Chapter 4 briefly describes the design of experiment approach to determine the main effect of the drawbead geometry on the drawbead forces, which served as a basis to formulate a novel drawbead selection criterion. A selection criterion for choosing an optimised drawbead geometry, as explained in Chapter 5, was necessary before developing an innovative and holistic methodology to design drawbeads. Chapter 6 discusses the proposed drawbead design methodology, and the experimental and numerical validation of the same is documented in Chapter 7. The overall conclusion, innovation and benefits to JLR and possible future extension of the research work are given in Chapter 8, 9 and 10 respectively.

Table 1.1 lists the submissions made throughout the EngD programme. Portfolio submission 1 describes the fundamentals of sheet metal forming and focusses on understanding tribology in the blankholder systems specific to aluminium alloys. This study provided exposure to the potential tribological factors that may influence the material flow over drawbeads such as the significance of draw speed on the coefficient of friction. The drawbead design principles and guidelines are discussed in detail in Portfolio submission 2. Portfolio submission 3 not only serves as an EngD placement

report but also a guide for setting-up finite element drawbead and deep drawing models. The drawbead simulations reported in this innovation report are an extension of the work described in Portfolio submission 3. Portfolio submission 4 consists of the results of a comparative investigation of different drawbead design approaches. These results were presented at the NUMISHEET 2016 conference and published in the form of a paper in Journal of Physics Conference Series by IOP Science 2016.

Table 1.1: Submissions

Sr.no.	Submissions	Report chapter no.
1	Tribology in the blankholder region for stamping of aluminium alloys	n/a
2	Drawbead design principles and methods	2
3	EngD placement report	3,7
4	Conference / journal publication	3
5	Personal profile	n/a

1.5 Deliverables

1. Developed an *innovative, holistic and scientific drawbead design approach*, which not only provides a coefficient of friction but also the optimised drawbead geometry to be used in the simulations. JLR is keen to exploit this methodology.
2. The capability to use the drawbead test as an efficient method to derive the coefficient of friction to be used in the forming feasibility simulations, eliminating the need for any physical press forming trials to confirm the correctness of the friction coefficient. Previously, the coefficient of friction was used as “fitting factor” to match simulation and physical results. This can also be extended to build a database of the coefficient of friction for a range of lubricants, die coatings and blank materials.

3. A fast and simple finite element model of the drawbead test to determine scientifically drawbead forces for aluminium alloys. Previously drawbead forces were altered until a satisfactory result from simulation was achieved. This approach can be extended to a range of materials and gauges to build a database to be used in the JLR's stampings standards.
4. Identified key drawbead geometry and process parameters influencing the DBRF and connecting this knowledge to the drawbead design process. This shall allow JLR to establish die tryout guidelines and procedures in their Stamping standards.
5. Formulated a drawbead geometry selection criterion that allows the stamping engineers to decide a drawbead reduction strategy in AutoForm^{TM}. In the reduction strategy, a dimension of drawbead such as depth, defined by the user, is changed systematically and manually in descending order until a satisfactory restraining force (automatically calculated by the software) is achieved.
6. Created a MATLAB code for the Stoughton model and for the Von Mises, Hill-48 and Barlat-89 yield functions to get an initial understanding of draw bead geometry and to update material cards in AutoForm^{TM} respectively.
7. As a contribution to knowledge, this research project highlighted that the actual flow of sheet material moving over the drawbead is asymmetric and is equally influenced by all the drawbead geometry parameters, namely, groove radius, bead radius and depth. In addition, a Coulomb friction model can be appropriately used in forming feasibility simulations. Earlier, it was assumed that the sheet metal flow through the drawbead was symmetric, i.e., conforms to the shape of the drawbead and that drawbead height was the single most influencing factor. It was also assumed that a non-linear friction model is necessary for contact representation in the simulation.

2 Review of drawbead design principles and methods

The chapter begins with the need for light weighting in the automotive industry and a brief introduction to sheet metal forming in the automotive industry. Differences between forming behaviour of aluminium alloys and steels and the working principle of drawbeads are also covered. The chapter also investigates both the academic research gaps and the shortcomings in the industrial practice for designing drawbeads.

2.1 Sheet metal forming in the automotive industry

The emission norms imposed by the European Commission are becoming stringent as shown in **Figure 2.1**. Thus, the vehicle manufacturers must attempt to reduce the carbon emissions of their vehicles. In order to meet the emission norms, the automotive OEMs are increasingly replacing steels with aluminium alloys to reduce the weight of a vehicle's body-in-white as seen in **Figure 2.2**. Lighter vehicles will produce lower carbon emissions. A body-in-white is an unpainted metal car body. The body-in-white panels are commonly manufactured using stamping operations and it was realised that the stamping die design practices based on extensive experience of forming steels for over a century, cannot be directly used for forming of aluminium alloys (Xu *et al.*, 1997). The aluminium parts split excessively when formed on dies used for forming of steels (Personal communication, 2013). These results, to some extent, were puzzling as aluminium alloys, being highly ductile, were thought to be easily formable when compared with steel. Hence, there was a need to understand the forming behaviour of aluminium alloys and a methodology to formulate die design practices for forming of aluminium alloys (Personal communication, 2013).

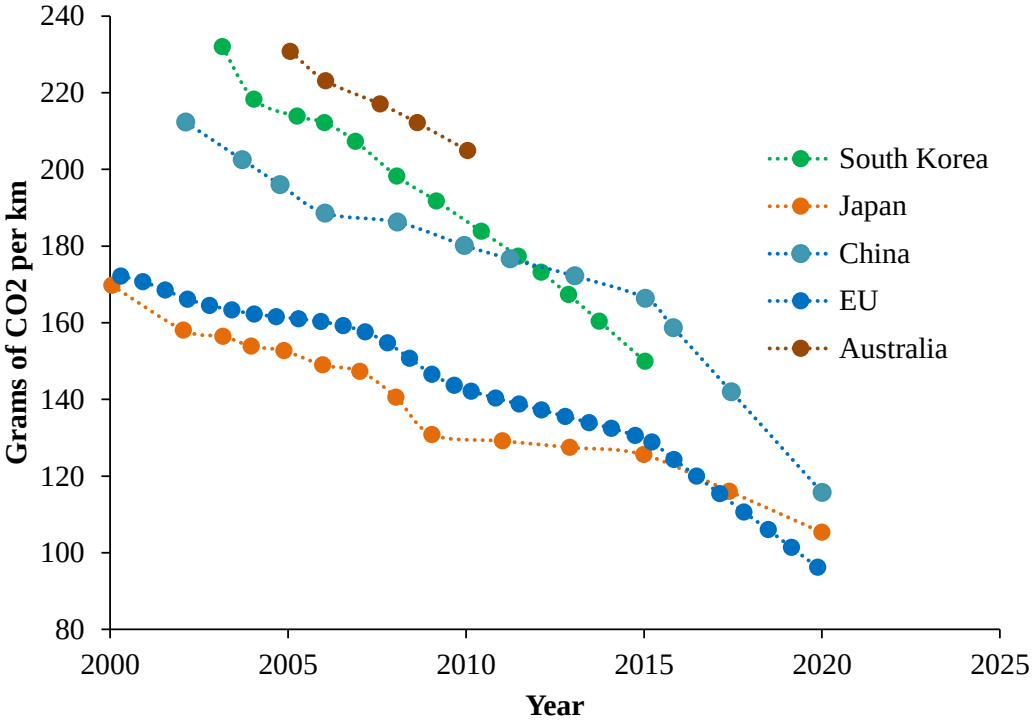

Figure 2.1: Reduction in carbon dioxide emissions as required by the national emission norms (European Aluminium Association, 2013)

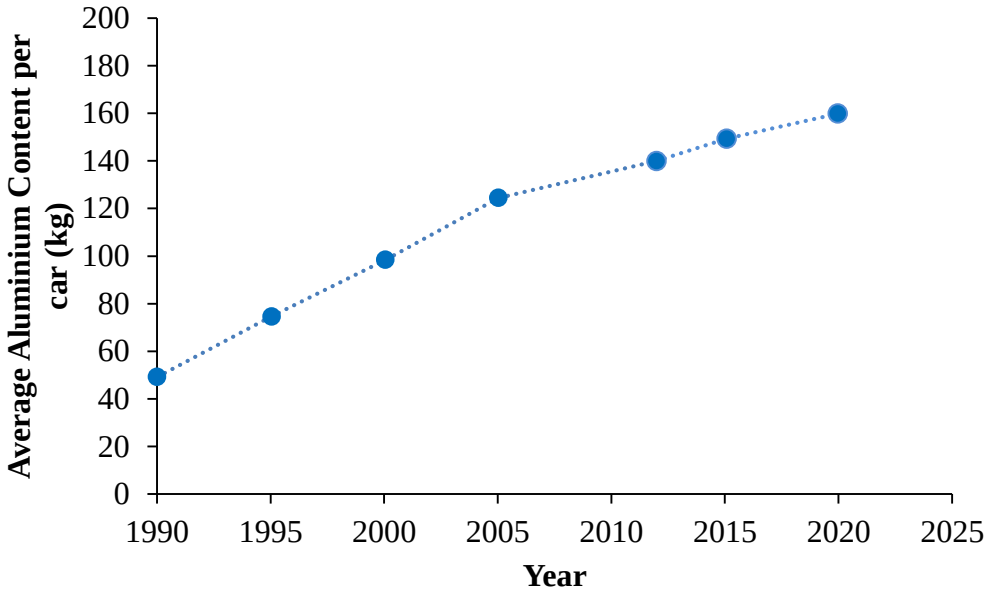

Figure 2.2: Increase in the use of aluminium alloys to reduce weight of cars (European Aluminium Association, 2013)

Forming is one of the five major manufacturing processes and can be classified into five types depending on the stress state experienced by the part being formed as illustrated in **Figure 2.3**. Commonly occurring sheet metal forming operations in the automotive industry are highlighted using an asterisk mark.

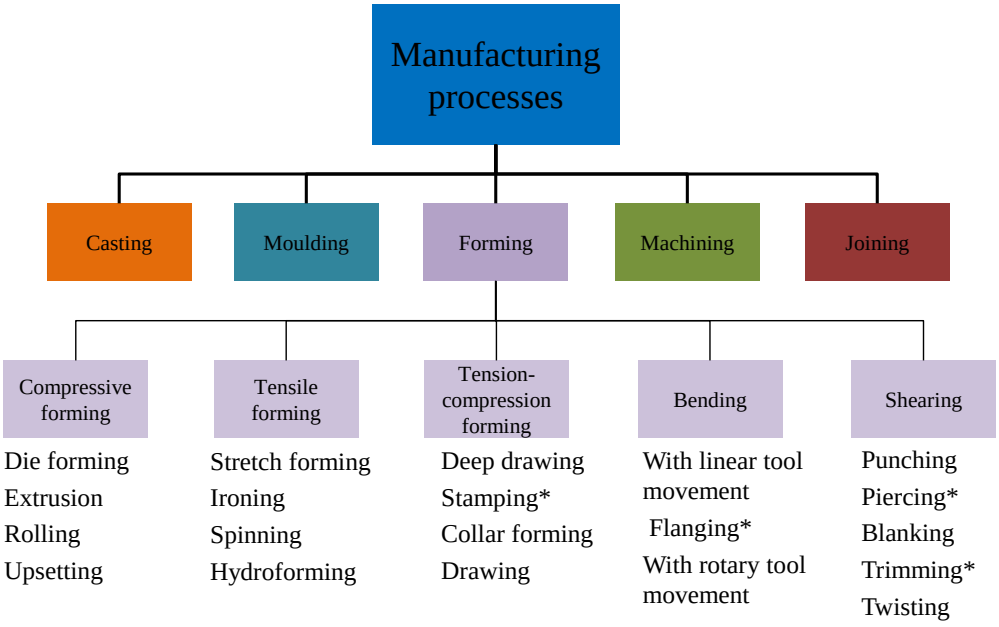

Figure 2.3: Classification of sheet metal forming operations, * indicates common use in the automotive industry

A deep drawing operation is shown in **Figure 2.4**a) and the forming operation of automotive panels using drawbeads, commonly known as stamping, is shown in **Figure 2.4**b). The depth of the part in stamping operations is smaller compared to deep drawing. Even though the stamping of automotive panels is typically done on a single action press, it primarily has two steps. In the first step, the upper blankholder moves down to position and clamp the blank securely and in the second step, the blankholder moves down drawing the blank over the punch to form the part.

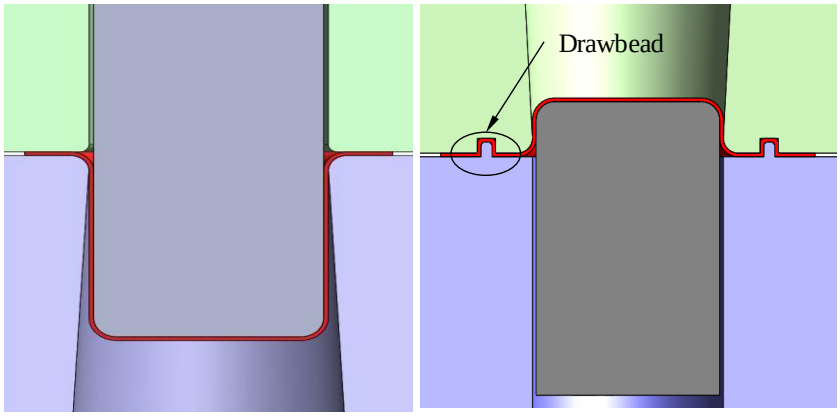

Figure 2.4: Schematic showing the difference between deep drawing a) and stamping b). Adapted from TALAT (1996)

A flat blankholder as shown in **Figure 2.4**a) imparts little braking resistance (restraining force) to the blank flowing into the die cavity. Friction between the blankholder and the blank may not be adequate to provide a restraining force necessary to control the metal flow and the blankholder force may be insufficient to prevent wrinkling in the formed panels (Zharkov, 1995). Drawbeads on the blankholder significantly increases the braking action by providing additional restraining force as the blank bends and unbends over the drawbead as it is being drawn through the blankholder and over the punch (Nine, 1978). Drawbeads provide advantages such as reduction in press capacity, smaller blank size and elimination of wrinkling. This has been discussed in detail in Submission 2.

A typical automotive die with drawbeads cut on the blankholder is shown in **Figure 2.5** and the terminology used in the stamping operation is illustrated in **Figure 2.6**. Although it has been referenced in the (Zharkov, 1995) that the drawbeads are located on the upper blankholder, the drawbeads were found to be located on the lower blankholder of the stamping dies used by Jaguar Land Rover (2014) and as such a common practice in the industry. Therefore, the stamping experiments and simulations

described in Chapter 7 have been carried out using drawbeads located on the lower blankholder.

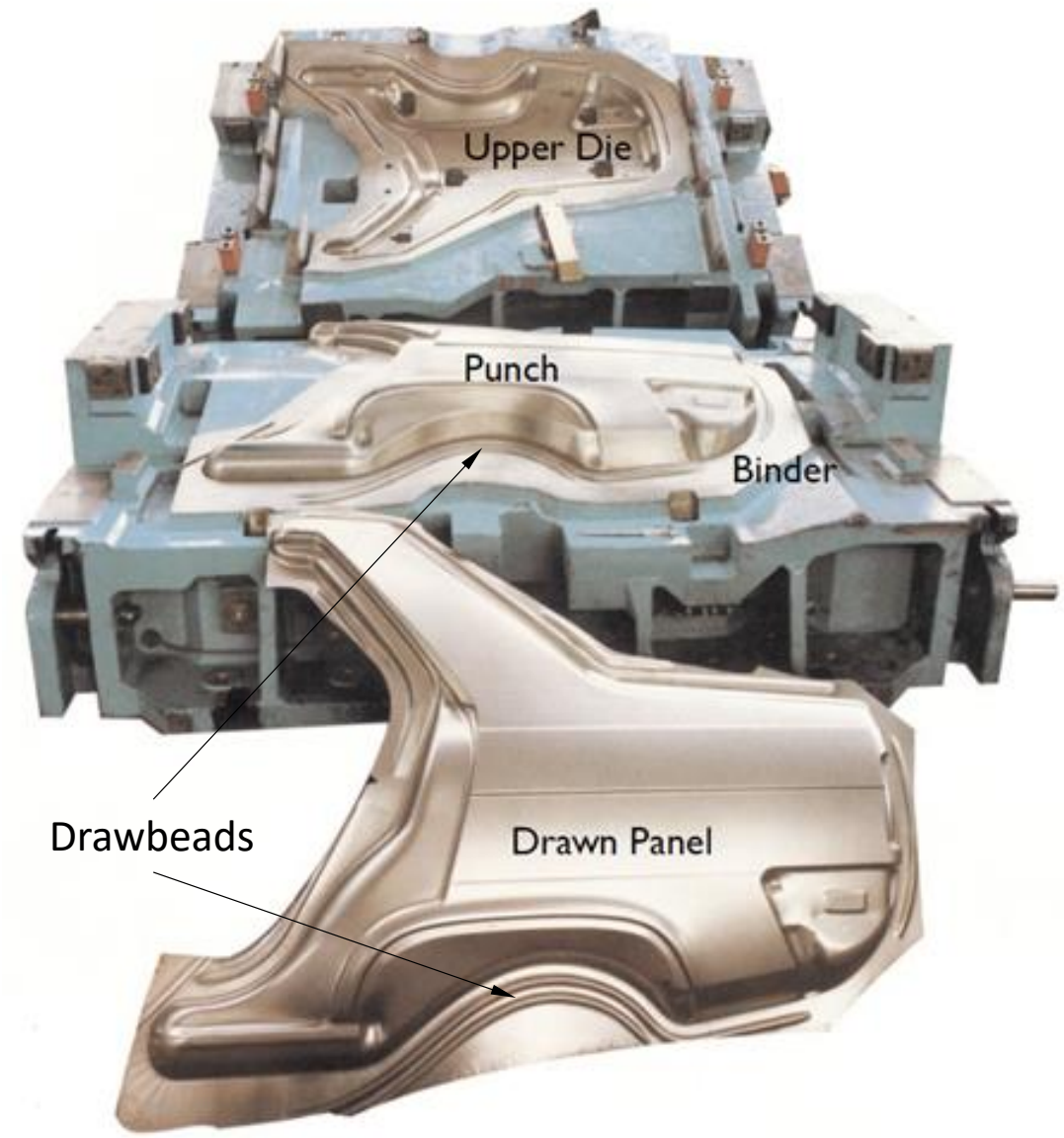

Figure 2.5: A typical draw die in automotive stamping. Adapted from Dutton Simulations (2014)

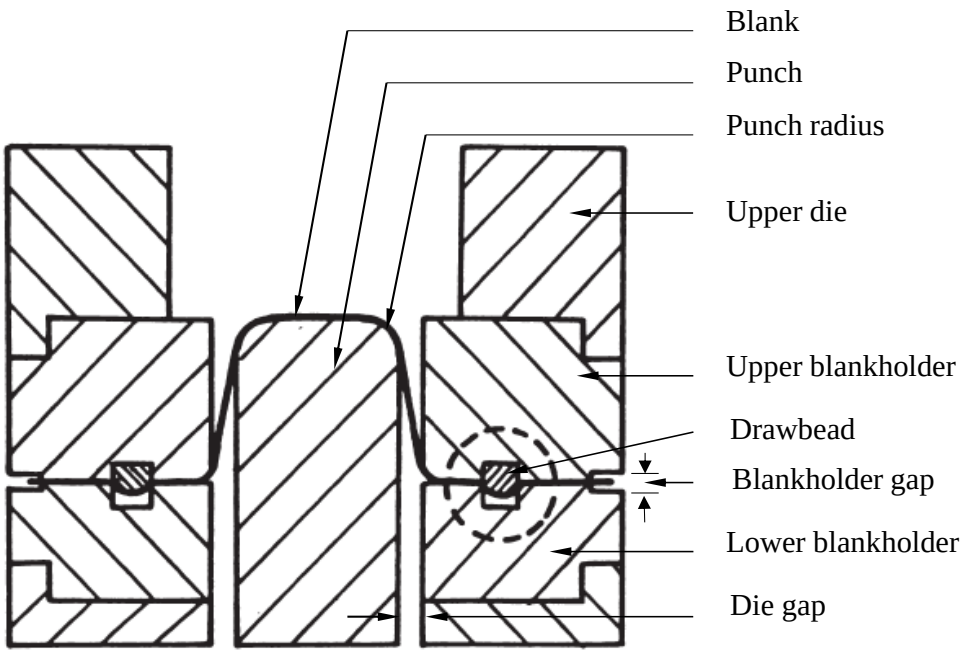

Figure 2.6: Die terminology used in the automotive sheet metal forming operations

2.2 Drawbead working principle

The drawbead restraining force (DBRF) is the force experienced by the blank when it is drawn over the drawbead. The drawbead restraining force is made up of two components, bending/ unbending force and frictional force as illustrated in **Figure 2.7**. The restraining force generated by a drawbead is due to the energy absorbed by the deformation of the sheet and the friction between the sheet and the drawbead system. A deformation or bending force is generated when the sheet bends over the first (entry) radius of the groove. When the sheet slides over the entry radius 'A', a friction force is also produced. There is no friction over the other side of the sheet, as it is not exposed to the bead. At point '2-3' the sheet unbends as the entry radius A terminates. Thus, this order of deformation (bending), friction (sliding) and straightening (unbending) produces all the restraining force from the first radius. Likewise, a restraining force is also created over the bead at 'B' and at the second or exit radius 'C' respectively. The DBRF is the summation of these individual restraining forces over the three radii.

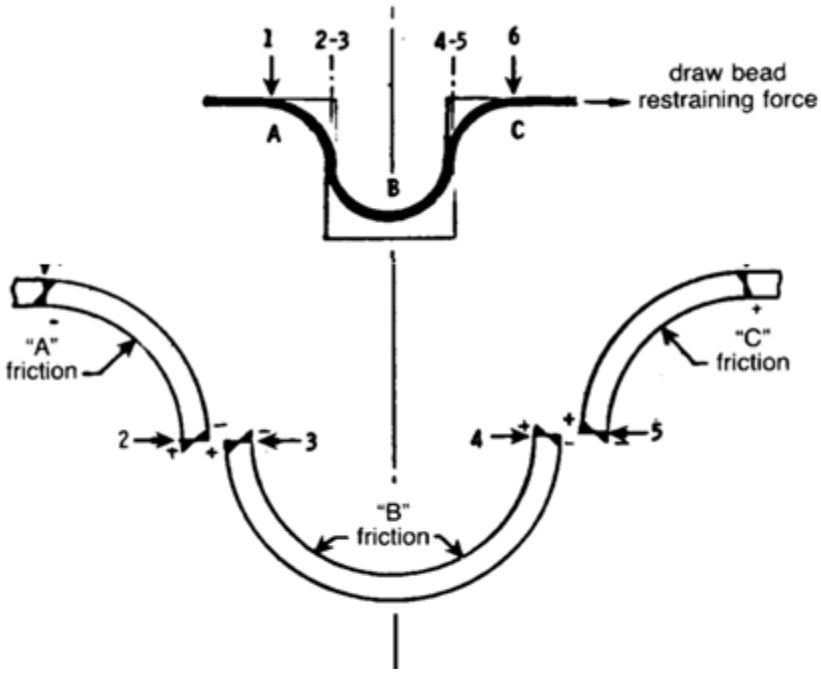

Figure 2.7: Development of deformational and frictional components of the drawbead restraining force over a conventional semi-circular drawbead (Nine, 1982b)

The blankholder force (BHF), **Figure 2.8**, is the force necessary to maintain the blankholder gap and in turn the drawbead depth and directly affects the press tonnage. The BHF should be greater than the uplifting force exerted by the blank. Drawbeads are only effective if the drawbead depth is properly maintained during the stamping operation. A smaller DBRF may allow more sheet material flow into die cavity causing wrinkling whilst a larger DBRF may lead to splits in the formed panels. The DBRF and BHF are primarily dependent on the drawbead geometry and on the material of the blank.

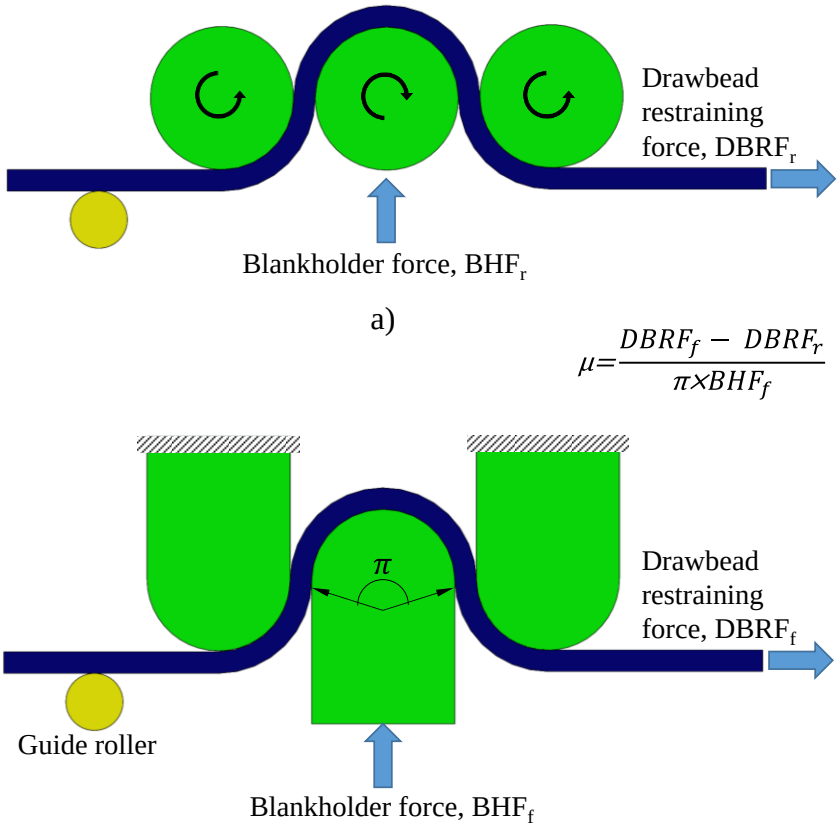

Figure 2.8: Drawbead test designed by Nine (1978) consists of roller drawbead set-up a) and fixed drawbead set-up b)

Drawbead tests have been mostly used to characterise different metal forming lubricants and in turn obtain coefficients of friction and DBRF (Nine, 1978). The principle of operation of the drawbead test is illustrated in **Figure 2.8**. The test set-up consists of two different drawbead arrangements; the roller set-up (a) has freely rotating rollers and the fixed drawbead set-up (b) has fixed semi-cylindrical bars that represent the groove and bead radii respectively. Identical strips of material are drawn through both set-ups for comparison. The guide roller is used to ensure horizontal and smooth entry of the strip and at the same time maintain a blankholder gap, **Figure 2.6**. Load cells attached to the grip used to draw the strip, and under the central bead record the restraining force and the blankholder force respectively. A strip when pulled over

the rollers experiences a restraining force because of work hardening due to a series of bending and unbending cycles; assuming there is negligible friction because of the rollers. A separate strip is then pulled over the fixed drawbead set-up. This strip experiences friction along with work hardening effects. The restraining force, in this case, is due to combined action of frictional and bending deformation forces. The coefficient of friction, μ, is determined using the formula shown in **Figure 2.8**. The frictional force is determined by subtracting roller setup's drawbead restraining force, $DBRF_r$, from the fixed set-up's drawbead restraining force, $DBRF_f$. This frictional force is then divided by the blankholder force, BHF_f, from the fixed set-up; π represents contact area angle in radians over the drawbead.

Drawbead shapes, bending and unbending principles, drawbead location and the application of drawbeads to mitigate forming defects are discussed in detail in Submission 2.

2.3 Formability comparison of steels and aluminium alloys

As stated in Jaguar Land Rover (2013), vehicles such as the Range Rover and Discovery are aluminium intensive. This is illustrated in **Figure 2.9**. 6000 series alloys are mostly used on exterior panels because of their low strength and high formability during the stamping operation. Since these alloys are bake-hardenable, the strength can be increased after the coat baking cycle during the painting process (Miller *et al.*, 2000). Amongst non-heat treatable alloys, 5000 series alloys have high strength and excellent formability making them suitable for both interior and structural components (Miller *et al.*, 2000). Hence, aluminium alloys belonging to these series namely AA5754-O and AA6111-T4 have been primarily used in the experiments conducted in this research.

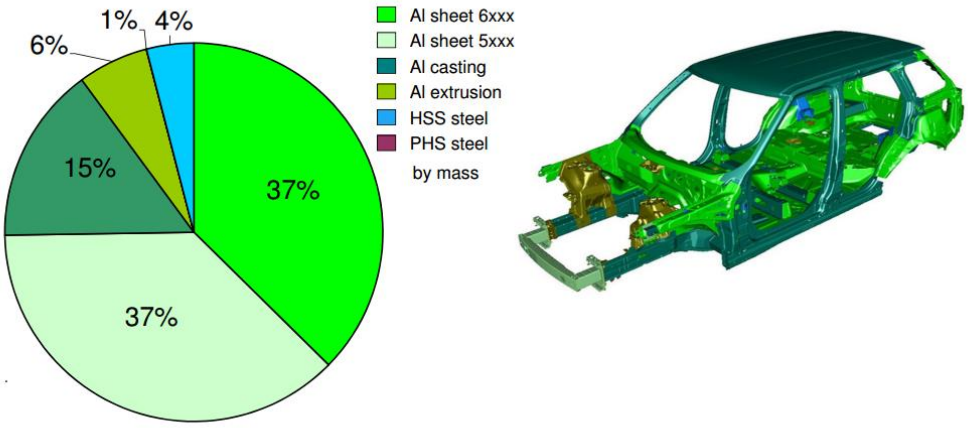

Figure 2.9: A full aluminium body-in-white of Range Rover Discovery showing extensive usage of AA5754-O and AA6111-T4 which are the materials used in this study (Jaguar Land Rover, 2013)

Formability is the ability of the material to deform plastically into the desired shape without necking or splits. It is understood that aluminium alloys have poor formability when compared to steels and it is, therefore, important to understand the fundamental difference between cold forming grade steels and aluminium alloys. There are various intrinsic material properties and process parameters that affect formability, however, the basic material properties can enable an initial formability comparison.

Figure 2.10a) identifies how mechanical properties are obtained from a tensile test and **Figure 2.10**b) illustrates typical stress-strain curve for low carbon steels and typical aluminium alloys. Steels have total higher elongation and Ultimate Tensile Strength than aluminium alloys. **Table 2.1** compares the mechanical properties of a common forming steel grade, Aluminium Killed Draw Quality (AKDQ), and aluminium alloys AA5754-O and AA6111-T4. These were the alloys selected for this study. The data for AKDQ was obtained from (Levy and Van Tyne, 2007) and for aluminium alloys from preliminary tensile tests conducted as part of this EngD research.

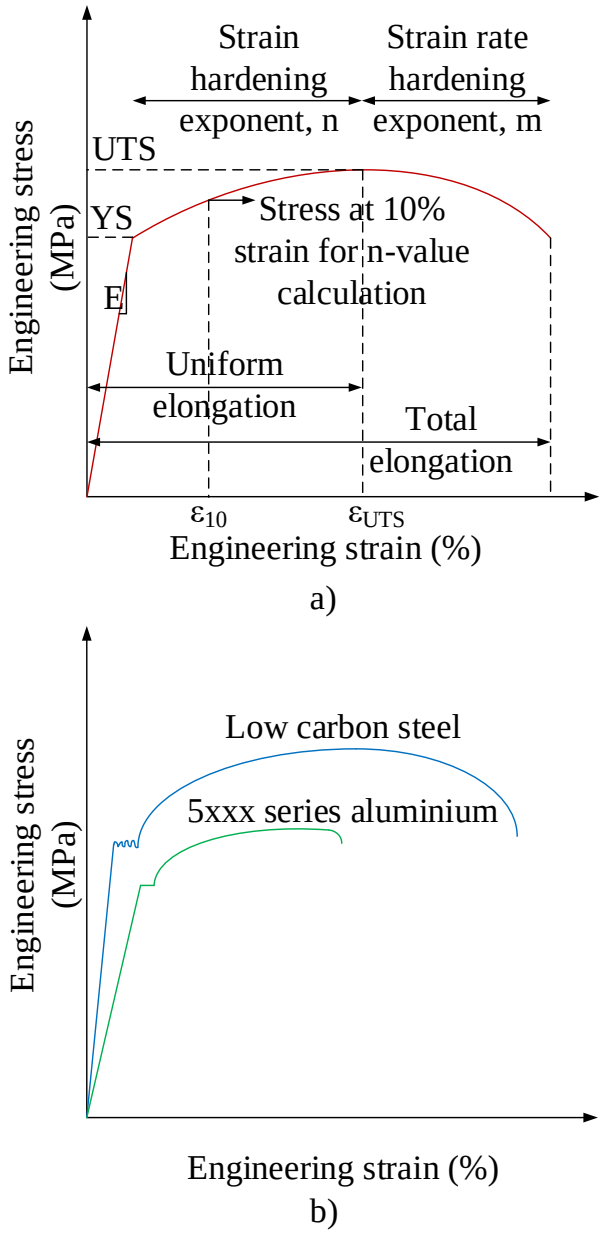

Figure 2.10: A typical stress-strain curve showing different material properties in a) and engineering stress-strain curves for low carbon steel and aluminium alloys in b)

The magnitude of Yield Stress (YS) and Ultimate Tensile Stress (UTS) cannot be directly related to formability. However, the smaller the difference between these two stresses, the larger is the ability of the material to undergo strain hardening and stretch less. It can be seen that aluminium alloys have a smaller difference between yield and ultimate tensile stress and may fail early while stretching as compared to steel.

The Young's modulus (E) of aluminium alloys is one-third of steel. Therefore, aluminium alloys will have higher elastic recovery upon release of external forces and higher springback as compared to steel.

The n-value is called the strain-hardening exponent and is an important measure in comparing formability. A higher n-value is normally good but for aluminium alloys, the n-value rapidly reduces leading to early necking and failure.

The m-value is called the strain-rate hardening exponent that indicates either increase or decrease in the flow stress as the rate of deformation is increased. AKDQ steel has positive m-value, which means that the material at the onset of necking gains strength in an attempt to retard the growth of necking and delay failure. Aluminium alloys have a negative m-value that results in losing strength at the onset of strain gradient, leading to rapid localised thinning and early failure. Thus, a negative m-value reduces the advantage of a better n-value in the case of aluminium alloys.

The Lankford coefficient ($\overline{r}$) is the ratio of true plastic strain in the direction of width to true plastic strain in the thickness direction (Hosford and Caddell, 2011). Higher Lankford coefficients indicate good resistance to thinning when subjected to plastic deformation. Aluminium alloys have a lower $\bar{r}$ value and hence a lower resistance to thinning than steels when bent and stretched over a radius. Therefore, using dies prepared for processing steels, which have a relatively low r/t value may result in splits when forming aluminium.

Table 2.1: Material properties comparison of steel and aluminium

Material	Young's modulus (MPa)	Yield stress (MPa)	Utimate tensile stress (MPa)	n-value	m-value	Uniform elongation (%)	Total elongation (%)	$\bar{r}$
AKDQ steel	210000	178	402	0.21	0.012	22	42	1.7
AA5754-O	70000	118	251	0.32	≤ 0	18	22	0.67
AA6111-T4	70000	131	253	0.28	≤ 0	19	22	0.58

Bendability, not shown in **Table 2.1**, is the ability of the material to bend over a radius without failure. An indicator of bendability is the ratio of the radius of the bend to the gauge (r/t) which is related to the material properties (Hosford and Caddell, 2011). Total elongation to failure along with n and m-values determines the bendability of the material. Hence, aluminium, as compared to steel, has less bendability and therefore a higher bending radius to sheet thickness (r/t) ratio.

An appropriate representation of forming behaviour in forming feasibility simulations is also necessary to enable a fair comparison of formability of aluminium and steel alloys. There are three requisites to define a material in any sheet metal forming's finite element model (Banabic, 2010):

1. Flow curve
2. Yield locus
3. Forming limit curve

The flow curve is obtained by fitting a suitable hardening rule to the experimental data obtained from the tensile test data after the yield point. Finite element software uses the flow curve to determine the effective flow based on the strain (nodal displacement) of the element. There are different hardening rules that are more appropriate to certain alloys. The Swift equation as seen in **Figure 2.11**, is an extension of the Power law (Marciniak *et al.*, 2002) and is commonly used for steels. However, based on an

analysis of the results of the aluminium alloys tested in this study, **Table 2.1**, the Voce hardening rule (Marciniak *et al.*, 2002) predicts the performance more accurately than the Swift equation as can be seen in **Figure 2.11**.

From the equations of the hardening rules in **Figure 2.11**, it can be seen that the Swift law is an extrapolation rule that provides an intercept K, a strength coefficient, and an exponent 'n', which is the hardening exponent. Thus, this hardening rule does not closely follow the experimental data and deviates towards the end of the flow curve. On the other hand, the Voce hardening rule is an interpolation equation that has an intercept and a saturation value. In this case, these are 113 MPa and 319 MPa respectively. Therefore, the Voce hardening rule fits better to the tensile test data collected.

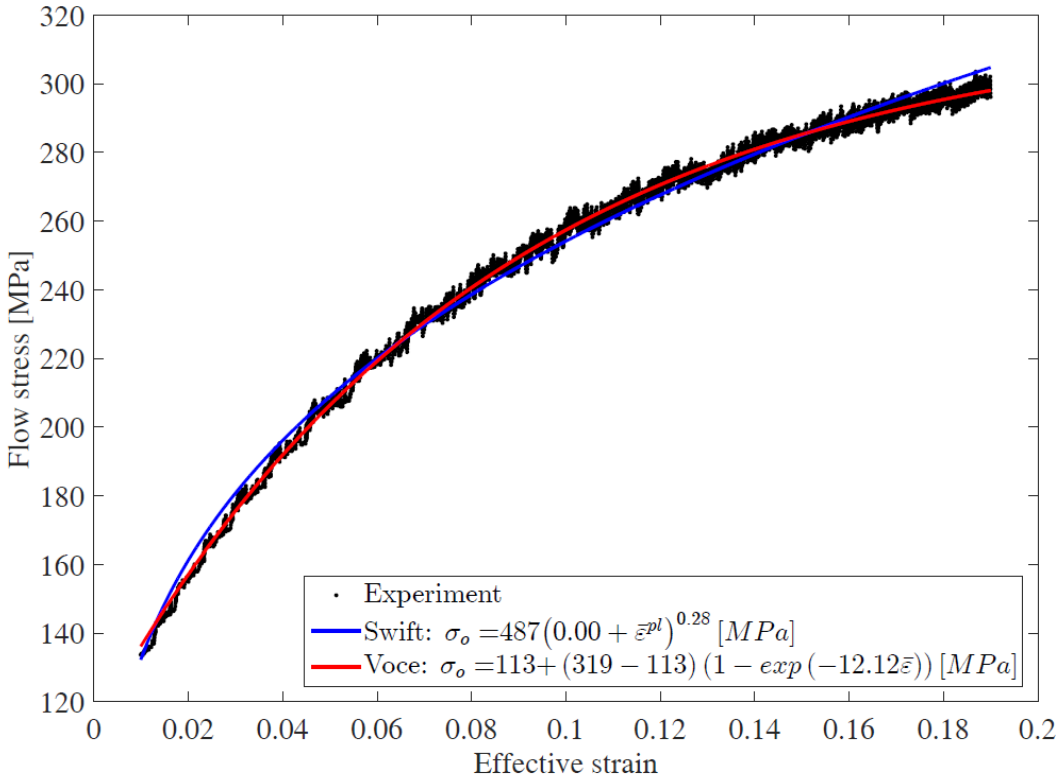

Figure 2.11: Fitting of hardening rules for tested AA5754-O

The yield locus is used to determine whether a current stress state or loading condition is large enough to begin or continue plastic deformation by comparing current yield stress of the material with the calculated stress. A yield function is used to determine a scalar value of current yield stress, also known as equivalent stress. Since this function is used to check the plastic flow, it is called a yield function. The function uses different tests pertaining to different stress states to determine a yield locus that represents the onset of plasticity.

Figure 2.12 illustrates an exemplary yield function with different stress states. It can be seen that these yield functions, especially Barlat-89 and BBC2005 show a slight difference in the plane strain tensile stress at 0° and 90° to the rolling direction. A strip whose thickness-to-width ratio is significantly large experiences a plane strain condition when passing through the drawbead during the drawbead test. Therefore, it can be concluded that advanced yield functions will not have a significant effect on the DBRF prediction. Hence, complex yield functions were not used in the finite element drawbead models. Advanced models are useful in an application such as deep drawing or stampings operations where biaxial stress states are encountered and where springback is important.

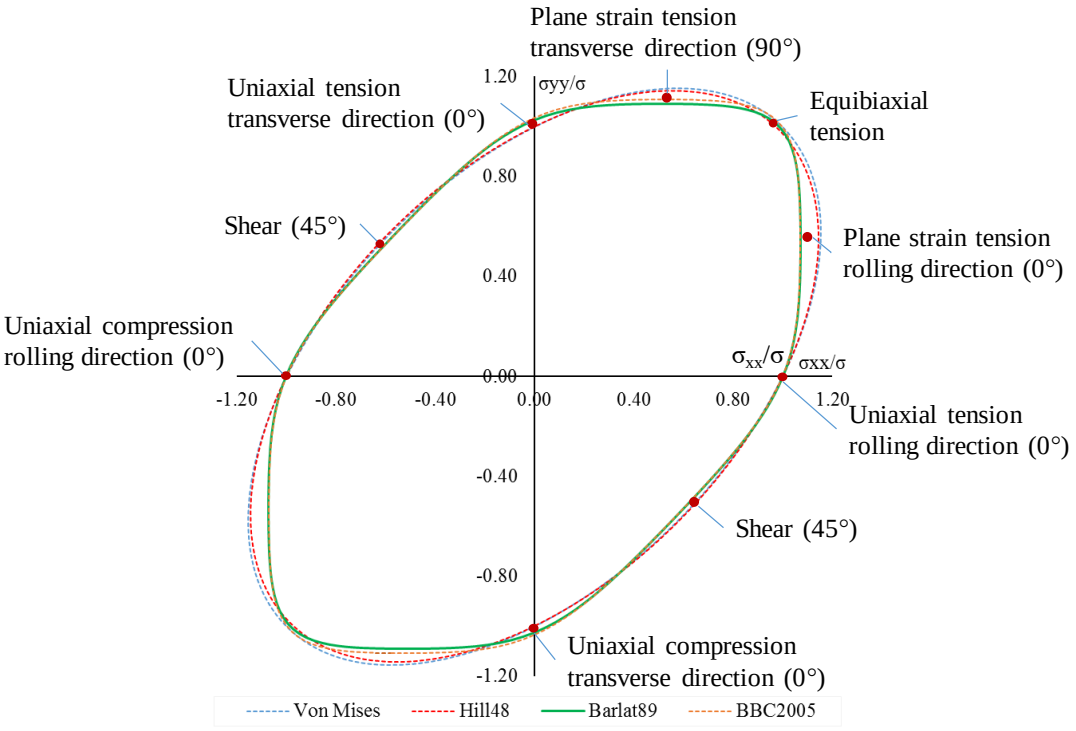

Figure 2.12: A comparison of different yield functions for AA5754-O

The forming limit curve (FLC) illustrated in **Figure 2.13**, essentially provides a failure criterion. It gives the maximum attainable plastic deformation before necking (failure) occurs under different stress states. Sheet flowing over drawbeads in the drawbead test experiences plane strain deformation that corresponds to the minimum point on the forming limit curve. Hence, the entire FLC was not required to be input into a material model for modelling sheet metal flow over drawbeads.

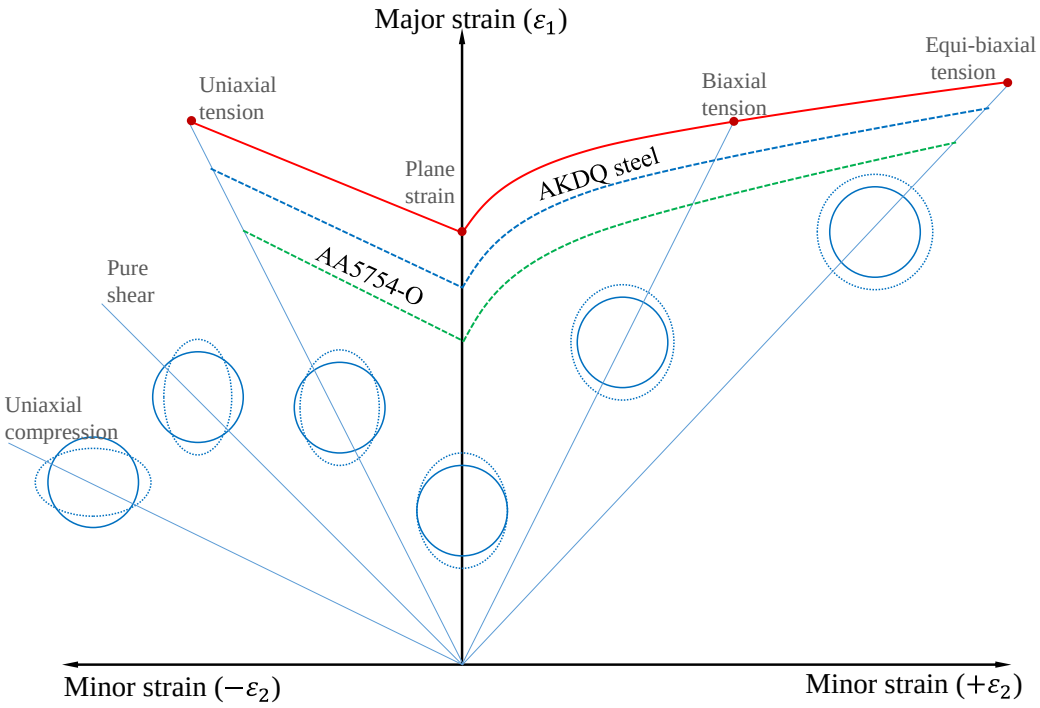

Figure 2.13: Forming limit diagram: a comparison of AA5754-O (green) and AKDQ steel (blue) with respect to critical forming limit curve (red)

2.4 Academic approach to drawbead design

An academic investigation of drawbead behaviour can be classified into three groups as shown in **Figure 2.14**a).Few studies focused on aluminium alloys as can be seen in **Figure 2.14**b) (Emblom and Weinmann, 2007; Taherizadeh *et al.*, 2009; Li and Weinmann, 1999) and Trzepieciński and Lemu (2014). Typical aluminium alloys used in research studies were AA2036, AA5251 and AA6111-T4.

Drawbeads and the sheet metal flow over the drawbeads have been studied from the academic point of view since the late 1970s when Nine (1978) designed a drawbead test to determine the coefficient of friction to be used in empirical formulae, such as Weidemann (1978) to calculate DBRF. Later on, the drawbead test, in its original or modified form was used to study different aspects related to drawbeads, which are explained below.

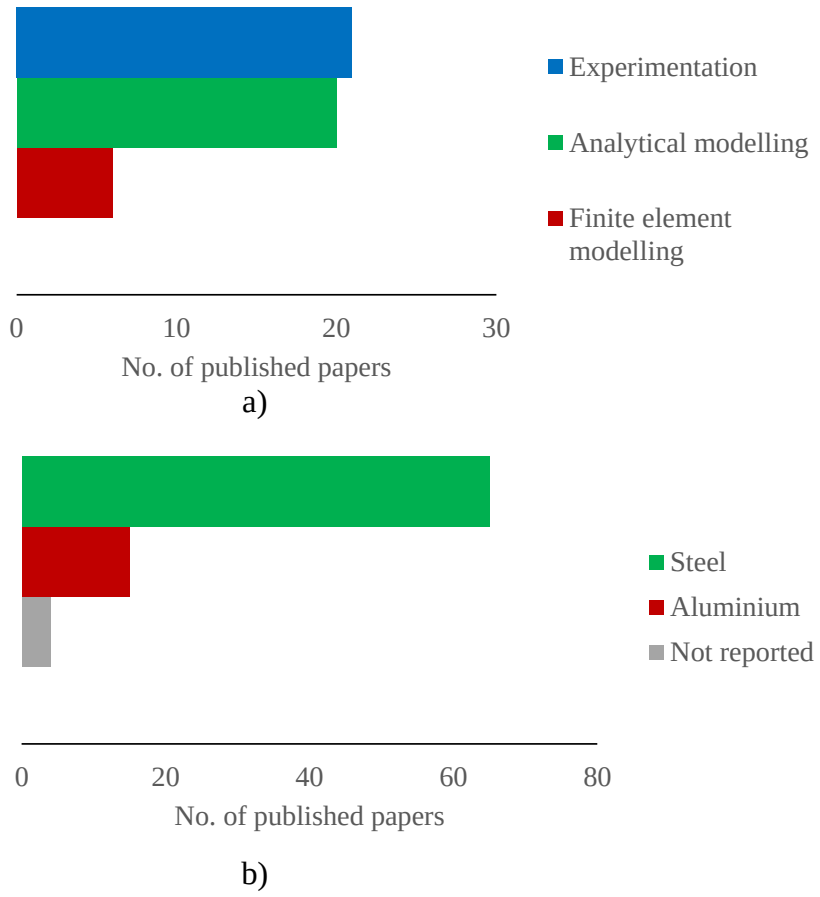

Figure 2.14: Review of 84 papers published between 1978 and 2017 indicated that finite element modelling of the drawbead process was limited a) and most of the experimentation and analytical modelling was done on steels b)

Schey (1996) used the drawbead test to look at the effect of lubricant viscosity and draw speed on the coefficient of friction and drawbead restraining force. The coefficient of friction reduced suddenly between 50 and 80 mm s^{-1} but remained largely unchanged between 80 and 240 mm s^{-1}. The DBRF followed a similar pattern and it was observed that the DBRF was largely unaffected after 80 mm s^{-1} as well. Nanayakkara *et al.* (2004) recognised that the drawbeads in the drawbead test are fully penetrated whereas on automotive stampings drawbeads are partially penetrated and therefore the coefficient of friction equation by Nine (1978) is not applicable.

However, the newly proposed coefficient of friction by Nanayakkara is not applicable for less than half of the drawbead penetration.

The experimental approach has also been used to design a novel "active drawbead system" which would potentially remove the need to determine and predict coefficient of friction and DBRF. Assuming that the drawbead penetration is the significant factor influencing sheet metal flow, (Weinmann *et al.*, 1994) proposed a modification of the fixed drawbead test set-up by incorporating a closed loop electronic system to actively change the drawbead depth and blankholder pressure to avoid splits and wrinkles. This option was also explored and further developed by (Li *et al.*, 2000) and later by (Emblom and Weinmann, 2007). However, the active drawbead system was not suitable in the production environment as the control system was too slow and complicated to be implemented effectively, especially due to the curvilinear profile of the drawbeads.

The second most popular approach adopted by researchers was to determine mathematically the effective bending radius of the strip to predict the DBRF and the blankholder force. These analytical models used different concepts to determine the DBRF such as:

a) Using bead radius as the effective bending radius of the strip (Weidemann, 1978)

b) Using parameters in the model derived from fitting of experimental DBRF in the Kluge model (Tufekci *et al.*, 1994),

c) Using the principle of virtual work (Stoughton, 1988) and

d) Using an iterative numerical procedure to determine effective bending radius of the strip and subsequently the drawbead forces (Sanchez and Weinmann, 1996).

Other recent analytical models were variations of the above models. For example, the Stoughton model was modified to take into account the Bauschinger effect (You, 1998; Lee *et al.*, 2008), to suit stepped and double beads (Keum *et al.*, 2001) and for square drawbeads (Firat, 2008).

The approach of using finite element modelling to model the drawbead test to predict the drawbead forces was first explored by Carleer *et al.* (1994). Assuming a plane strain condition, 2D drawbead models were set-up for pre-determined circular and square drawbead geometries for low carbon steel. These models gave acceptable results. Hence, the models were used to study the effect of drawbead shape on the DBRF, frictional shear stress and strain in the upper, lower and mid-surfaces. The drawbead restraining forces from the models were compared with the forces determined experimentally. After trial and error, the 'fitted' coefficient of friction that gave near-to-experimental results was assumed realistic. This was the drawback of the model as the coefficient of friction was used as a fitting factor. A fitted coefficient of friction value may cover shortcomings in the material model and the FE model itself. In addition, the same value may not work for FE models with different drawbead geometries.

Maker (2000) was a more comprehensive work. Experiments with pre-determined drawbead geometries were conducted which were then compared with 2D, 3D and equivalent drawbead models. Even though the 2D and 3D drawbead models did not accurately predict the forces, they matched the trend. It was also noted that the equivalent drawbead model, although quicker to use, under predicted the draw-in. Although this research did not mention the coefficient of friction used in the

simulations, it showed that 2D and 3D models were able to predict the drawbead force reasonably.

2.4.1 Academic research gaps

- Most drawbead tests were used to determine the coefficient of friction at full drawbead penetration while stamping dies only have partial drawbead penetration (Demeri, 1993) and (Jaguar Land Rover, 2014).
- The academic research focused on individual aspects of drawbeads such as the influence of draw speed and draw depth on DBRF but does not look into a complete drawbead design process.
- Analytical models over predicted the drawbead forces and were only validated with drawbead experiments on steel. None of the models were tested using the aluminium alloys investigated in this study.
- Equivalent drawbead models are quicker to use but need the coefficient of friction and DBRF as an input that might underestimate the sheet material thinning effect.

2.5 Industrial approach to drawbead design

One of the most significant parts of the dies are drawbeads that directly affect the quality of the part. These are located in the blankholder area and allow die design engineers to locally control the material flow by increasing the restraining force where the draw depth and material flow is lower and additional stretch is required, or reduce the restraining force and increase material flow where draw depth is high. Drawbeads are also helpful in mitigating two of the most commonly occurring defects, splits and wrinkling. Although the significance of drawbeads is widely acknowledged, their design, particularly for aluminium alloys, is not well understood.

The finite element method (FEM) is a popular tool in sheet metal forming to simulate various sheet metal forming operations. In the field of automotive stampings, FEM is widely used to determine the blank shape, obtain process parameters, such as the blankholder pressure, and to design forming dies. With developments in the computing technology, simulations can run faster and the entire tool geometry can be used in the forming feasibility studies. Such advancement is balanced by the intricate design of sheet metal parts and lead times for die design and manufacturing being shortened. Hence, complicated areas of die geometry such as drawbeads, which would need small elements to capture its geometry, are simplified using equivalent models. Although simulations with equivalent models gave acceptable results, they are not suitable for understanding the sheet metal behaviour over the drawbeads.

2.5.1 Industrial drawbead design practice

Three industrial automotive guidelines identified in the literature, **Table 2.2**, namely, the American (Smith, 1990), German (Xu *et al.*, 1997), and Russian (Zharkov, 1995) provide recommendations on typical drawbead geometries to be used for forming steels based on empirical data acquired over many years. Similar drawbead design standards for aluminium have not been found. Therefore, the industrial drawbead design practice for aluminium forming is based on trial and error.

Table 2.2: List of industrial automotive guidelines for drawbead design based on forming of steels

Sr.no	Country of origin of automotive forming guidelines	Reference
1	Germany	(Xu *et al.*, 1997)
2	Russia	(Zharkov, 1995)
3	America	(Smith, 1990)

A simplified die design process map based on industrial practice and focusing on design, validation and tryout is shown in **Figure 2.15**. Tooling project management, engineering change control and quality assurance activities have been excluded for clarity.

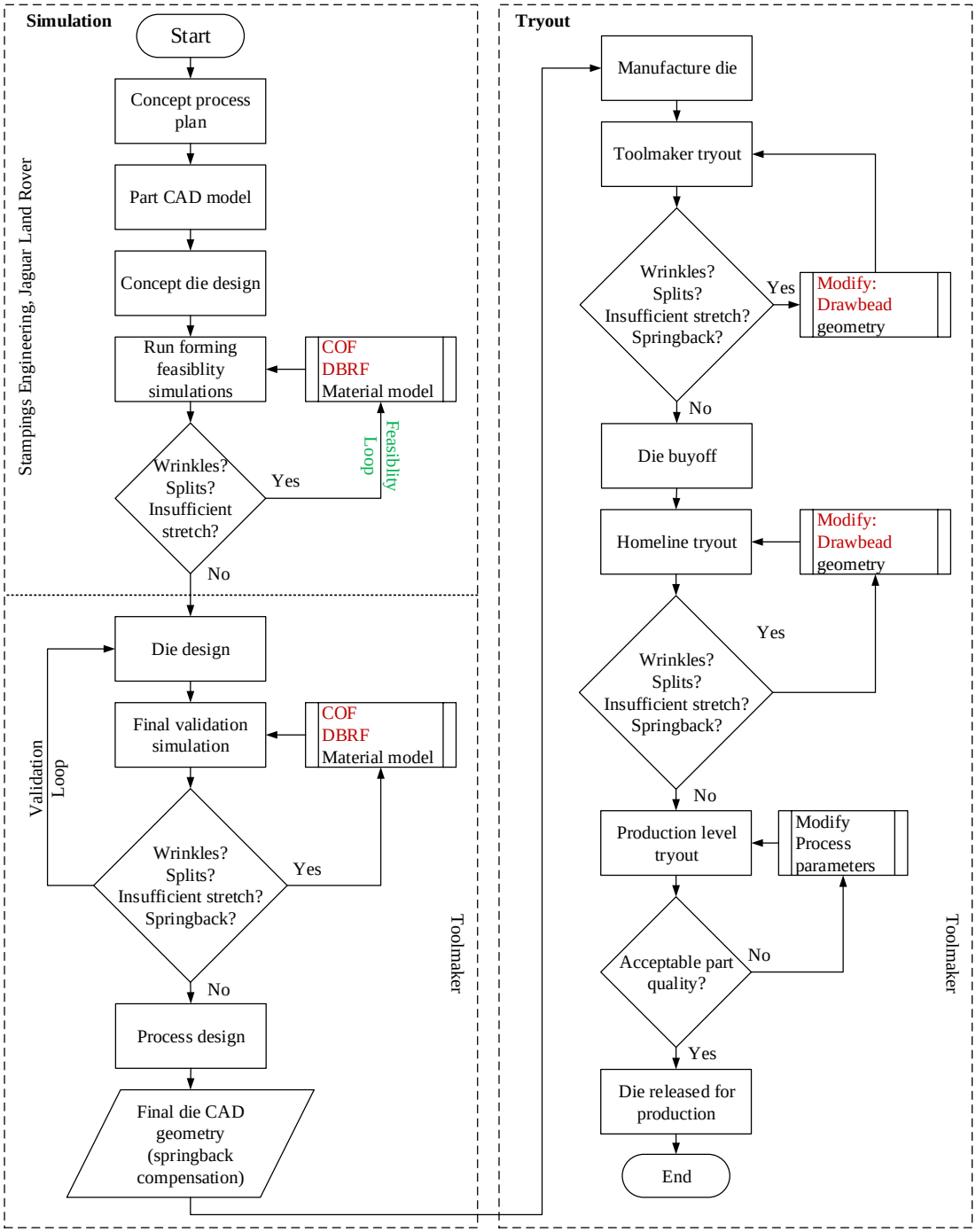

Figure 2.15: Flow chart indicating the main stages of industrial drawbead design practice

A part design is received from JLR's Body Engineering team. The simulation engineer imports it into a finite element package and then a conceptual die design is created with the help of the software to conduct a forming feasibility study. In this initial study, the formability of a part is checked and the resolution of defects such as insufficient stretch, splits and wrinkles is attempted. The main inputs to the simulation are the material model, DBRF and the coefficient of friction. The two main inputs that are changed are a DBRF and a coefficient of friction. A DBRF is assigned using a line of force along the periphery of the die. In most cases by changing values of these two inputs, defects can be mitigated. In some cases where draw depth is big enough to cause excessive thinning or the bend radius is close to sheet thickness, the Body Engineering team is advised to change the geometry of the part. Once the initial feasibility study is successful, then a die design is created which includes corrections in the die geometry from initial process plan stage to reduce forming defects such as wrinkles and splits. Also, process parameters such as appropriate blankholder pressure, determined by trial and error or based on previous experience, are set. These final changes are validated in the final validation stage and then the file is handed over to a toolmaker. This is the completion of the simulation part of the process.

The toolmaker creates a prototype from the die CAD file. Based on experience, the toolmaker assigns a physical drawbead geometry that is machined onto the blankholder. Then around 30 panels are formed and draw-in is measured, the thickness in the critical areas identified by the simulation is also measured. Usually, the drawbead geometry is adjusted until the draw-in is matched with simulation results. Other rework may include spotting of dies where there is uneven contact and adjusting

the blankholder pressure. Once the prototype is successful, the die is then tried on an in-house press in Jaguar Land Rover. This is to make sure the part quality is acceptable after the change of press. Here the drawbead geometry may be altered. After this stage, the die is finally tried out on the production line and commissioned after a number of successful production runs.

Changes to the drawbead and die geometry increases the tryout time and the number of test panels required. The prototype and the in-house die tryout is only accepted if 30 successive panels are formed within acceptable limits in each stage. The final production tryout may involve forming of 4000 to 12000 panels. The die design and tryout process, depending on the complexity of the part, can take anywhere between 6 months and 18 months. This is assuming that the inputs to the simulation are correct. The tryout process may need to be repeated if the inputs to the simulation are incorrect which can seriously affect the die commissioning deadline and the final car launch date.

Even though the drawbead force can be predicted either analytically or by numerically modelling the material flow over the drawbeads, there is no defined process to select an appropriate drawbead geometry. In addition, no parameter/method to evaluate and compare different drawbead geometries exists. Thus, there is a need to scientifically determine the simulations inputs and DBRF, along with an appropriate coefficient of friction, rather than rely on a trial and error basis.

The drawbead design is determined by trial and error during the forming feasibility study before sending the die design to the toolmakers. This is time-consuming. The commercial FE packages apply the analytical drawbead model, such as the Stoughton drawbead model, in the background to generate an equivalent drawbead force and

blankholder force from the entered drawbead geometry parameters (AutoForm, 2013). It will be proven in Section 3.2 that the analytical models overestimate the drawbead forces. The predicted drawbead forces may excessively restrain the blank and predict splits on the part. To mitigate splits the Stamping Engineer may reduce the drawbead height and or the coefficient of friction. This approach leads to a false representation of the frictional contact as the coefficient of friction is used as an "adjusting parameter". Thus, the contribution and effect of the drawbead geometry is "masked" and using this geometry on the physical dies may lead to a mismatch between the simulation and tryout results. The improved methodology will be demonstrated in Chapter 6. When trying out the die before production, the drawbead geometry often still needs to be changed. The tool makers and stamping engineers do not have a clear method/strategy to change the drawbead shape to successfully form the part (Jaguar Land Rover, 2014).

The equivalent drawbead model used in simulations are not fully capable of representing the material flow behaviour over drawbeads. In addition, using full part geometry in the simulation to study the effect of drawbeads often masks the local thinning and strain hardening of the sheet. Although the software allows 3D drawbead geometry to be defined and changed using a reduction strategy, the selection of drawbead geometry may still need many iterations.

2.5.2 Industrial research gaps

- Industrial guidelines for drawbead geometry were based on decades of experience from stamping of steels. As shown in Section 2.3, aluminium and steel differ in properties and therefore the same drawbead geometries and process parameters cannot be used.

- Drawbead design for aluminium largely is still a trial and error process
- Determination of coefficient of friction, DBRF and subsequently drawbead geometry in the simulations is an iterative process with limited scientific understanding.

2.6 Conclusion

Comparison of academic and industrial drawbead design approaches is summarised in **Table 2.3**.

- Academia has not come up with a holistic approach to determine a drawbead geometry, which can be easily implemented within the industry. Innovative solutions such as active drawbeads could solve the problems during die tryout. Alternatively, re-machining of an incorrect drawbead geometry, but these do not give correct inputs to be used in the forming feasibility simulation.
- Industry, because of the complexity of analytical drawbead models and friction models, and due to a large amount of experimentation required, has relied on a less scientific trial and error approach to determine the coefficient of friction and drawbead geometry. A simplified approach determining the coefficient of friction and the drawbead geometry in the simulation does not exist.

From the literature review in Section 2.3, it was understood that academia has focused on different aspects of drawbeads such as the effect of speed on the coefficient of friction and DBRF and determining the coefficient of friction for partially penetrated drawbead whereas industry has relied on a trial and error approach to determine DBRF in the simulations. Academia focused on experimentation to determine DBRF and used the drawbead as part of a larger research subject to reduce springback. Industry in a

way has also relied on experimentation to determine drawbead geometry by modifying it during the die tryout stages.

Table 2.3: Comparison of industrial and academic approaches for modelling drawbeads

	Industrial approach	**Academic approach**
Basis	• Using commercial sheet metal forming packages to determine iteratively DBRF and coefficient of friction through equivalent models. • Remachining of drawbead geometry during tryouts to get acceptable panels	• Physical testing to determine the coefficient of friction and the DBRF. • Mathematical modelling of sheet metal flow. • Optimisation techniques to determine drawbead geometry.
Measures	• Blank material utilisation and cost. • Die manufacturing cost. Process complexity and lead-time.	• Complexity and accuracy of physical tests and models.
Inputs	• Material model and Process parameters. • Coefficient of friction. • DBRF and or drawbead geometry.	• Material properties. • Coefficient of friction. • Drawbead geometry.
Outputs	• Information on forming feasibility, material and die costs.	• Scientific understanding of the behaviour of blank over drawbeads. • Mathematical models which can be incorporated into commercial forming packages.
Advantages	• Standardised process. • Easy to follow.	• Objectivity. • Scientific rigour.
Limitations	• Inaccurate inputs such as DBRF and COF can lead to excessive corrective action during die tryout. • Potential to be biased by personal preferences of Stamping Engineer and toolmaker. • Lacks conversion of DBRF into a physical geometry.	• Highly focused on certain aspects of drawbeads. • Unique test set-up and model formulation, which may not represent press shop environment and industry, needs. • Needs extensive material characterization. • Model formulation and results difficult to understand and implement.

3 Investigation of drawbead design methods

The three approaches, experimental, analytical and numerical, for designing drawbeads identified in Chapter 2 are investigated in this chapter. This chapter verifies the assumptions made in each approach and simultaneously attempts to eliminate the insignificant factors so that a simplified approach for designing drawbeads can be derived. The investigation process is illustrated in Appendix A.

3.1 Experimental approach

Sheet material when being drawn over drawbead experiences a restraining force due to a series of bending and unbending cycles and frictional contact. When analytically and numerically modelling this restraining force, a coefficient of friction value is necessary to represent the frictional contact. Nine (1978) designed a drawbead test to determine the coefficient of friction which can be used in the mathematical models. The DBRF and the BHF are other outputs from the test. Since material flow over drawbeads is more severe than over the punch and die radii in a conventional forming process, this test was later used to evaluate lubricants (Dalton and Schey, 1991; Figueiredo *et al.*, 2011).

Nine (1982a) proved that even though the friction over drawbeads is a complex phenomenon dependent upon the sheet and die material surface properties, lubricant properties and contact pressures, the coefficient of friction formula based on the Coulomb's friction law, **Figure 2.8**, is representative of the physical phenomenon. The underlying assumption, however, is that the contact remains as a thin film lubrication. A change in lubrication regime, due to increased contact pressure may invalidate the application of Coulomb's law. An example of the breakdown of Coulomb's law by comparison of DBRF and BHF was seen in experimental work done by (Nine, 1982a)

as shown in **Figure 3.1**. The sheet material was 0.9 mm AA2036-T4 aluminium alloy lubricated with mill oil. The drawbead groove and bead radii were 4.76 mm and the strip was 50 mm wide. The draw speed was 85 mm s^{-1}. A similar comparison in this project was carried out in identifying drawbead geometry combinations and process parameters that do not follow Coulomb's law of friction.

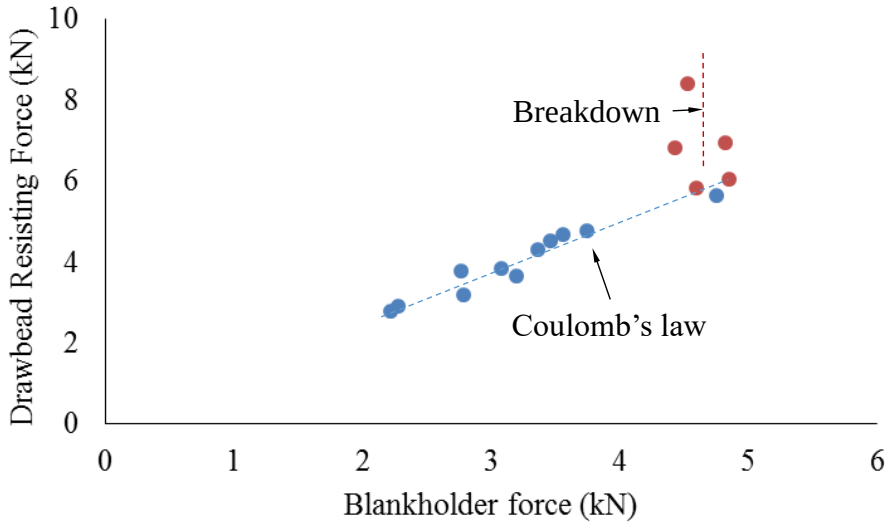

Figure 3.1: Breakdown of Coulomb's friction law with increasing blankholder force during the drawbead test (Nine, 1982a)

The Drawbead simulator at WMG is shown in **Figure 3.2** and the drawbead geometry used in the investigational experiments is shown in **Figure 3.3**.

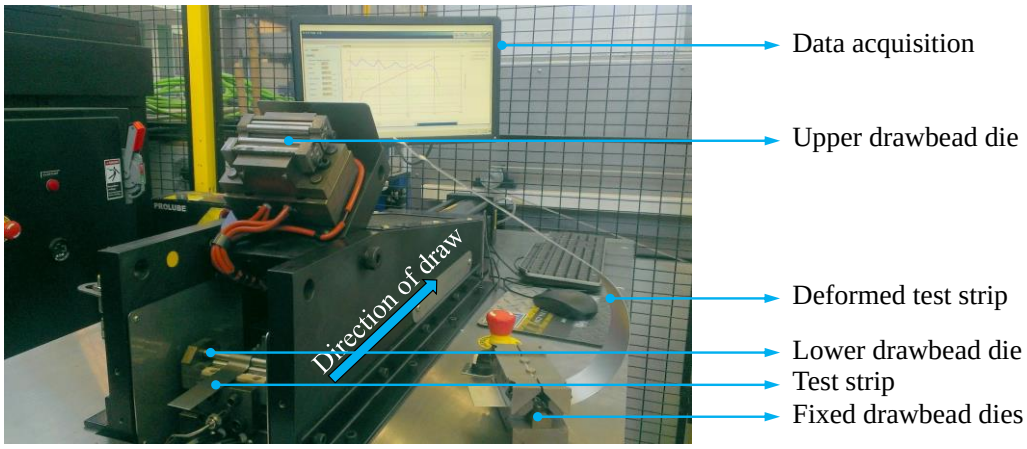

Figure 3.2: Drawbead simulator at WMG in the open position showing the drawbead set-up

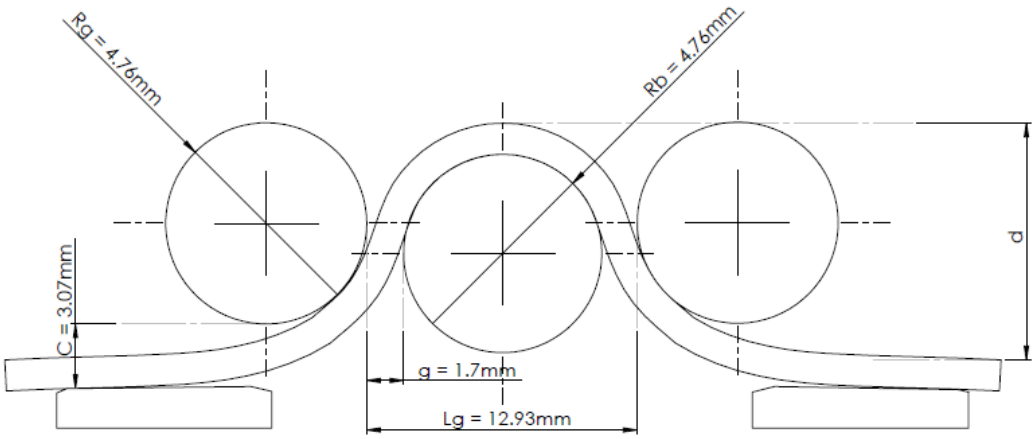

Figure 3.3: Drawbead geometry used in the current experiments and simulations

3.1.1 Draw speed

An experimental investigation to understand the influence on the change in draw speed was carried out. This was driven by a desire to understand further the impact of an increase in SPM. In a press shop, the press speed, measured in strokes per minute (SPM) is increased to achieve a higher production rate. An increase in SPM essentially increases the draw speed that may influence the DBRF due to a change in frictional conditions between the blank and blankholder. Therefore, this experimental investigation was done to understand the influence of a change in draw speed on the DBRF, the bead load and coefficient of friction. This investigation was also necessary to determine the draw speed that should be used in the further experiments. For this purpose, 50 mm wide AC600 aluminium strips belonging to the 6000 series (such as AA6111-T4), of 0.9 mm thickness lubricated with ALUBVS forming lubricant oil were used. The draw stroke was 200 mm. The draw speeds were varied from 10 to 100 mm s^{-1} on both roller and fixed bead set-up, as these were the minimum and maximum speeds available on the drawbead simulator for this test. Each experimental run was repeated three times. The deviation in observed forces was negligible, less than 1%, and hence error bars are been not shown in **Figure 3.4** below. (Please refer to Appendix

B1 for the full results table). The data shown is from the fixed bead set-up that also includes the effect of frictional contact between the drawbeads and test strip.

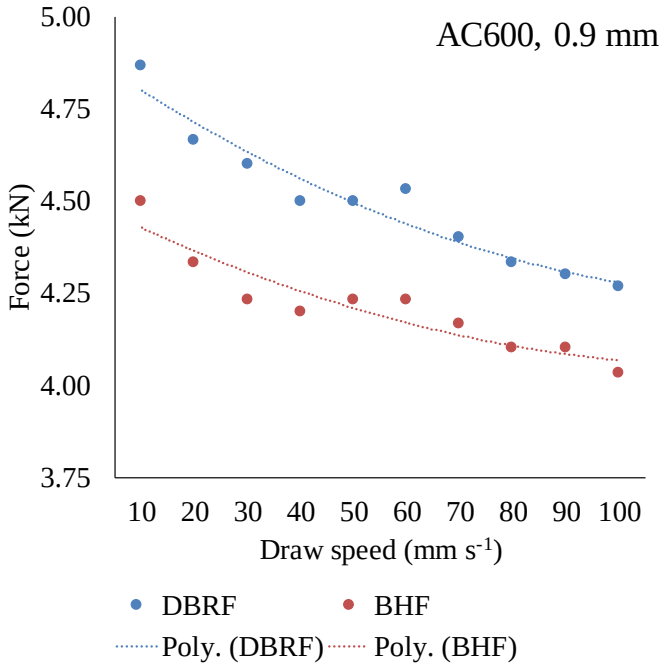

Figure 3.4: Effect of draw speed on the Drawbead Restraining Force (DBRF) and Blankholder Force (BHF)

The draw speed was found to have a significant influence on the drawbead forces and the relationship nonlinear in nature. The rate of change of drawbead forces was higher from 10 mm s^{-1} to 60 mm s^{-1}. The drawbead forces reduced significantly due to the reducing friction with the increasing speed. This maybe associated to the contact between the test strip and drawbead moving from boundary lubrication regime to mixed lubrication regime. There is more metal-to-metal contact in the boundary lubrication than in the mixed lubrication regime where the contact load is shared by lubricant and high points on surfaces in metal-to-metal contact. However, the rate of change of drawbead forces remained relatively unchanged in the range between 70 and 100 mm s^{-1}. This is quite typical when a contact is in a mixed lubrication regime and the rate of change of contact forces is smaller (Schey, 1983). This speed range is

similar to the draw speeds on an actual press (Schey, 1996). It was decided to select a draw speed of 85 mm s^{-1} for future drawbead tests, based on a desire to benchmark the work conducted here against earlier work by Nine (1978). The anomalous data point at 60 mm s^{-1}, also seen in **Figure 3.5**, did not fit the general data. Identical result was obtained on repeating the experimental run. However, a conclusion could not be reached as to why the data point did not fit with the rest of the data as the process parameters such as the lubricant, lubricant film thickness and temperature were maintained constant. Probably, there was an unidentifiable phenomenon arising from lubrication-surface interaction at 60 mm s^{-1}.

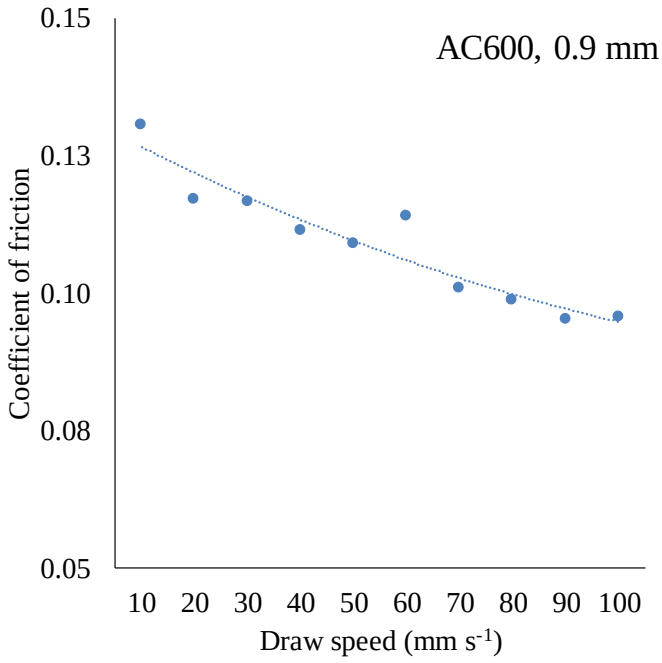

Figure 3.5: Effect of draw speed on the coefficient of friction

The influence of draw speed on the coefficient of friction can be seen in **Figure 3.5**. As coefficient of friction is a function of frictional (DBRF) and to normal component (BHF) of contact forces, it follows a trend similar to the drawbead forces. There is no significant drop in coefficient of friction between the ranges of 70 to 100 mm s^{-1}. This

further allows making a safe assumption that the effect of draw speed on coefficient friction would not be significant and a single draw speed value, 85 mm s^{-1} in this case, can be used in the future drawbead tests.

3.1.2 Strip thickness

It was evident that the bending and unbending effect and consequently the drawbead forces are a function of the bead radius (R_b) and blank thickness (t) (Levy and Van Tyne, 2009). In the body-in-white manufacturing process, parts come in various thicknesses. Drawbead tests to study the material flow over the drawbeads and deriving the drawbead forces for each material and gauge would be enormously time-consuming. Therefore, a need for determination of the significance of sheet thickness on drawbead force was identified.

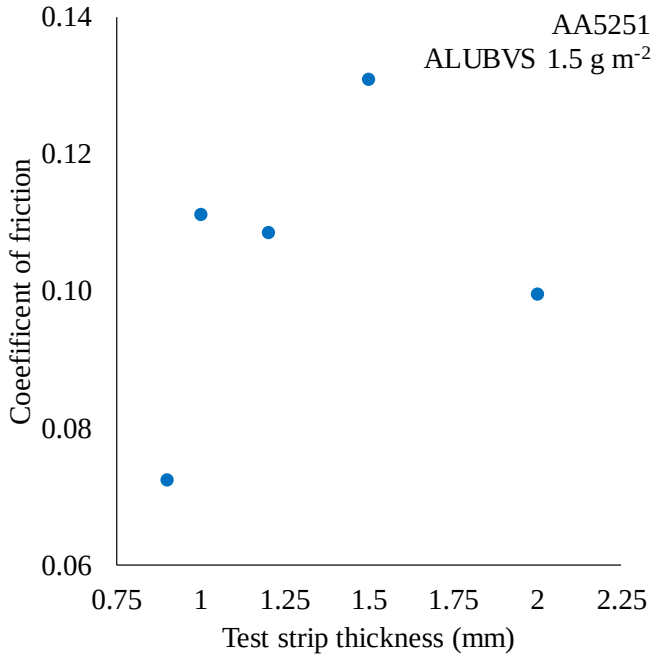

Figure 3.6: The coefficient of friction as a function of test strip gauge for AA5251

AA5754-O and AA6111-T4 were not readily available in a sufficient range of gauges. Therefore, AA5251, which also belongs to the 5000 series, was chosen, as it was

available in a range of gauges such as 0.9, 1, 1.2, 1.5 and 2 mm. The 50 mm wide test strips were lubricated with ALUBVS forming lubricant oil. The draw stroke was 200 mm and the draw was fixed at 85 mm s^{-1}. Again, both roller and fixed bead set-up were used and each experimental run was repeated three times. The variation observed for drawbead forces was less than 0.1 kN and consequently, only ±0.003, in coefficient of friction and was considered negligible. Hence, error bars were not shown in **Figure 3.6**.

The coefficient of friction was calculated from the formula proposed by Nine (1978) as illustrated in **Figure 2.8**. Friction is a function of the tribological system that includes the nature of the surfaces in contact and the lubrication. More on tribology in sheet metal forming is discussed in Submission 1. In this experiment, the surface roughness of the test strips and the drawbead remain unchanged. The amount of the lubricant on each strip was also kept constant. All the strips were drawn in a direction parallel to the rolling direction. Ideally, with the process conditions such as the blankholder force, draw speed and lubrication remaining constant, the coefficient of friction should be constant for all the strip thicknesses. However, it can be seen from **Figure 3.6** that such is not the case.

The coefficient of friction was also shown to vary with changes in strip thickness in the drawbead tests conducted by Hance and Walters (1999). The drawbead geometry used in their experiments was the same as that used in this test. Six AKDQ steel strips with thicknesses ranging from 0.5 to 1.5 mm were used and the calculated coefficient of friction was found to reduce with an increase in strip thickness. Duarte and Oliveira (2005) also investigated the effect of a change in thickness for both AKDQ steel and 2036-T4 aluminium alloys. Good correlation was seen between experimental and

simulation results. However, the drawbead forces increased with increasing thickness for both the alloys, which is similar to observations in this research project. Neither set of researchers provided explanations for their results that were contradictory in the case of AKDQ. This means there is an underlying disadvantage in the drawbead test method to determine the coefficient of friction when it comes to different test strip gauges. Hence, it was decided to use only one sheet thickness for further drawbead tests.

3.1.3 Blankholder gap and blankholder force

In all the drawbead tests conducted in this chapter, the engagement of drawbead was stroke controlled. The set-up also closely resembled the stamping operation on an automotive press in which the dies are gap-controlled to ensure that the dies did not open due to the uplifting force exerted by the strip when drawn through the drawbeads. If a certain blankholder gap is maintained, it is obvious that any excess blankholder force will have no contribution to the DBRF or the coefficient of friction.

3.1.4 Drawbead depth

This experimental investigation was done to understand the influence of a change in drawbead depth on the coefficient of friction. For this purpose, 50 mm wide AA5754-O aluminium strips of 1.5 mm thickness lubricated with ALUBVS forming lubricant oil were used. The draw stroke was 200 mm and the draw speed was set at 85 mm s^{-1}. Tests were conducted on both roller and fixed bead set-ups. Each experimental run was repeated three times. The deviation in observed forces was negligible and hence error bars were not shown in **Figure 3.7** (Please refer to the Appendix B2 which has the results table).

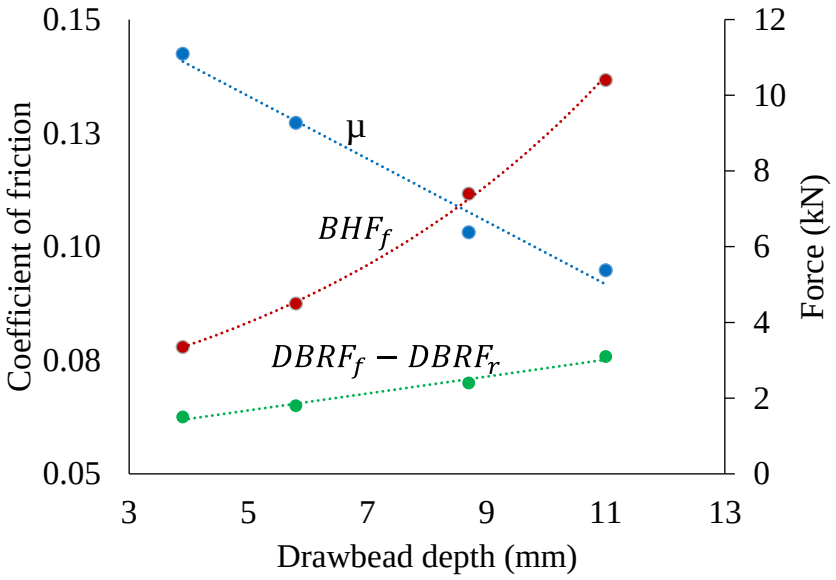

Figure 3.7: Relationship between coefficient of friction and BHF/DBRF for varying drawbead depths for 1.5 mm AA5754-O

It was stated early in Section 2.2 that the coefficient of friction formula for the drawbead tests is based on Coulomb's friction law. This means that the coefficient of friction for all the drawbead depths should remain constant unless there is a change in the lubrication regime. However, as seen in **Figure 3.7**, the coefficient of friction drops when the drawbead depth is increased. Visual inspection of the drawn surfaces of the test strips showed no evidence of severe surface deformation which can account for this. Therefore, the observed drop in coefficient of friction is not due to the tribological occurrences. One reason could be the ratio of frictional force ($DBRF_f$ - $DBRF_r$) to the blankholder force (BHF_f). The exponential increase in the blankholder force because of the increase in drawbead depth results in a lower coefficient of friction, **Figure 3.7**. In addition, π in Nine's formula, representing the contact area over the drawbead, does not appropriately represent a reduced contact area at lower drawbead depths.

3.1.5 Summary

The drawbead test is a simple method to determine the drawbead forces and coefficient of friction for a given drawbead geometry. However, this method has some underlying limitations as an experimental approach.

In the drawbead test, the work hardening behaviour of the test strip material clearly affects both the coefficient of friction and drawbead forces, which is a significant disadvantage. Therefore, in the forming simulations or analytical drawbead models, the coefficient of friction and DBRF must be determined for the particular combination of material and gauge being studied. Moreover, the coefficient of friction also varied with a change in drawbead height. This contradicts Coulomb's friction law and leads to presumption that a friction model to predict the coefficient of friction is required.

3.2 Analytical approach

Physical drawbead testing to determine the drawbead forces is an expensive and time-consuming process. Therefore, analytical drawbead models have been developed to 'estimate' the DBRF needed to input in simulations, and the blankholder force to determine the required press capacity. An analytical drawbead model must be able to predict the thinning of the strip as it passes over the drawbead. In order to do so, the model should closely represent the material and contact behaviour depending on the change in drawbead geometry. Moreover, the model should be comparatively easy to implement in the industry.

3.2.1 Selection of drawbead analytical models

Several analytical drawbead models have been formulated, of which the four most commonly occurring in the literature are compared in **Table 3.1**.

Weidemann (1978) proposed a very simple model to calculate the DBRF by supposing that the effective bending radius of the strip is the same as the bead radius. However, this assumption is only valid at the full drawbead depth. The drawbead on physical stamping dies never achieves full depth making this model inappropriate. The stresses through the cross section of the strip are assumed constant, however, due to the series of bending and unbending cycles, different layers through the strip's cross-section experience either tension or compression. This implies that the experimental drawbead forces might be lower than the ones predicted by the analytical model. Therefore, the Weidemann model was not chosen.

Table 3.1: Comparison of inputs and outputs of common drawbead analytical models

		Weidemann (1978)	Stoughton (1988)	Kluge (1992)	Sanchez & Weinmann (1996)
INPUTS	**Material model**				
	• Rigid plastic	X	X	X	X
	• Strain hardening		X	X	X
	• Rate dependant plasticity	X	X	X	X
	• Yield function	Isotropic	Hill anisotropic	Isotropic	Hill anisotropic
	• Bauschinger effect				X
	Friction model	Coulomb	Coulomb	Coulomb	Coulomb
OUTPUTS	**Strip's effective bending radius**		X		X
	Restraining force	X	X	X	X
	Uplift force		X		X
	Thinning		X		X
	Complexity	Low	Moderate	Low	High

The Kluge model which was an improvement of the Weidemann model (Tufekci *et al.*, 1994), used the same underlying principles but included the strain hardening effect. The semi-empirical approach of this model meant that parameters had to be acquired by least squares fitting of the experimental data. Even though this increased the accuracy of DBRF prediction, the need for experimentation to determine the coefficient of friction and drawbead forces still existed. Moreover, like the Weidemann model, the Kluge model is only applicable at full drawbead penetrations. Tufekci *et al.* (1994) compared the drawbead forces predicted by Kluge model with experimental

forces from experimental work done by Nine (1978). The model over-predicted the forces by 20% for aluminium 2036-T4. The effect of anisotropy that influences the plane-strain flow stress is not included in the model formulation. Since aluminium alloys are significantly anisotropic, the Kluge model was not used to predict the drawbead forces for aluminium alloys in this project.

Sanchez and Weinmann (1996) developed the most advanced analytical models which not only takes into account the effect of the sheet's anisotropic behaviour but also the Bauschinger effect. The Bauschinger effect is illustrated in **Figure 3.8**. By dividing the strip thickness virtually into fibres, the effective bending radius, effective through thickness strain and flow stress could be calculated at each bending and unbending cycle. To do this, a numerical iterative procedure was developed which made it possible to account for the cumulative effect of a series of bending and unbending cycles. As seen in **Table 3.1** the Sanchez & Weinmann model predicted the strip's effective bending radius, restraining forces and thinning that are essential for forming simulation. However, this model was not chosen for use in this study due to the extensive material testing required to characterise the Bauschinger effect and the need for a complicated numerical iterative procedure as well.

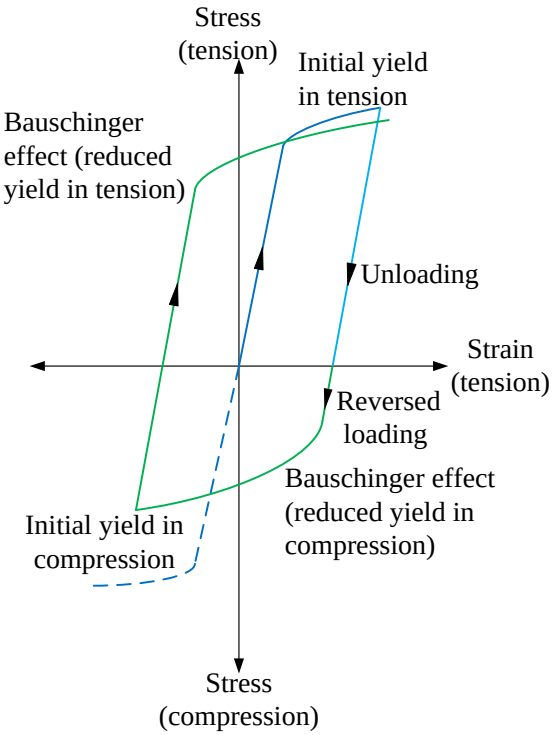

Figure 3.8: Bauschinger effect

Stoughton (1988) proposed an analytical model based on the principle of virtual work of deformable bodies in which the (external) work needed to pull the strip through the drawbead is equated with the (internal) work necessary to bend and unbend the strip and overcome the frictional resistance. This approach does not require the use of regression on the experimental data to obtain parameters for prediction of drawbead forces like the Kluge model. The Stoughton model not only attempts to predict the restraining force and the blankholder force but also calculates the effective bending radius of the strip. Thus, it is applicable to both partial and full drawbead penetrations, unlike Weidemann and Kluge models that are only suitable for full drawbead depths. Moreover, since the force calculations are in the closed form, not iterative like in Sanchez and Weinmann, the parameters and outputs directly relate to mechanical parameters obtained from a tensile test and to the drawbead geometry used. Hence, it is a good formulation for understanding the significant factors in the drawbead design

and their influence on the drawbead forces and thinning of the strip. Therefore, it was decided to investigate the analytical approach of designing drawbeads with Stoughton model in its original formulation. Improving and developing this model to give better results was out of the scope of the project.

3.2.2 Comparison with experiments

A MATLAB program was developed to code the Stoughton model and predict the drawbead forces. The steps involved in calculating the drawbead forces and the MATLAB code have been documented in Appendix C. The DBRF predicted by the Stoughton model in the frictionless case and in the presence of friction, are shown in **Figure 3.10**. In the frictionless case, the coefficient of friction in the exponent form is zero. Therefore, a linear increase in the restraining force with increase in drawbead depth is observed. In the presence of friction, the DBRF grows exponentially. In both cases, the Stoughton model over predicts the restraining forces determined experimentally by 41%, **Figure 3.10**a), in the roller set-up and by 57 %, **Figure 3.10**b), in the presence of friction at the highest drawbead depth. However, the Stoughton model correctly predicts the trend.

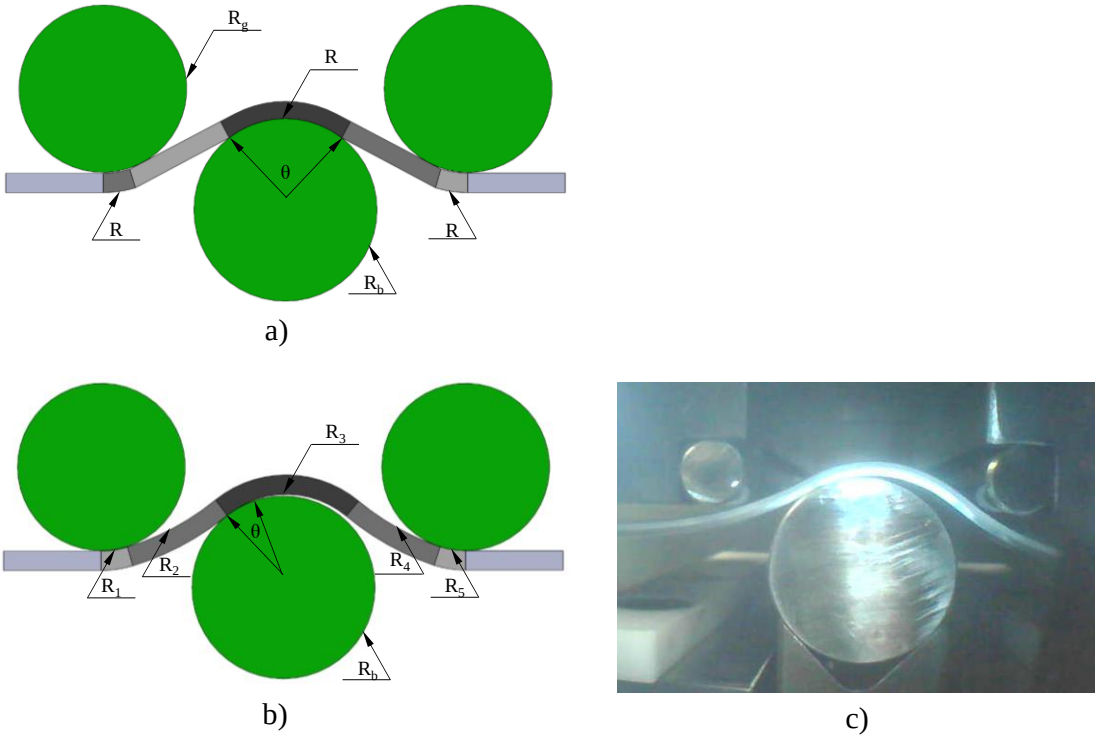

Figure 3.9: The strip geometry in the analytical model is assumed to be symmetric (a) but in reality (b) & (c) is asymmetric

The model requires calculation of the contact between the material and the bead to determine the effective bending radius. To simplify the calculations, the model assumes symmetric contact of the strip. This results in the prediction of a higher contact angle and consequently a smaller effective bending radius than seen in experiments. As the drawbead height increases, the effective bending radius of the strip comes closer to the radius of the bead and simultaneously, the strain in the outer most fibre of the strip increases because of increased tension. Therefore, the predicted restraining force also increases. However, it was observed in the experiments in this project that the strip does not conform to the bead radius in partial drawbead penetrations, **Figure 3.9**b) & c), so the symmetric contact and the effective bending radius of the strip is larger than the bead radius R_b.

The Stoughton model uses Hill-48 yield function to predict the effective flow stress which over predicts the effective flow stress required to initiate or sustain the plastic deformation of the strip. Therefore, the associated effective plastic strains produced by the Levy-Mises flow rule are also higher and as is the predicted restraining force.

Another reason for over-prediction of drawbead forces, especially at full drawbead penetration, is that the Stoughton model assumes isotropic hardening and does not account for the Bauschinger effect. The sheet moving over the drawbeads undergoes cyclic deformation. Under such deformation, the successive compressive yield stress after tensile loading reduces and is lower than the initial (or previous) tensile stress. However, with isotropic hardening, the effective stress is equal or more than the initial tensile stress which may lead to the prediction of larger forces (Sanchez and Weinmann, 1996).

The blankholder force, **Figure 3.10**c) and **Figure 3.10**d), is a vertical component of the restraining force. Therefore because of the reasons mentioned above, the Stoughton model over predicts the blankholder force as well as shown in **Figure 3.10**.

3.2.3 Summary

In this section, the need for analytical drawbead models was discussed. Four commonly cited analytical models were compared and the Stoughton model was chosen. The model correctly predicts the trend but overestimates the DBRF and the blankholder force. This is due to its assumptions that effective sheet flow over the drawbeads, especially in partial penetrations, is symmetric in nature. Hence, the Stoughton model over predicts effective through thickness plastic strains resulting in larger predicted drawbead forces than observed in the experiments conducted here.

Therefore, the use of analytical drawbead models for predicting the DBRF and the blankholder force in forming feasibility simulations may lead to erroneous results such as splits in the part.

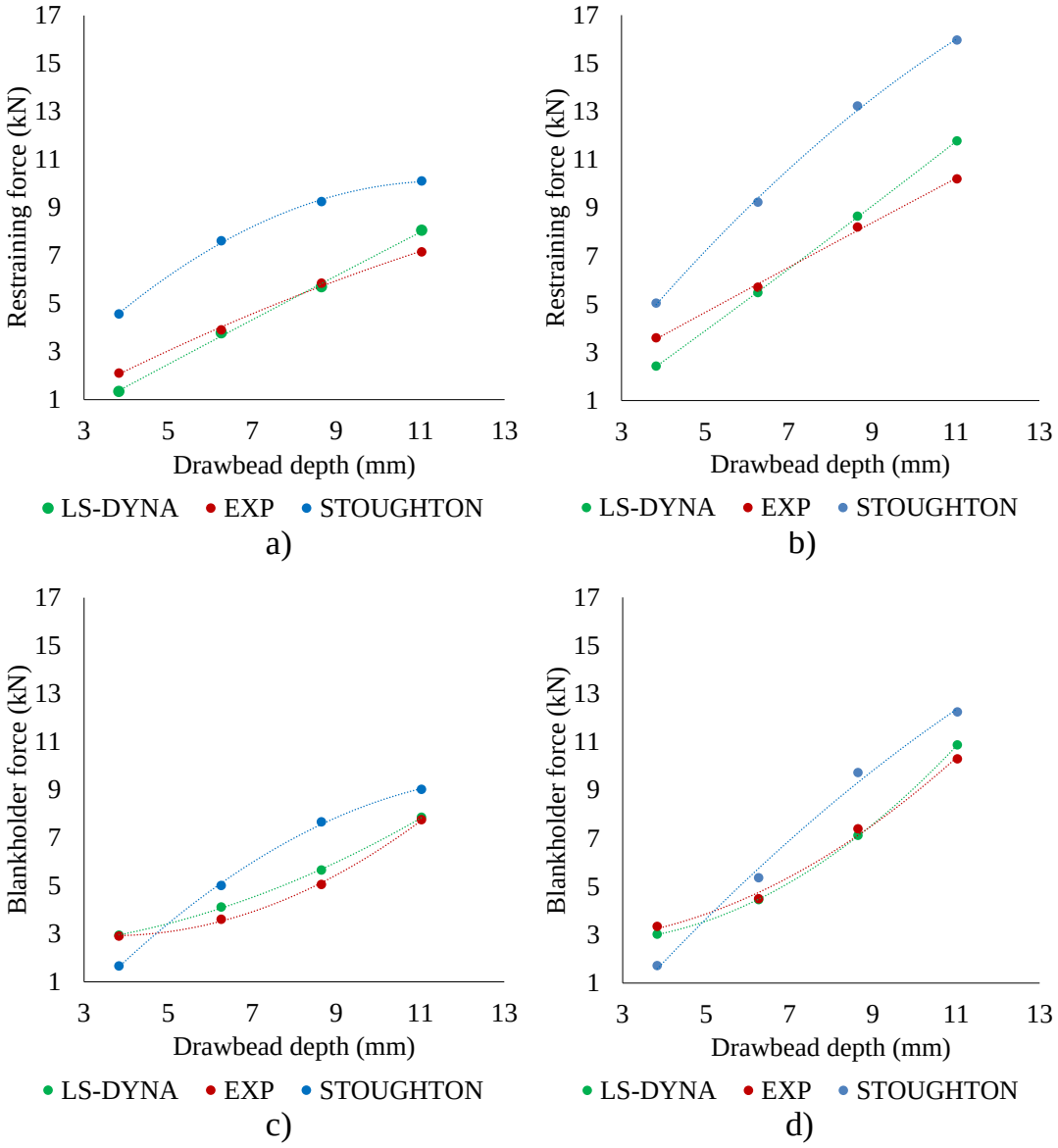

Figure 3.10: Comparison of drawbead restraining forces obtained from experiments, Stoughton model and LS-DYNA model at μ=0 a) and μ=0.15 b) and comparison of blankholder forces at μ=0 c) and μ=0.15 d)

3.3 Finite element modelling approach

The third approach in determining the DBRF and studying the behaviour of sheet metal flow is through finite element modelling of the drawbead test. The finite element method is a popular tool in sheet metal forming and there are several commercial software packages for forming finite element analysis. Four such packages are AUTOFORM^{TM}, DYNAFORM^{TM}, HYPERFORM^{TM}, and PAMSTAMP^{TM}. These finite element codes are for commercial use and therefore are used mainly for industrial applications. LS-DYNA is a general purpose finite element code suitable for varied applications such as automotive crashworthiness, explosions and sheet metal forming (LS-DYNA Theory Manual, 2014). For sheet metal forming simulations, it offers:

- metal forming pre and post processor suite
- the ability to choose from a number of material models for metal forming applications
- special contact types suitable for metal forming applications
- a facility to set-up equivalent drawbead models

LS-DYNA has been used successfully for studying drawbeads and sheet metal forming processes by a number of researchers, for example Xu and Weinmann (1996), Chen and Weinmann (2003), Sheriff and Ismail (2008), Firat and Cicek (2011) and Raghavan *et al.* (2014).

3.3.1 Plane strain deformation model

Drawbeads usually run parallel to the outline of the die and consist mostly of straight sections. On a die, the width of the blank passing over drawbeads is usually much larger than its thickness. Typically in bending operations, if the width to thickness ratio

of a flange is more than 8 then a plane strain condition can be assumed (Ren *et al.*, 2009). In the experiments described in Section 3.1, the width of the strip is 50 mm and the thickness is 1.5 mm giving a width-to-thickness ratio of 33. The assumption of plane strain simplifies the stress state by reducing it from a three-dimensional to a two-dimensional state. Several numerical studies relating to drawbeads were conducted using 2D plane strain model (Carleer *et al.*, 1994; Maker, 2000; Bae *et al.*, 2012; Ren *et al.*, 2009) and it has been demonstrated (Joshi *et al.*, 2016) that a 2D plane strain finite element model can replicate the bending behaviour of the sheet over the drawbeads in an appropriate way. This approach also allows for the use of different contact models. Hence, to understand the effect of drawbead geometry, at such a preliminary stage, it was easier and quicker to set-up a drawbead model in 2D rather than using a 3D model.

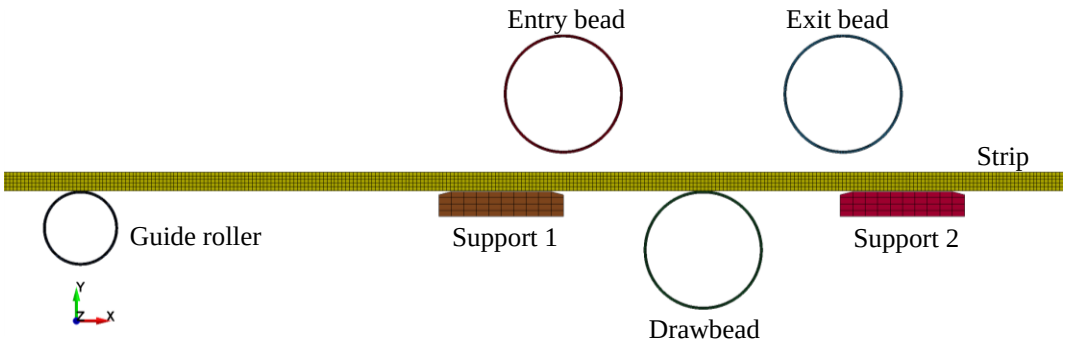

Figure 3.11: Schematic of the 2D finite element drawbead model

Figure 3.11 illustrates the 2D model set-up in LS-DYNA. The location of the supports is as per the drawbead test set-up. There is a clearance of 1.1 times the sheet thickness between the entry bead and the drawbead.

3.3.2 Element formulation

LS-DYNA has only one type of plane-strain element formulation, ELFORM_13. The entry bead, exit bead and drawbead are modelled as 2D cylinders with approximately 360 elements around the circumference to allow for a good contact with the strip. The strip is 1.5 mm thick and has five elements through the thickness. This is the optimum value, which is determined from the convergence study as described in Submission 3.

3.3.3 Material model

MAT_20_RIGID was used to model the drawbeads and the supports as rigid steel. The strip was modelled using the MAT_24_PIECEWISE_LINEAR_PLASTICITY material model. The required flow curve was obtained from the constants of the Voce hardening rule as this showed a better correlation with the tensile test data than the Power law as seen in **Figure 2.11**. Other material properties are listed in **Table 3.2**.

Table 3.2: AA5754-O material properties

Density (kg/m^3)	**Young's modulus (MPa)**	**Poisson's ratio**	**Lankford coefficient $\bar{r}$**
2700	70000	0.33	0.67

3.3.4 Boundary conditions

The entry and exit rollers were fixed. The bead was given a vertical degree of freedom in the Y-direction. The bead was displacement controlled and not load controlled. This was similar to the experimental set-up. Fixed bead displacements of 3.9, 5.8, 8.7 and 11 mm were used. Both the ends of the strip were allowed to move in the X-direction only and a displacement of 60 mm was assigned to the front-end of the strip. It was seen in the experimental restraining force vs time plot that the DBRF stabilised after

50 mm. This is shown in **Figure 3.12**. The displacement of the strip was started only after the bead achieved its vertical position.

3.3.5 Contact

A commonly used penalty stiffness based contact type, AUTOMATIC_SURFACE_TO_SURFACE was used in the 2D finite element model. This contact type is recommended where a large amount of relative sliding between the two surfaces occurs (LS-DYNA Theory Manual, 2014). In addition, this contact does two node/surface penetrations checks, i.e., on either side of the surfaces in contact. This is especially important for the coarser mesh of the strip coming in and out of contact with the fine mesh of the bead surfaces. The Coulomb friction model with a maximum allowable stress was used to limit the frictional shear stress to a value less than the yield stress of the strip material. More on contacts in LS-DYNA is explained in Submission 3. A coefficient of friction of zero is used to model the roller-drawbead (frictionless) set-up whilst the coefficient of friction for the fixed drawbead set-up was adjusted iteratively until a good agreement with the experimental drawbead forces was observed. In this case, a good agreement between simulation and experimental results for a fixed drawbead set-up was found at the coefficient of friction of 0.15.

3.3.6 Comparison with experiments

It can be seen in **Figure 3.12** that the DBRF predicted by 2D plane strain model shows a good correlation with the experimental DBRF. Both the forces show similar transition characteristics and stabilise after 50 mm of draw length. To calculate the drawbead forces from the simulations the average value of forces from 50 to 60 mm of draw length were used.

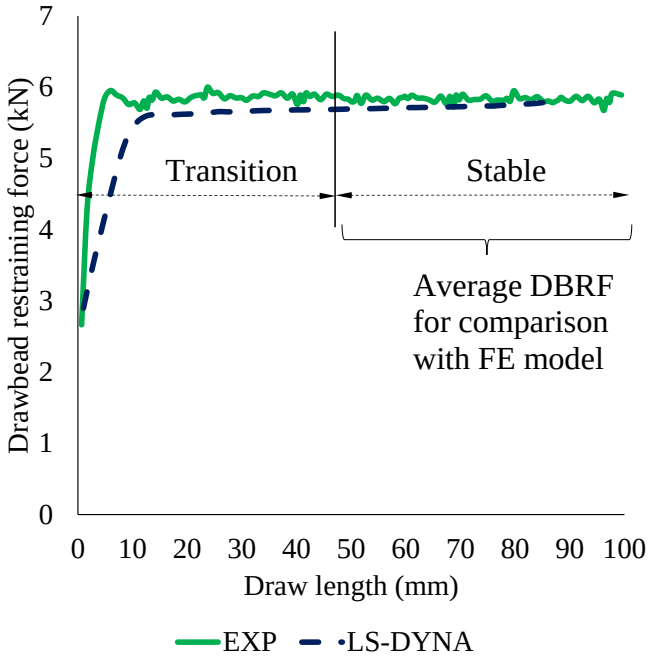

Figure 3.12: Comparison of drawbead restraining forces obtained from the drawbead test and LS-DYNA

Figure 3.10 compares the drawbead forces obtained from experiment and simulation with the coefficients of friction of zero and 0.15 respectively. In the case of DBRF, the simulation underestimates the force by almost 36% at a lowest drawbead depth of 3.9 mm and overestimates the force at 11mm drawbead depth by 12%. However, there is good agreement at the two remaining drawbead depths, with the error less than 3%. In the presence of friction (the coefficient of friction = 0.15) the simulation under predicts by 32% for the lower drawbead depth and overpredicts by 15% at high drawbead depths. For other depths, the error is less than 5%. Thus, apart from lower depths, the 2D finite element models predicted both the DBRF and the blankholder satisfactorily. This is shown in **Figure 3.10**c) and **Figure 3.10**d).

The reason the simulation underestimates DBRF at lower drawbead depth is illustrated in **Figure 3.13**. DBRF is an interior force obtained from the displacement of nodes at the cross-section of the strip. It also includes the tangential component of the sliding

contact force. At 3.9 mm penetration, only three strip nodes are in contact with the bead, as shown in **Figure 3.13**a), whereas there are 24 nodes in contact for the depth of 8.7 mm where there is a good agreement between simulation and experiments. This can be seen in **Figure 3.13**b). At low penetration, the effective bending radius of the strip is much larger than the radius of the bead resulting in almost 'point' contact instead of a good surface contact. Hence, further refining of the mesh will not solve the problem but only increase computational time. This has been demonstrated in Submission 3.

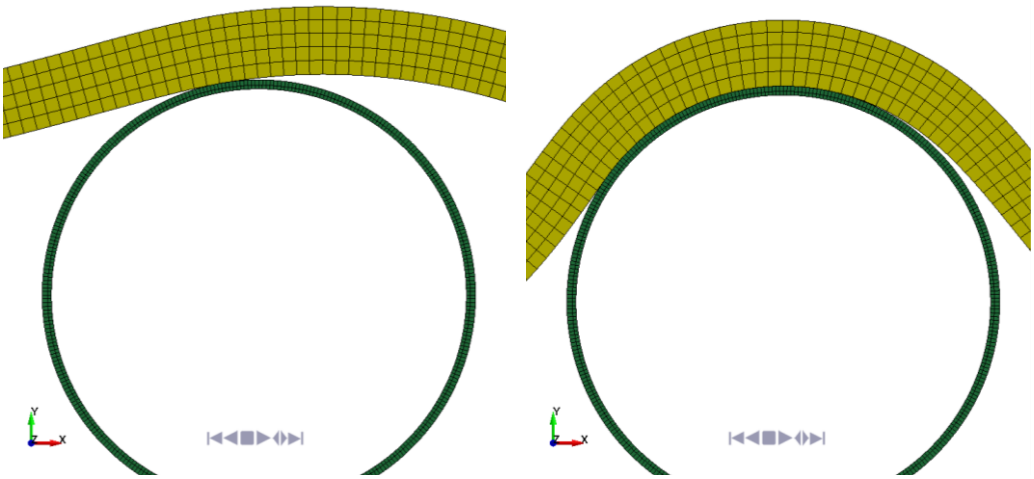

a) b)

Figure 3.13: Length of contact at depth of 3.9 mm a) and at a depth of 8.9 mm b) in the 2D drawbead finite element model

The blankholder force is essentially a normal component of a sliding contact and is read directly at the contact surface. **Figure 3.10**c) and **Figure 3.10**d) shows a comparison of blankholder forces obtained from simulations and experiments. There is a good agreement between the simulation and experimental results with a deviation less than 5 % in both frictional and frictionless contact. Thus, the 2D model also predicts the blankholder force accurately.

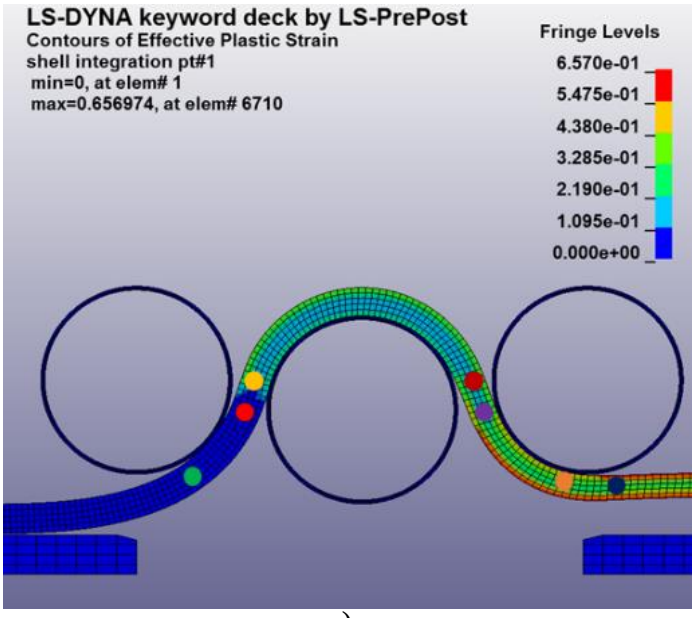

a)

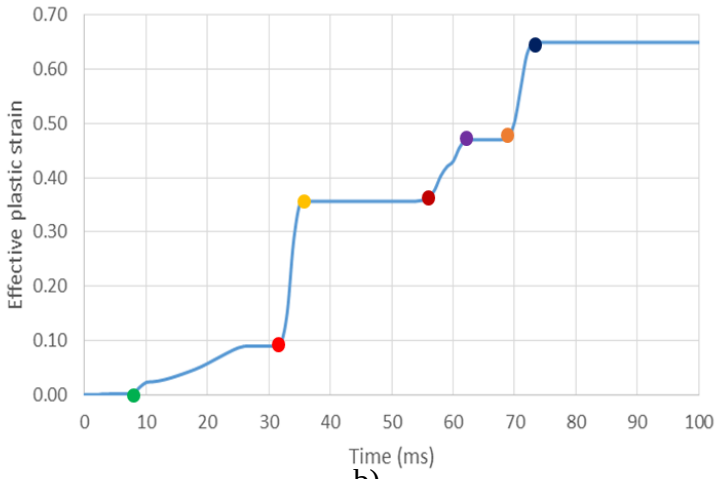

b)

Figure 3.14: Locations of bending and unbending points a) and graphical representation of effective plastic strain at respective locations b), at d=11 mm & μ=0.15.

Figure 3.14a) and **Figure 3.14**b) show the development of effective plastic strain in the strip. During a tensile test, the maximum strain at the point of instability (necking) is 0.19. This value is surpassed after the first unbending of the strip. The maximum plastic strain observed at the exit of the drawbead is 0.67 due to the work hardening effect. LS-DYNA extrapolates the flow curve. When effective stresses and strains encountered during simulations fall beyond the given range this can lead to an over-prediction of the DBRF.

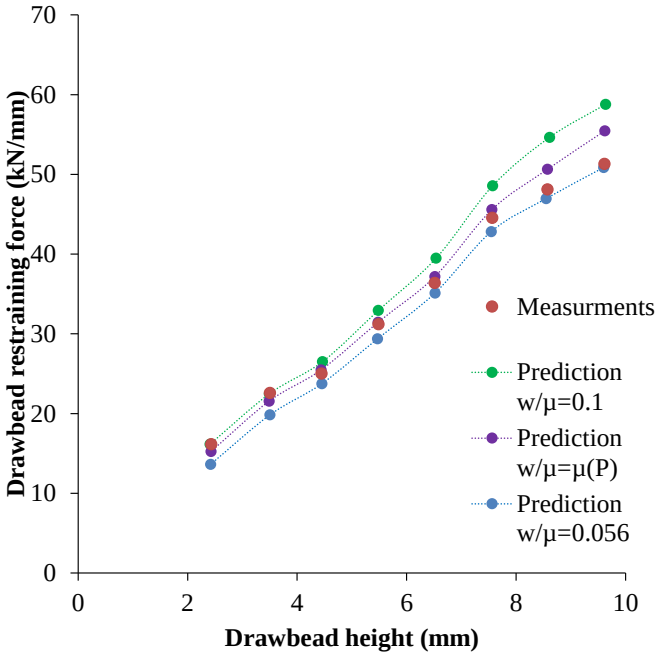

Figure 3.15: Comparison of drawbead restraining forces for coefficients of friction, obtained from Coulomb's model and non-linear friction model for different drawbead depths (Ren *et al.*, 2009)

The underestimation of DBRF at lower depths and overestimation at higher depths was also observed in drawbead test simulations conducted by (Ren *et al.*, 2009) for AKDQ steels. The study concluded that one friction coefficient cannot be used to determine drawbead forces at different drawbead depths and a non-linear friction model was necessary to improve the correlation between experimental and simulation results. If this was true then there should have been better agreement with between the experimental and simulation drawbead restraining forces in the frictionless case as can be seen in **Figure 3.10**a). In addition, it can be seen in **Figure 3.15** that using a contact pressure based non-linear friction model, $\mu = \mu(p)$, only slightly improved the deviation at lower and higher depths. Therefore, it can be concluded that friction is not the primary cause for such deviation and a simple Coulomb's friction law can be used. An added benefit of this approach is that additional testing and experimental fitting is not required.

3.3.7 Summary

- A finite element model using a plane strain assumption was set-up. The model parameters such as mesh size, the number of integration points and coefficient of friction were obtained from the parametric studies, as detailed in Submission 3.
- A Coulomb friction law can be appropriately used to represent the contact. The coefficient of friction of 0.15 gave the best agreement with the experimental results. Non-linear friction models require additional tests, data fitting and do not significantly improve DBRF prediction.
- The Voce equation is more suitable for the fitting of tensile test data of aluminium alloys than the Power and Swift equations.
- The 2D drawbead model can appropriately represent the bending and unbending behaviour of the strip and contact.

3.4 Conclusion

Analytical models such as the Stoughton model over predict the restraining force. Simple models such as the Weidemann model and the Kluge model do not give sufficient information, such as blankholder force and thickness prediction, whereas complicated Sanchez and Weinmann model require additional testing and numerical procedure to determine drawbead forces and thickness information. However, these can act the first point of reference to estimate the drawbead forces and to study the effect of drawbead geometry on the forces.

The choice of a 2D drawbead model as the design methodology for determining the coefficient of friction and drawbead forces was driven by the finding that the 2D drawbead FE models are able to predict both the trend and the magnitude of the

drawbead forces accurately. The FE models do not give accurate results at lowest and highest depths due to insufficient contact length and extrapolation of the flow curve respectively. The accuracy of the FE models is better than the analytical models. The analytical model over predicts the drawbead forces with an error of 60% whereas the FE models predict the drawbead forces with less than 15% error.

4 Influence of drawbead geometry parameters on drawbead restraining force

Drawbead geometries commonly observed on automotive draw dies often use a groove radius different from the bead radius. There are many workable drawbead geometry combinations and manufacturing of these for investigation using physical drawbead tests would be expensive. Previous work has established that the drawbead depth is the most significant geometrical parameter. However, no research work was found in which the individual and combined effects of the drawbead geometry parameters was studied. Understanding these effects will help in establishing a strategy for drawbead geometry design and selection. Therefore, it is essential to understand the sensitivity of the DBRF to the various geometrical parameters.

4.1 Design of experiments

One of the most powerful statistical tools for systematically studying the relationship between the input variables and the output is the design of experiment (DoE). The design of experiments involves selecting factors or inputs to the process that can be either controllable or uncontrollable. For the drawbead experiments, *controllable factors* include the drawbead geometry parameters and process parameters whereas an example of an uncontrollable factor would be ambient temperature. To understand the influence of factors, it is required to divide the range of each factor into different *levels*. For example, in this case, the drawbead depth is investigated and will be varied at four levels, 3, 5, 8 and 10 mm. Depending on the number of factors and respective levels, a *structure* or layout for the experiments needs to be designed. There are two types of design of experiments, fractional and full factorial. Full factorial experiments involve testing every combination of factors and levels where each combination is called an

experimental run. An experiment involving three factors varied at two levels is referred to as a 2^3 design and requires $2^3 = 8$ runs. Where there are several factors varied at many levels and testing all the experimental runs is not feasible, a fractional factorial design based on a carefully chosen subset of the full factorial design can be used. Although this is economically beneficial, it compromises on the understanding of interaction effects between factors. Hence, in this study, full factorial experimentation is undertaken. The design of experiment to study the influence of drawbead geometry on the DBRF is shown in **Figure 4.1**.

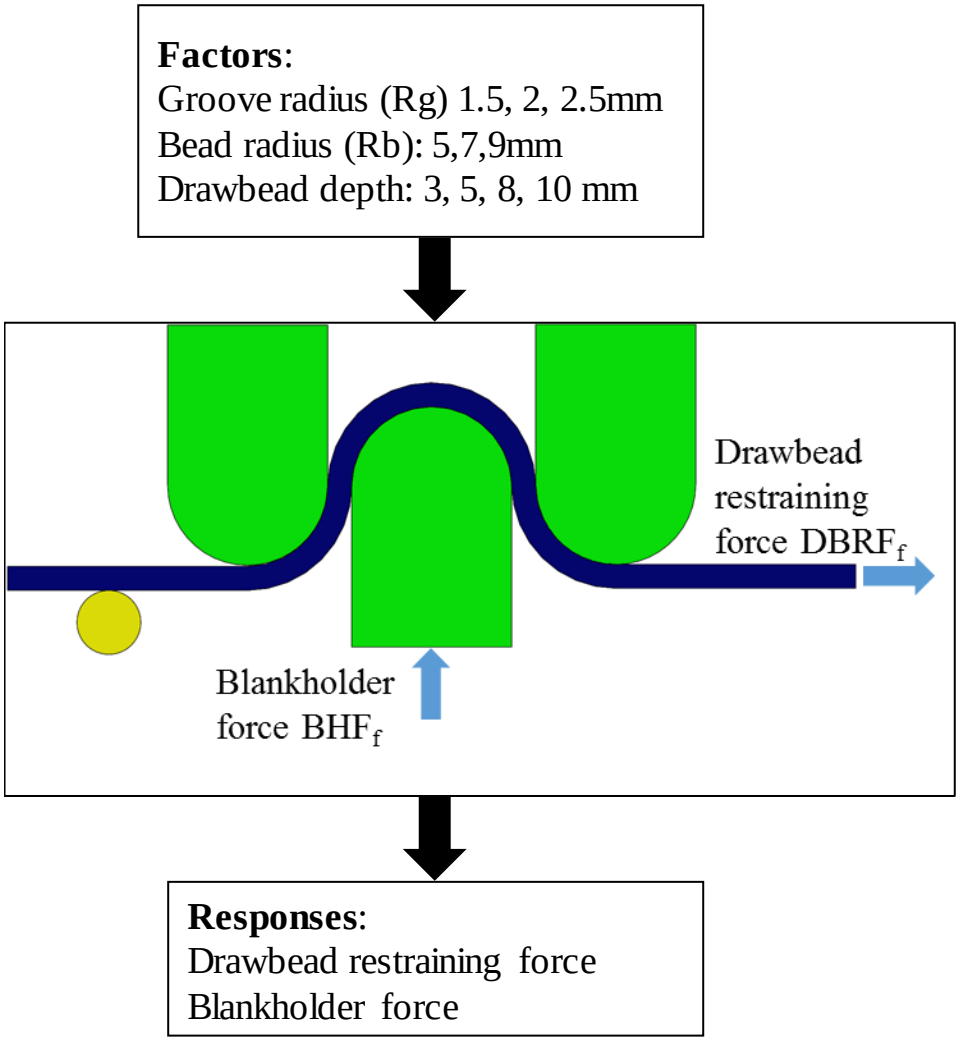

Figure 4.1: Design of experiment approach to study the influence of drawbead geometry on drawbead forces

The selection of factors, or drawbead geometry parameters in this case, were based on those identified across the literature, on stamping dies at JLR's press shop and trial drawbead tests conducted in this work. The range was set such that it covered the upper and lower limits for all the parameters individually. The minimum groove radius was set to 1.5 mm, which was equal to the test strip thickness. The maximum groove radius was set to 2.5 mm, as it was the maximum groove radius found on the stamping dies in the JLR press shop (Jaguar Land Rover, 2014). From the various drawbead tests carried out in the literature (Samuel, 2002), it was identified that the minimum bead radius was at least three times the test strip thickness to avoid locking of the material flow through the drawbead. Therefore, the minimum bead radius was set to 5 mm. 4.5 mm could have been ideal but 5 mm bar stock was readily available at the time of manufacturing the test set-up.

The maximum bead radius was found to be no more than six times the test strip thickness as test strip might not experience work hardening due to gentle bending (Lange, 1986). Hence, the maximum bead radius was set to 9 mm. During a visit to JLR's press shop (Jaguar Land Rover, 2014) it was found that the maximum bead radius of 9 mm was in use within the press shop. Therefore, to duplicate the press shop conditions, this bead radius was used for the experiments.

In order to be able to identify the impact of the drawbead height, it was opted to keep the groove and the bead radius constant. For a semi-circular drawbead, it is normal practice that the maximum drawbead depth is equal to the bead radius. For these experiments, drawbead height was varied between 25 to 100% of the drawbead radius, i.e., 25, 50, 75 and 100%. This gave drawbead depths of 3, 5, 8 and 10 mm, which were used for the experimental work. The experiment was repeated three times to

ensure the consistency in the results. From this experimental work, the drawbead depth used for this investigation were selected as 5 mm as depth of 3 mm was inadequate to restrain the test strip, 8 mm cause severe thinning and 10 mm made the test strip tear. However, it must be noted that the depth results may vary if the grove and bead radii are changed.

Process parameters such as the lubricant type, lubricant coat weight, draw speed and the blankholder force, blankholder gap were kept constant. Only the drawbead geometry parameters were changed.

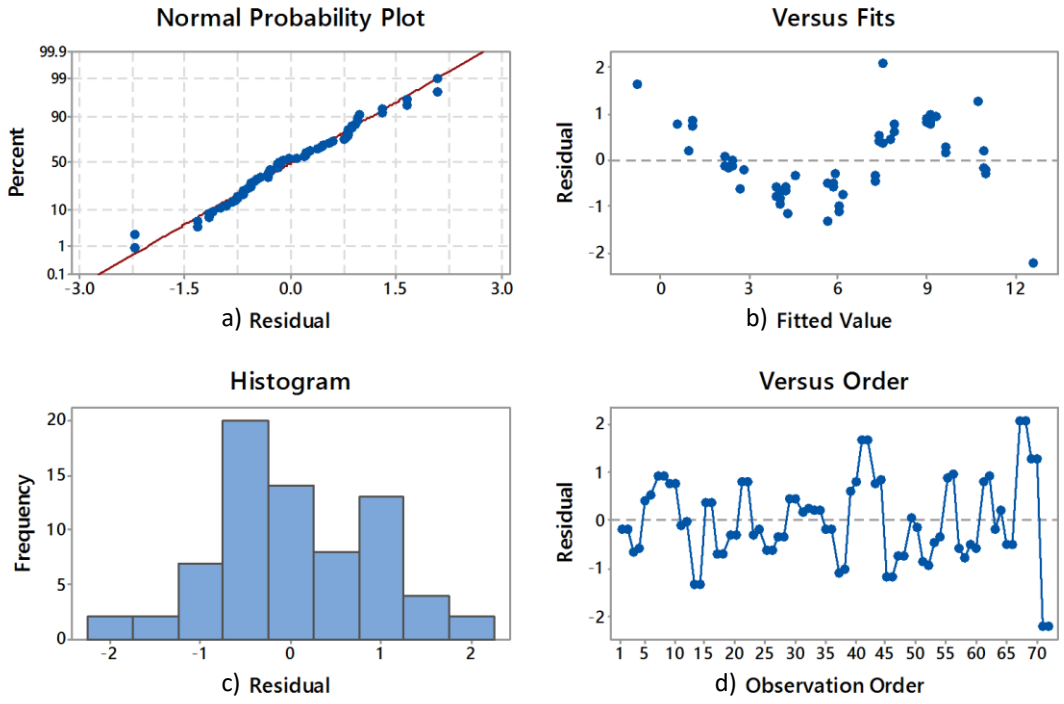

Figure 4.2: Residual plots obtained from Minitab

After running the experiments for all the combinations, MINITAB^{TM} statistical analysis software was used to compute and analyse the experimental data. The adequacy of the design was checked using the residual plots shown in **Figure 4.2**. The Normal Probability Plot, **Figure 4.2**a), for the residuals, shows that the results data (blue dots) is normally distributed around the line of fitted means of the data (red line).

There are two outliers at runs 71 and 72 as seen in **Figure 4.2**d. Whilst the values obtained from runs 71 and 72 gives the appearance of being outliers, these readings can be attributed to the maximum limit of and are therefore considered to be valid results.

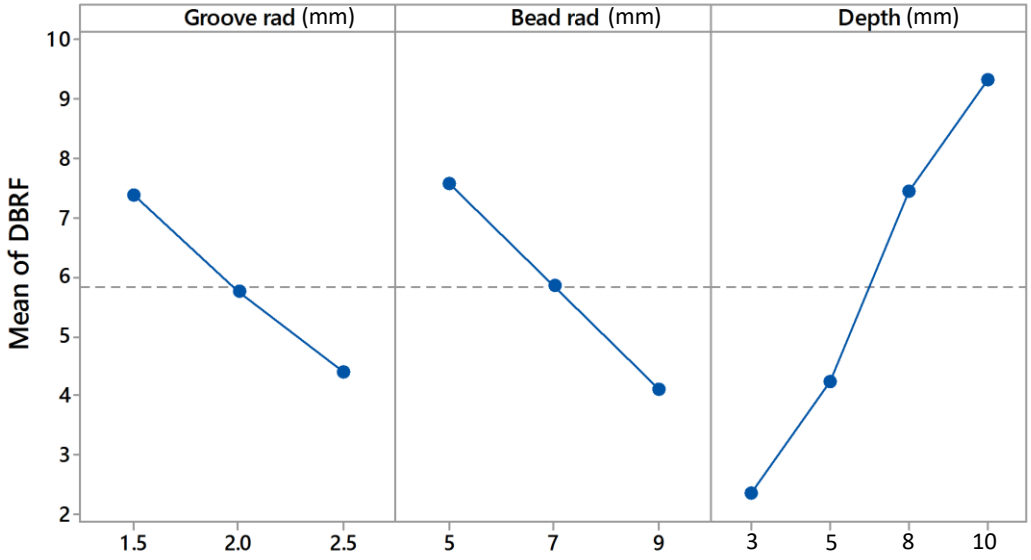

Figure 4.3: Main effect plot obtained from Minitab

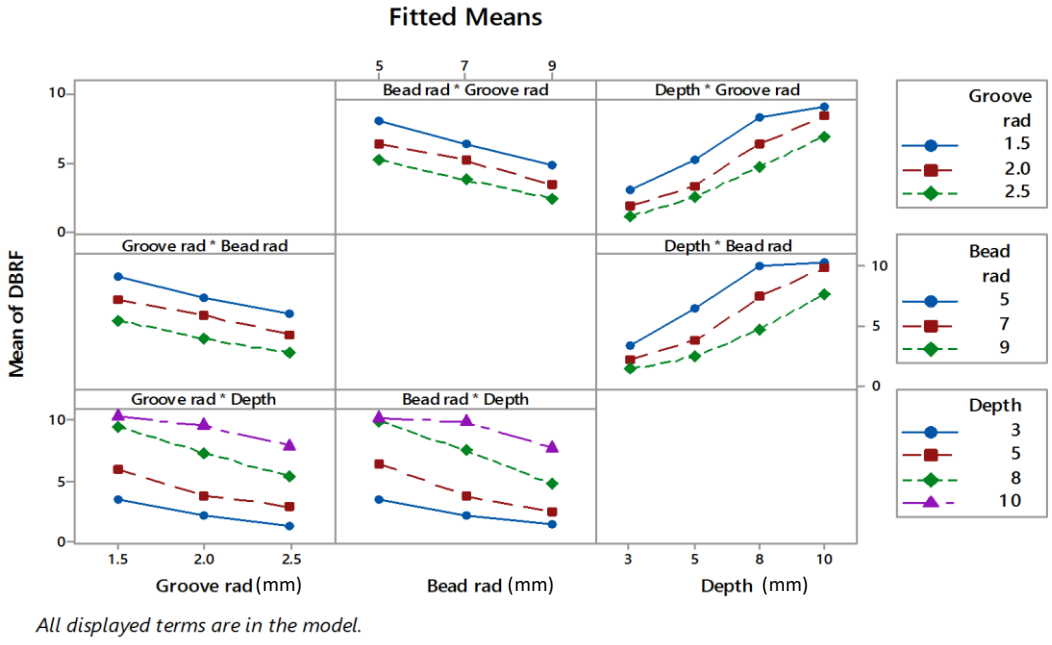

Figure 4.4: Interaction plots obtained from Minitab

The main effect plot, **Figure 4.3**, suggests that all the individual drawbead geometry parameters have a significant influence on the DBRF, as the lines of the effect are not parallel. The groove radius and bead radius both have a negative slope showing that an increase in radii leads to a decrease in the DBRF. This is to be expected since bending over a larger bead radius reduce the effective bending radius of the strip and produces smaller tensile strains in the outermost fibre of the strip resulting in a lower restraining force. However, the DBRF increases steeply with the increase in the drawbead depth. This indicates that the drawbead height is a more significant drawbead geometry parameter than either the groove or the bead radius.

The interactions between bead radius, groove radius and depth are shown in **Figure 4.4**. It can be seen that there are interaction effects, as the lines of the effect are not parallel, but the slope of interaction effects are not steep as seen in the main effects **Figure 4.3**. The two-way interaction between the groove and bead radii is not as significant as that of drawbead depth and groove radius or bead radius. This is to be expected because the drawbead depth defines the tightness of wrap of the test strip around the groove and bead.

The level of significance of main effects and interaction effects is established using an ANOVA table as shown in **Table 4.1**. It can be seen that the p-value, which corresponds to the significance level for all the square and 2-way interaction are larger than 0.05. Only the main and interaction effects with p-values less than 0.05 have a significant effect on the response. Therefore, for the DBRF, in this case, the interaction effects were not significant.

Table 4.1: ANOVA table from Minitab

Analysis of Variance

Source	DF	Adj SS	Adj MS	F-Value	P-Value
Model	9	405.085	45.009	42.82	0.000
Linear	3	403.903	134.634	128.07	0.000
Groove rad	1	57.122	57.122	54.34	0.000
Bead rad	1	72.450	72.450	68.92	0.000
Depth	1	274.331	274.331	260.96	0.000
Square	3	0.625	0.208	0.20	0.897
Groove rad*Groove rad	1	0.233	0.233	0.22	0.641
Bead rad*Bead rad	1	0.109	0.109	0.10	0.750
Depth*Depth	1	0.283	0.283	0.27	0.608
2-Way Interaction	3	1.401	0.467	0.44	0.723
Groove rad*Bead rad	1	0.203	0.203	0.19	0.664
Groove rad*Depth	1	0.702	0.702	0.67	0.421
Bead rad*Depth	1	0.497	0.497	0.47	0.498
Error	26	27.332	1.051		
Total	35	432.416			

4.2 Conclusion

A study of the main and interaction effect of groove radius, bead radius and drawbead depth on the DBRF have provided the following conclusions.

- The influence of drawbead geometry on the DBRF is critical in the drawbead design process. From the main effects plot, drawbead depth had the most significant impact on the DBRF followed by bead radius and groove radius.
- It was found that the individual impact (main effect) of drawbead geometry parameters have more significant influence on the DBRF than the combined influence (interaction effect).
- When creating a database of drawbead geometries and DBRF, although drawbead depth alone was a significant parameter, the effect of groove and bead radii should not be ignored.

5 Criteria for selection of optimised drawbead geometry

5.1 Need

The restraining force generated by the drawbeads is not only a function of the drawbead geometry but also of the tensile strength of the blank material, its thickness and the blankholder gap. The drawbeads will only be able to produce an effective restraining action if the blankholder remains closed throughout the draw stroke. As discussed in Section 2.3, drawbeads exert an uplifting force. A blankholder force greater than the uplift force must be applied to maintain a correct blankholder gap that may demand extra press capacity. Therefore, a larger blankholder force will be required to suppress higher uplifting force exerted by smaller drawbead radii and/or higher depths. The sheet thickness and tensile strength of the blank also contribute to the uplifting force. For example, under the same drawbead geometry, the uplifting force for a thicker blank will be higher than the thin blank. The same is valid for a blank material with higher tensile strength. Therefore, drawbead selection criteria must take into account the effect of drawbead geometry, blank thickness and material type on the blankholder force and consequently on the press capacity required to form a particular part.

Drawbead geometry selection is not a straightforward process, especially when using analytical drawbead models. There can be several combinations of different drawbead geometries, which may give the same drawbead force. Therefore, to be able to determine the optimum geometry, researchers used various statistical optimisation algorithms. Naceur *et al.* (2001) developed optimisation algorithms (regression analysis) using a Newton-Raphson iterative procedure in two stages. Firstly to determine the optimum DBRFs and secondly to determine the optimum drawbead

geometry using the Stoughton drawbead model on the optimum DBRF determined in the first stage. In both optimisation stages, the range and initial estimate had to be entered in the optimisation programme, which was a significant drawback as the output was greatly influenced by the value of the initial estimate. Moreover, the optimisation software could only include one objective function, for example, minimization of variation between the experimental and predicted thickness, and could only provide one optimum geometrical parameter as an output.

Artificial neural networks (ANN) are predictive algorithms, which attempt to simulate internally the relationship between the input and the output variables and can potentially eliminate the guesswork in the optimisation programmes. ANN models are required to be "trained" by giving numerous different input and output scenarios so that it "learns" the relationship between them. This option was explored by Han *et al.* (2006) to determine the optimum DBRF to form a truck side door panel. The results presented were in terms of mean square error between the results from the numerical simulation and the artificial neural networks. It was observed that the mean square error came within acceptable limits after training the model with over 20 different scenarios, in this case, the combination of groove and bead radius. However, physical experiments were not carried out to verify the model.

Esener *et al.* (2013) compared optimisation algorithms (regression analysis) and an artificial neural network approach for determining the DBRF using fixed bead set-up drawbead test with three different penetrations, 1.25, 3.73 and 6.75 mm on seven different forming steel grades with six thicknesses, 0.8, 1, 1.2, 1.5, 2, and 2.5 mm. The work concluded that optimisation algorithms over predicted the DBRFs by almost 30% and the ANN models by over 40%.

Hence, it was concluded that optimisation algorithms and artificial neural networks, in spite of being sophisticated techniques, give inaccurate predictions, and more importantly are difficult to implement and understand. Therefore, a simple relative measure to evaluate drawbead geometries and to narrow down the selection to determine the optimum geometry is desired.

5.2 Concept

The drawbead restraining force and the blankholder force work together to bring in a desired level of stretch in the part. The stretch in the part is measured in terms of effective through thickness plastic strain. Therefore, a method that takes into account the combined influence of DBRF, blankholder force and effective through thickness plastic strain will prove useful in evaluating the effectiveness of the drawbead geometry. The effect of blankholder force is significant as it directly affects the press tonnage requirements.

From the review of research done by academia and industry in section 5.1, it was clear that a parameter to compare and select a geometry does not exist. Therefore, a parameter that allows a qualitative comparison of the performance of different drawbead geometries will help in the selection of a drawbead geometry that is suitable for a given material and thickness. Based on the key parameters described above, it was thought that the outputs from the drawbead test namely, DBRF, BHF and effective through thickness strain would prove useful in relative comparison of the drawbead geometries under consideration.

To this end, a geometry effectiveness parameter (GEP), which is a ratio of the maximum through thickness plastic strain to the proportion of the blankholder force required to maintain the blankholder gap, is proposed in Equation 5.1. The ratio of

through thickness plastic strain to restraining force factor gives a measure of how much the drawbead forces are contributing to the strain experienced by the test strip. The factors used in GEP can be determined either experimentally or numerically.

$$\boldsymbol{GEP = \frac{\varepsilon_t}{R_{ff}}} \qquad \text{Equation 5. 1}$$

ε_t is the through thickness plastic strain in the strip, defined as

$$\boldsymbol{\varepsilon_t = \frac{original\ thickness - final\ thickness}{original\ thickness}} \qquad \text{Equation 5. 2}$$

R_{ff} is the restraining force factor, which in turn is a ratio of the drawbead restraining force to the blankholder force, BHF_f, in N mm^{-1}

$$\boldsymbol{R_{ff} = \frac{DBRF}{BHF}} \qquad \text{Equation 5.3}$$

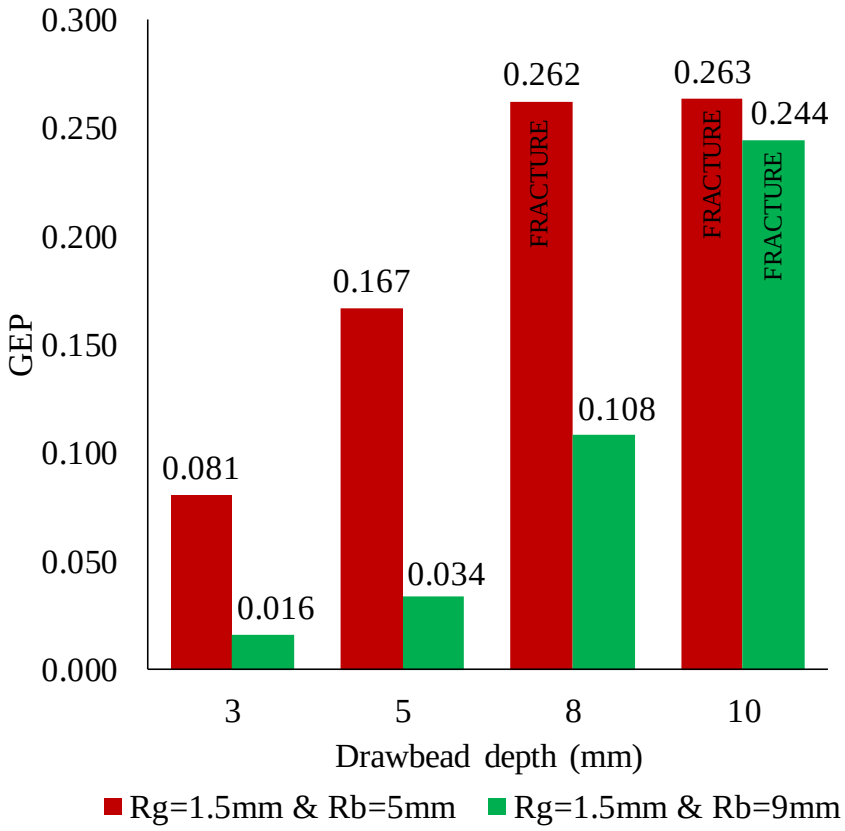

Figure 5.1: Illustration of concept of GEP as a relative measure to compare drawbead geometries for 1.5 mm AA5754-O

Figure 5.1 illustrates how GEP can be used to compare two drawbead geometries, R5 (Rb = 5 mm) and R9 (Rb = 9 mm), represented by red and green bars respectively. The GEP was calculated for the drawbead geometries that were used with the 1.5 mm AA5754-O material. It can be seen that for R5 drawbead geometry, the test strip fractured where higher GEP values were observed, particularly at a high drawbead depth of 8 and 10 mm. In addition, larger GEP values were also recorded for depths of 3 and 5 mm, which was due to severe thinning of the test strips at the exit of drawbead. In comparison, the R9 drawbead showed lower values of GEP across all depths. The very low GEP value at 3 mm depth was due to there being insufficient stretch imparted by the drawbead geometry while a better stretch was imparted at a depth of 5 mm. From the results, it can be understood that the R5 drawbead geometry is not suitable

for 1.5 mm AA5754-O whilst R9 drawbead with a depth of 5 mm appears to impact sufficient stretch. This suggests that the GEP value can be used as a qualitative guide.

5.3 Application

The GEP is a simple way of quantifying and comparing the effect of changes not only in drawbead geometry but also in the overall blankholder system. **Figure 5.1** showed a specific example of the practical application of Geometry Effectiveness Parameter (GEP) in which eight drawbead geometry combinations were evaluated. If the DBRF alone is considered, as shown in **Figure 5.2**, then there is less distinction between the different drawbead geometries, i.e., drawbead depths of 5 and 8 mm for Rg=1.5mm give similar DBRF but their GEP values are quite different. Hence, it can be seen that the GEP can be useful in giving a relative comparison of the drawbead geometries. A comparison using DBRF alone cannot give an indication of the effectiveness of the drawbead geometry because the drawbead geometry giving higher DBRF will always be considered "effective" and vice versa.

Using GEP, it can be seen that higher GEP values, 0.244 to 0.263, corresponding to higher DBRF led to severe thinning or fracture that is undesirable in stamping operations. Similarly, lower GEP values, 0.016, indicate that corresponding DBRF is not sufficient in bringing in sufficient strain the sheet material. Overall, it can be observed that the R5 drawbead geometry relative to R9 gave higher GEP values that may result in severe thinning or fracture of the sheet material. In addition, it is also observed that the R9 drawbead geometry may impart sufficient strain in the sheet material with a drawbead height of 5 mm as 8 mm results in conditions that are closer to fracture due to more severe thinning. Thus, GEP allowed narrowing the choice of drawbead geometries from eight to one. Therefore, it can be safely concluded that the

final depth of 5 mm is suitable for 1.5 mm AA5754-O. Further work is required to determine how 'critical' GEP values could be determined for different materials to allow drawbead design optimisation.

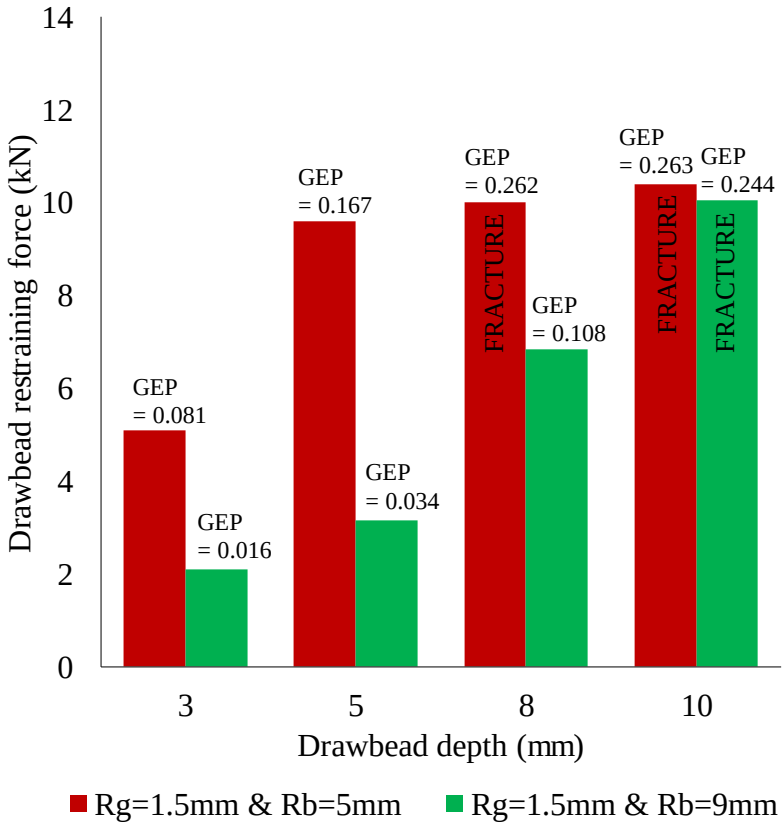

Figure 5.2: Geometry Effectiveness Parameter (GEP) for range of drawbead geometries tested for AA5754-O

The GEP presented in this research work was used to compare the drawbead geometries and is based on the output of the drawbead test, namely, DBRF, BHF and through thickness strain. This research work has shown the effectiveness of the GEP measure in the conditions used in this study. However, GEP measurements that have been proposed could be applied to other scenarios. For example, to compare different shapes or single, double or triple rows of drawbeads. However, further work would need to be carried out to demonstrate its effectiveness under these conditions.

GEP should be used with caution. The drawbead geometry giving higher GEP may have larger through thickness strains which may lead to necking of the blank in the wall area after bending over the die radius. The increase in drawbead depth gives higher GEP. However, the required press tonnage also increases and new press with a larger capacity may be required. Lastly, the GEP should not be used to compare different blank materials directly. Different blank materials will exhibit different plastic deformation behaviour over a range of drawbead geometries. In this case, the GEP should be determined separately for each blank material and thickness keeping the drawbead geometry constant.

5.4 Conclusion

- It was shown in the literature review that using optimisation models and (ANN) is a complicated process and does not offer any significant advantage in predicting the DBRF. In addition, these methods do not allow easy correlation between the inputs and the outputs.
- GEP is a simple method that takes into account the combined influence of thinning and the amount of blankholder force needed to maintain the drawbead gap. Thus, it is possible to select a drawbead geometry without affecting the press capacity.
- Even though GEP is larger at higher drawbead depths, it is not suitable for stamping large panels, as there is significant thinning at the exit of the drawbead. There may be splits on the part during the stampings operation due to excessive restraining action.

- Based on the GEP analysis, drawbead geometries with groove radius of R1.5 and bead radii of R5 and R9 were selected for evaluation through a stamping operation.

6 Proposal for designing drawbeads for aluminium alloys

A research methodology is proposed based on the findings from the literature review outlined in Section 2.3 and 2.4 and the initial investigation described in Chapter 3 respectively. This chapter outlines the proposed route to design drawbeads. Drawbead tests using the roller and the fixed set-up were conducted to generate drawbead forces to compare with the frictionless (roller set-up) and frictional (fixed set-up) contact numerical models. Then simulations were conducted for a range of groove radii, drawbead radii and depths using the design of experiments approach to obtain the drawbead forces. Finally, the Geometry Effectiveness Parameter (GEP), described in Section 5.2 was used to compare and select the optimum drawbead geometry.

6.1 Proposed drawbead design process

The analysis conducted in this project has shown that the process for drawbead geometry selection should be based on the following:

- It should provide the coefficient of friction, drawbead forces and through thickness strain behaviour of the blank over the drawbeads for use as an input into forming feasibility simulations.
- It should require minimal experimental work and/or new test tooling to determine required parameters.
- The process should not rely on analytical drawbead models.
- It should be easy to follow and implement.
- The process should have a method to rank the effectiveness of drawbead geometries.
- It should be easy to set-up in a finite element software and the model should be quick to run.

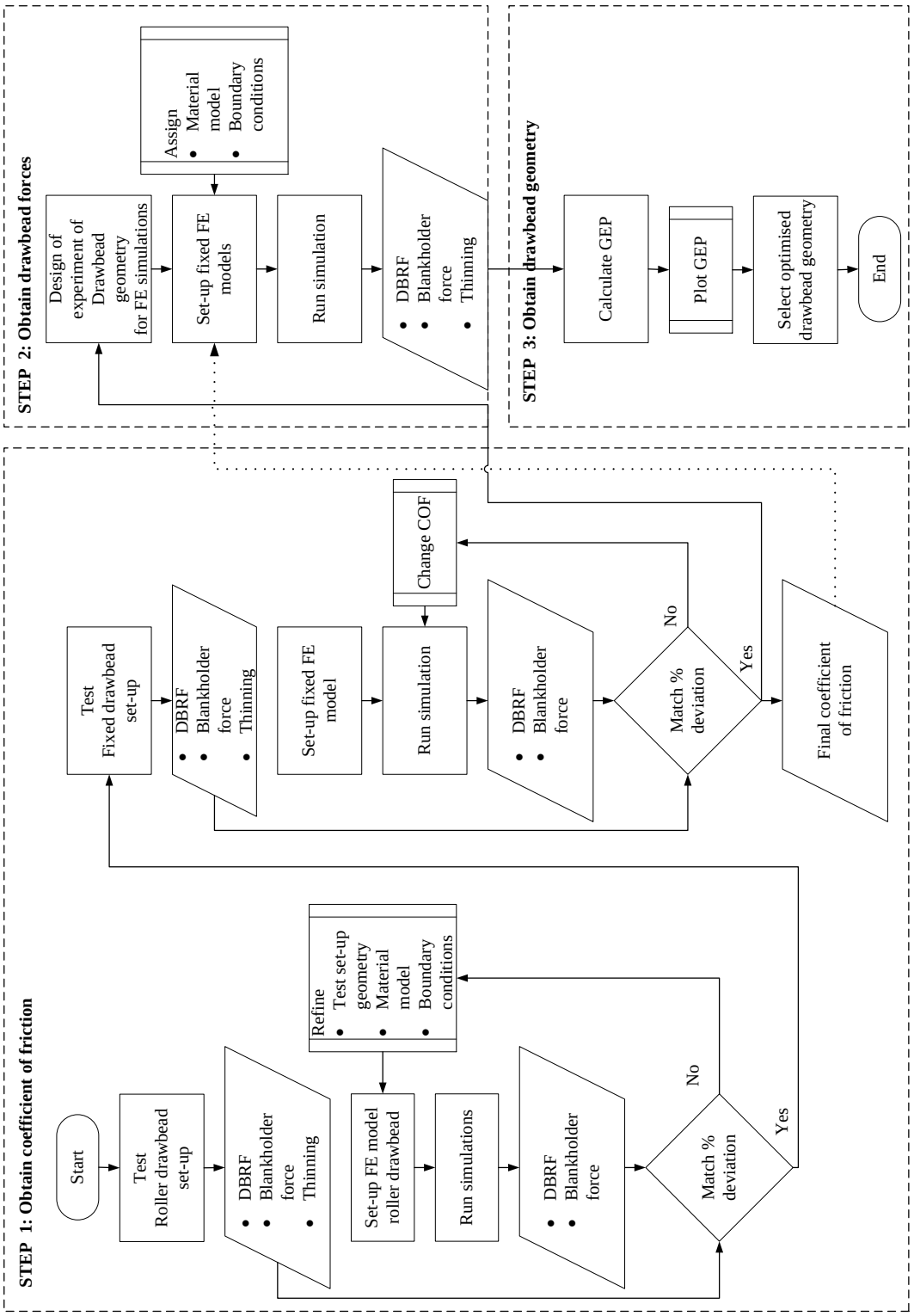

Figure 6.1: Proposed methodology for arriving at optimised drawbead geometry

Based on the knowledge gathered from the investigation of drawbead design approaches, Chapter 3, and understanding the influence of the drawbead geometry on the material flow, a drawbead design approach was formulated as shown in Figure 6.1. The process is divided into three stages. Firstly, a coefficient of friction should be obtained by calibrating the FE model with the results from the roller drawbead tests. Next, fixed drawbead simulations using the obtained coefficient of friction for different drawbead geometry combinations should be performed to determine predicted drawbead forces and through thickness strains. Lastly, GEP must be used to select the optimum drawbead geometry.

6.2 Process verification

All the experimentation and finite element modelling conducted so far used AA5754-O. In order to test the model, AA6111-T4 was used to demonstrate that the process is applicable equally to a different aluminium alloy. This was because AA6111-T4 alloy showed a slight difference in material properties as compared to AA5754 as per **Table 2.1**. Nominally, AA6111-T4 had a higher yield and ultimate tensile strength tensile than AA5754-O. (CES Edupack, 2014). The yield stress for AA6111-T4 is reported to be 150 MPa, which is higher than that of AA5754-O, 100 MPa. In addition, the ultimate tensile strength of AA6111-T4 is reported to be larger than that of AA5754-O, 300 MPa and 220 MPa respectively. Therefore, it was expected that AA6111-T4 might comparatively experience a higher restraining force due to its larger yield stress. The following sub-section shows the process implementation sequentially as illustrated in the process flowchart in **Figure 6.1**.

6.2.1 Coefficient of friction

6.2.1.1 Roller drawbead test

A roller drawbead test similar to that described in Section 3.1 was conducted using 1.5 mm AA6111-T4. The strip size was 500x50 mm with ALUBVS applied at a coat weight of 1.5 g m^{-2}. The strips were drawn at 85 mm s^{-1} for 200 mm. Three strips were drawn for each drawbead depth of 3, 5, 8 and 10 mm. The restraining force and the blankholder force are shown in **Figure 6.2**a) and **Figure 6.2**b), respectively. It can be observed that the characteristics of the drawbead forces are similar to those obtained for AA5754 in Section 3.1, **Figure 3.10**. This did not follow the hypothesis stated earlier because there was only a marginal difference in the material properties of the AA5754 and AA6111-T4 material used in the work as seen in **Table 2.1**. In addition, it could be attributed to the change in mechanical properties of AA6111-T4 over time, also known as age hardening (Dierke *et al.*, 2007). The material properties were obtained from tensile tests conducted almost 9 months apart from the drawbead tests described in this section. However, the A6111-T4 material was stored at -20°C between the tensile tests and the drawbead tests to slow age hardening effect. Further tensile tests to confirm age hardening were not carried out.

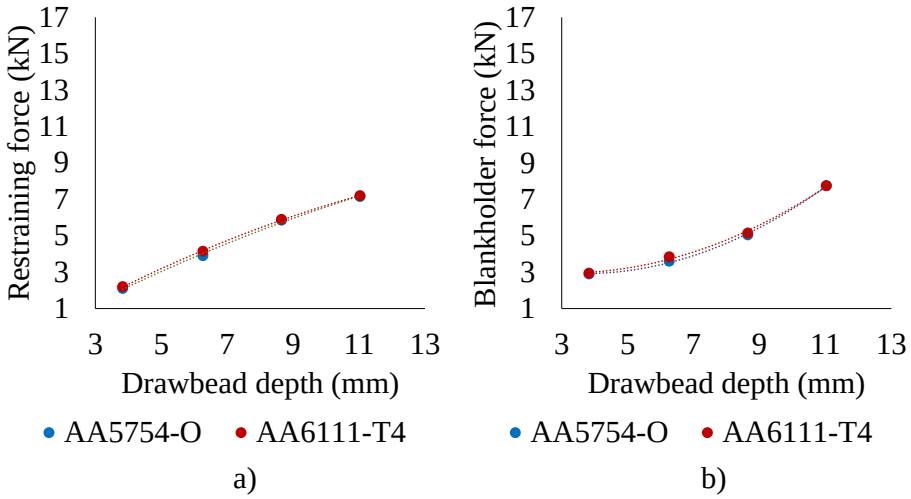

Figure 6.2: Comparison of experimental drawbead restraining force a) and blankholder force b) obtained from roller drawbead set-up for AA5754-O and AA6111-T4

6.2.1.2 FE model of the roller-set-up

A roller FE model, similar to that described in Section 3.3.1 was used. The coefficient of friction was entered as zero to simulate the frictionless roller drawbead test. The DBRFs and the blankholder force predicted by the model are compared with the experimental results in **Figure 6.3**.

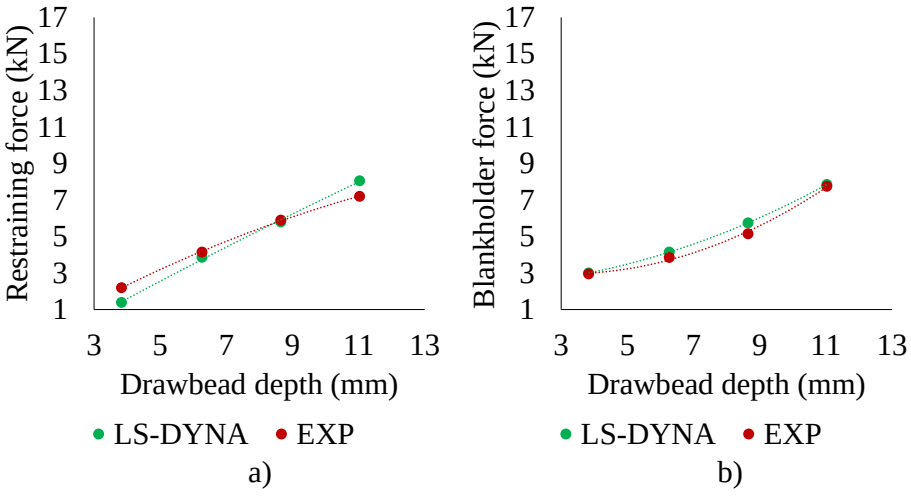

Figure 6.3: Comparison of simulated and experimental drawbead restraining force a) and blankholder force b) for μ=0 for AA6111-T4

6.2.1.3 Drawbead test, fixed set-up

A fixed drawbead test similar to that described in in Section 3.1 was conducted using 1.5 mm AA6111-T4. The strip size was 500x50 mm with ALUBVS applied at a coat weight of 1.5 g m^{-2}. The strips were drawn at 85 mm s^{-1} for 200 mm. Three strips were drawn for each drawbead depth of 3.5, 5.8, 8.7 and 11 mm respectively. The restraining force and the blankholder force are shown in **Figure 6.4**. It can be observed again that the characteristics of the drawbead forces are similar to drawbead forces obtained for AA5754-O in Section 3.1.

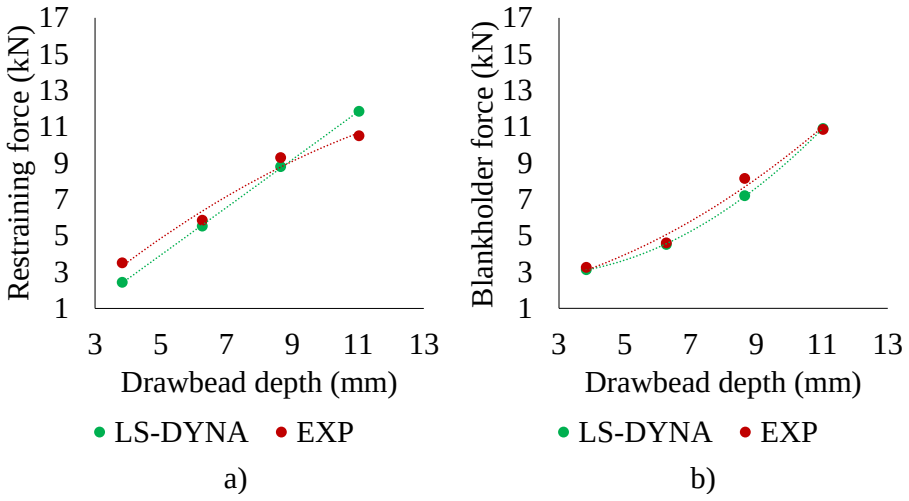

Figure 6.4: Comparison of numerical and experimental drawbead restraining force a) and blankholder force b) at μ=0.15 for AA6111-T4

6.2.1.4 FE model of fixed drawbead test set-up

In this model, the drawbead geometry, strip geometry and other parameters used in the frictionless model remained constant, apart from the coefficient of friction, which was adjusted until a good agreement with the experimental results, was achieved. An example of a change of drawbead forces with coefficient of friction is shown in **Figure 6.5**. It can be seen that out of the four coefficient of friction values evaluated, the value of 0.15 gave predictions with less than 10% error in drawbead restraining force, (**Figure 6.5**a)), and blankholder force, (**Figure 6.5**b)) for two of the drawbeads

considered. Lower coefficient of friction values under predicted the drawbead force by more than 25% and higher values over predicted the forces by almost 20%, especially for the maximum depth of 10 mm. It can be seen in **Figure 6.4** that the restraining force and the blankholder force predicted by using the coefficient of friction value of 0.15 correlated well with the experimental forces.

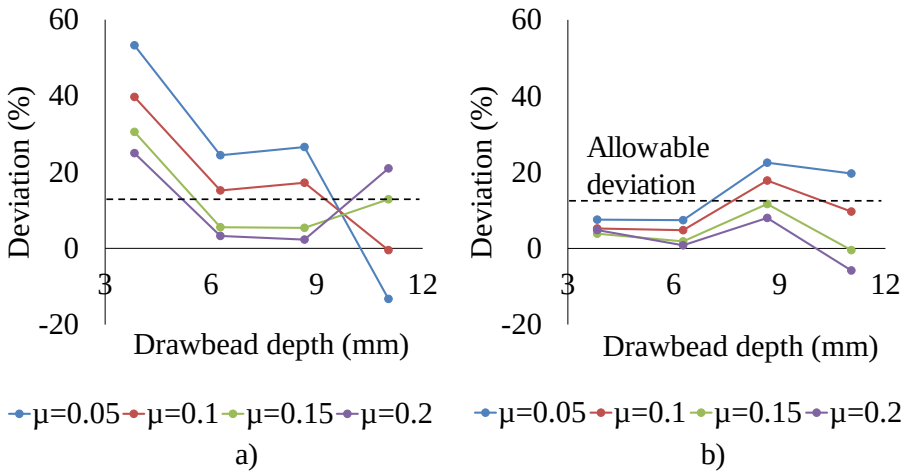

Figure 6.5: Percentage deviation between experimental and numerical drawbead restraining force a) and blankholder force b) for various coefficients of friction for AA6111-T4

6.2.2 Drawbead restraining force and thinning prediction

6.2.2.1 Setting of design of experiments

As previously noted in Chapter 4, the drawbead geometry has a significant influence on the sheet metal flow. Hence, it is advised to perform a full factorial experiment to understand the influence of drawbead geometry on the DBRF. The range of drawbead geometries used in the design of experiment is listed in **Table 6.1**. The design has two factors, groove and bead radius, with three levels and one factor, drawbead depth, with four levels resulting in 36 simulation runs.

Table 6.1: Range of drawbead geometries used in design of experiments for FE simulation

Groove radius, R_g (mm)	Bead radius, R_b (mm)	Drawbead depth, d (mm)
1.5, 2, 2.5	5,7,9	3, 5, 8 and 10

6.2.2.2 Obtaining drawbead forces

The simulations for different drawbead geometry combinations were run using a coefficient of friction of 0.15, which was derived in Section 6.2.1 in the FE models set-up in Step 5 above. Drawbead experiments with the same geometry combinations were conducted to verify that the drawbead forces obtained from simulations are correct. As an example, the drawbead restraining forces and the blankholder forces for a combination of Rg=1.5 mm & R_b=5 mm and Rg=1.5 mm & R_b= 9 mm is shown in **Error! Reference source not found.**. There is a good agreement between the experimental and predicted drawbead forces for both the drawbead geometries. Hence, it can be concluded that accurate drawbead forces can be determined using the coefficient of friction derived in Section 6.2.1.

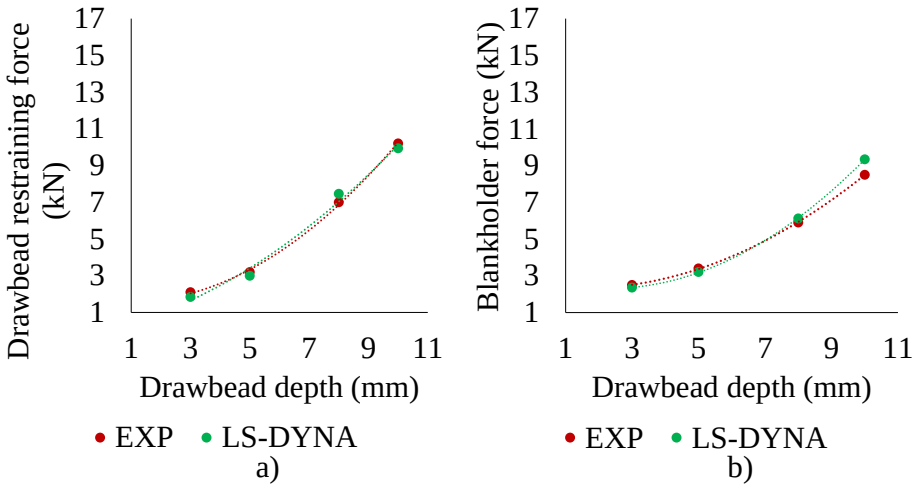

Figure 6.6: Comparison of experimental and simulated drawbead restraining force a) and blankholder force b) for drawbead geometry of Rg=1.5 mm and Rb=9 mm at μ=0.15 for AA6111-T4

6.2.3 Selection of optimised drawbead geometry

GEP is a useful measure to determine the optimised geometry. It not only takes into account the drawbead forces but also the thinning at the exit of the drawbead. The procedure to determine the GEP is described in Section 5.2. The GEPs for AA6111-T4 are shown in **Figure 6.7**. It can be seen that a drawbead geometry of R_g=1.5 mm & R_b= 5 mm, resulted in higher GEP values. At a depth of 5 mm, severe thinning was observed and fracture of the strip occured at higher depths.

For a drawbead geometry of Rg=1.5 mm & Rb= 9 mm no fracture occurred although severe thinning at depths of 8 and 10 mm was observed. At a depth of 3 mm, the BHF was higher than DBRF whereas, at 5 mm, the DBRF was greater than BHF. Hence, the drawbead geometry of R_g=1.5 mm, R_b=9 and d=5 mm was found to be optimum.

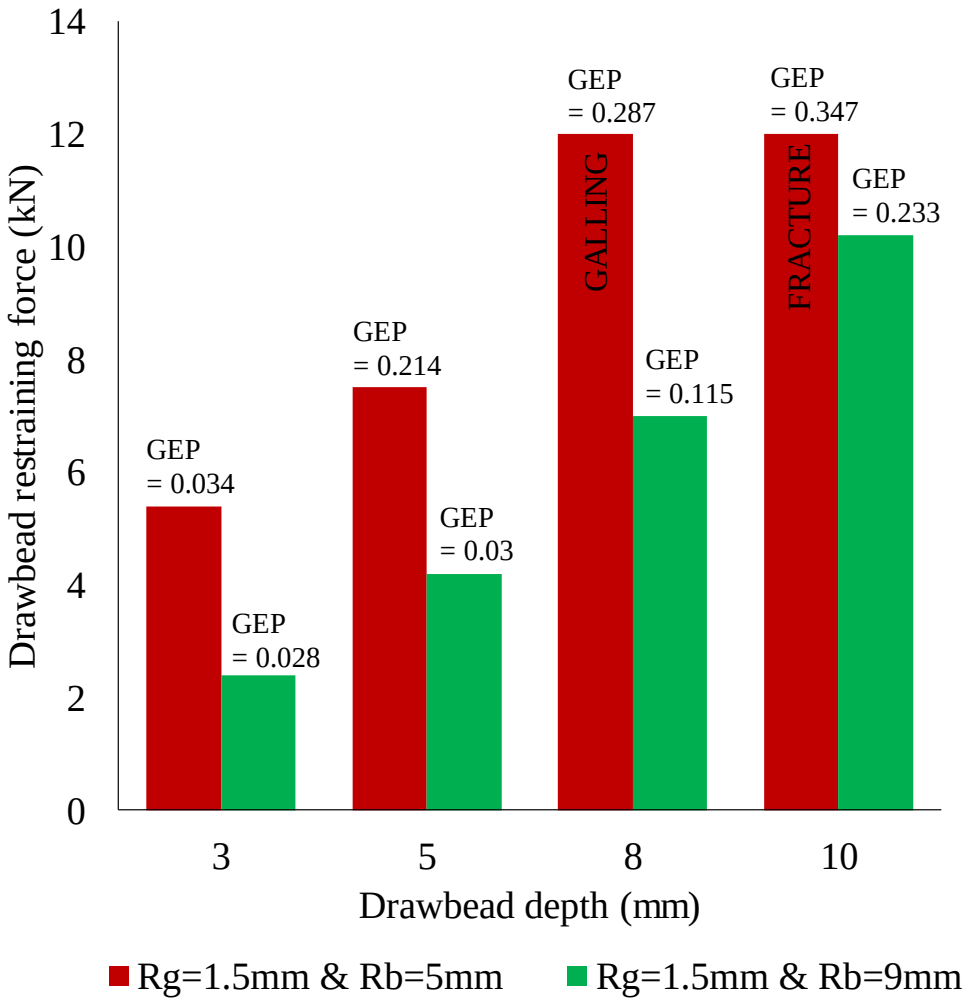

Figure 6.7: Geometry Effectiveness Parameter (GEP) obtained from simulation for the range of drawbead geometries for AA6111-T4

It was observed in **Figure 6.2**a) that the DBRF force for the two aluminium alloys under study was identical. This could lead to the postulation that the same drawbead geometries could be used for both AA5754-O and AA6111-T4. However, after comparing GEPs for AA5754-O and AA6111-T4, in **Figure 5.2** and **Figure 6.7** respectively, it can be seen that AA6111-T4 has higher GEP values than those of AA5754-O. This was expected because of the higher restraining force (due to larger yield stress) and greater thinning effect (due to lower $\bar{r}$ value) demonstrated by AA6111-T4, which led to higher GEP values consequently. Since the test strips were drawn in the rolling direction, r_0 were more relevant than $\bar{r}$. The r_0 for AA5754-0 was

0.67 and that for AA6111-T4 was 0.58. Thus, AA6111-T4 had lower resistance thinning as compared to AA5754-0 and hence the difference in the GEP values.

6.3 Conclusion

There was a good correlation between the experimental and predicted drawbead forces by applying a piecewise linear plasticity material model in 2D plane strain FE simulations.

- The experimentation in this methodology is limited to a) obtaining material parameters such as the flow curve, n-value and $\bar{r}$-value through uniaxial tensile testing and b) roller and fixed set-up drawbead tests. For the drawbead test, only three experimental runs for each set-up are necessary. Further fixed drawbead physical tests for verification of the some of the results from the FE simulations based on design of experiments may be required.
- The coefficient of friction value, 0.15 in this case, obtained by adjusting the coefficient of friction in the FE model calibrated to the results from the roller drawbead test, gives satisfactory predictions of the drawbead forces for various combinations of drawbead geometry. This was verified by conducting experiments with R_g=1.5 mm and R_b =9 mm for four different depths. The error between the experimental and predicted drawbead forces was within 10%.
- The Geometry Effectiveness Parameter (GEP) is easy to compute, simplifies the process for drawbead selection, and eliminates the use of optimisation software packages.
- Based on GEP, R5 with 3 mm depth and R9 with 5 mm depth was selected for final validation by stamping of rectangular pans.

7 Validation of the proposed drawbead design approach

The research methodology for the drawbead design was established and implemented to select the drawbead geometry for use with 1.5 mm AA6111-T4 in Chapter 6. In this section, the selected drawbead geometry is verified by application to drawing a rectangular pan. Stamping experiments and simulations using two distinct drawbead geometries were performed on AA6111-T4 1.5 mm blank. Simulations for each drawbead geometry were conducted with both equivalent and geometric (modelled drawbeads) drawbead models. The results from the simulations, namely, punch force, thinning and draw-in were compared with the experiments. Lastly, a list of recommendations for setting up models for forming feasibility simulation is provided.

7.1 Stamping experiment

The selected drawbead geometries, a) R_g= 1.5 mm, R_b= 5 mm, d= 3 mm and b) R_g= 1.5 mm, R_b= 9 mm, d= 5 mm, were tested on a rectangular pan as the simple geometry allows the study of the effect of the drawbead. The drawbeads were positioned on the longer side of the rectangular part.

7.1.1 Experimental set-up

Stamping experiments were carried out using a 1000 kN Interlaken ServoPress 225. A single action, gas-spring actuated die with interchangeable draw bead geometries and blankholder was manufactured to carry out the stamping experiments with different drawbead geometry combinations. The experimental set-up is illustrated in **Figure 7.1**. The die moves down to position and clamps the blank against the blankholder. The gap between the die and blankholder is controlled by spacers that are1.1x the blank thickness. The blankholder pressure, initially 10 MPa, is applied by the cushioning system consisting of gas springs. Next, the die and the blankholder move downward

together, at a velocity of 2 mm s^{-1}, to draw the blank over the punch to form a rectangular pan. The draw stroke was 26.5 mm. Each experimental run was repeated three times per drawbead geometry combination.

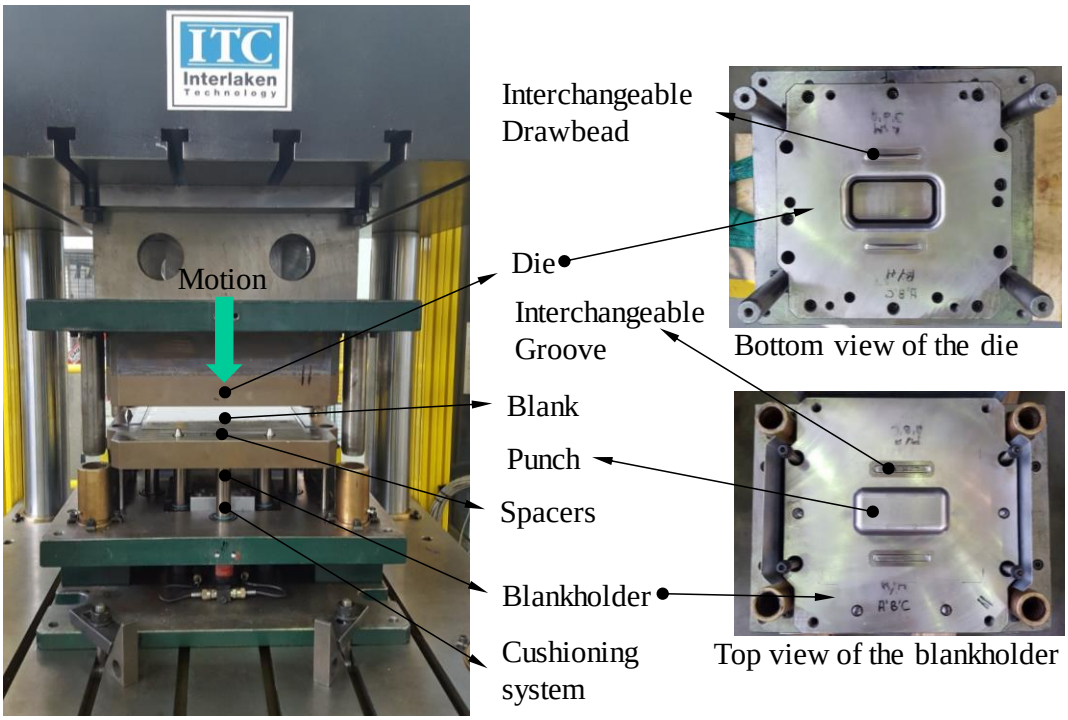

Figure 7.1: Experimental set-up for stamping of rectangular pans

AA6111-T4, 1.5 mm thick, was cut into a blank size of 250x290 mm. The edges of the blank were deburred to avoid scratching the die and blankholder surfaces. The blanks were lubricated using ALUB-VS with a coat weight of 1.5 g m^{-2}.

7.1.2 Results

It can be seen from **Figure 7.2** that there is not much difference in the punch force for R5 and R9 drawbeads, although the punch force from R5 drawbead is slightly higher, as expected. The difference in the observed punch forces is not significant as the drawbead depth for R5 drawbead is 3 mm and that for R9 is 5 mm.

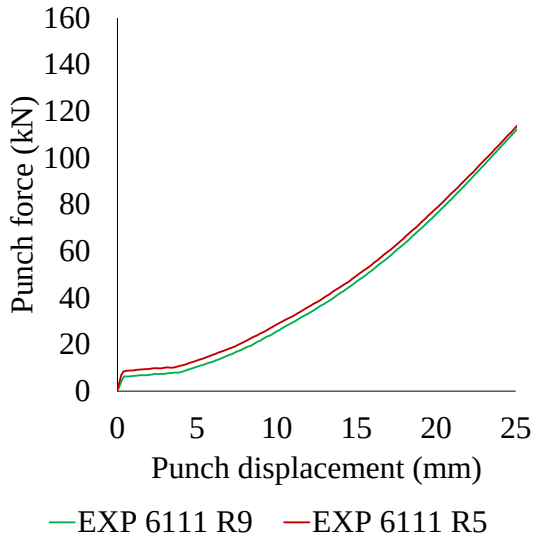

Figure 7.2: Experimental punch force vs draw stroke for R5 and R9 drawbead geometries

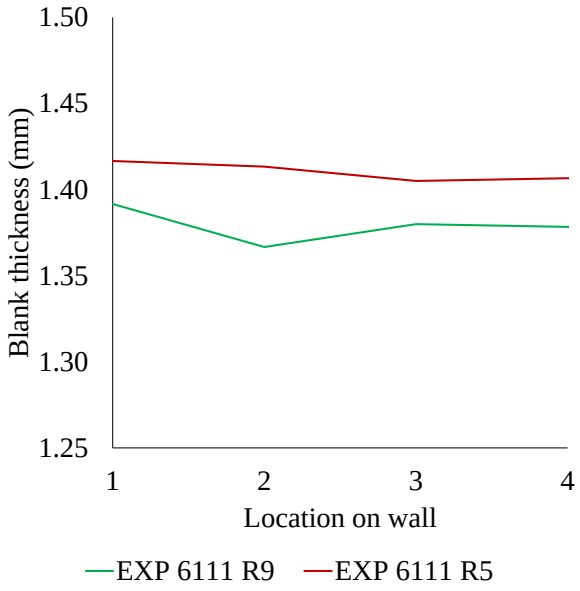

Figure 7.3: Thickness profile of wall section for R5 and R9 drawbead geometries

Figure 7.3 shows the thinning observed in the wall for both the drawbead geometries. The difference between thinning is more pronounced than the punch forces. In addition, it can be seen that the R9 drawbead provides more stretch than the R5 drawbead because of the higher depth. For JLR, the allowable thinning is 15% of the sheet thickness (Personal communication, 2013), which results in a final sheet

thickness of 1.275 mm. The stretch offered by R9 drawbead is closer to the thinning limit and hence gives the desired stretch.

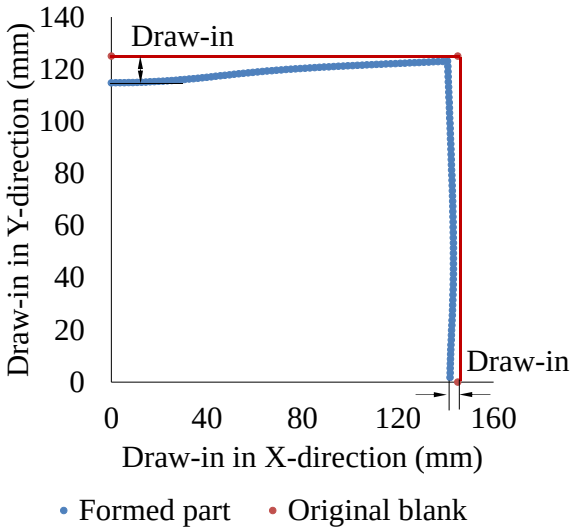

Figure 7.4: Schematic of draw-in measurement locations along the profile (blue) of the formed part

The draw-in represents the amount of material drawn into the die cavity. It is measured by the difference between the original and the formed profile of the blank at a given location as seen in **Figure 7.4**. From **Table 7.1**, it can be seen that draw-in for R9 drawbead is slightly more than R5 because of the higher wrap around the drawbead coming from larger bead radius (R_g) and greater drawbead depth (d). In addition, it can also be observed that the drawbeads do not have a significant impact on the draw-in where drawbeads are not placed (X-direction).

7.1.3 Summary

The stamping experiments were conducted on AA6111-T4 blank using interchangeable drawbeads and blankholder. The achieved draw stroke was 26.5 mm. Therefore, the punch force, draw-in and thinning from the simulation will be compared at draw stroke of 26.5 mm. Other observations were:

- The punch forces for R5 and R9 drawbeads do not show a significant difference in the entire draw stroke.
- Even though R5 drawbead required the highest punch force, the stretch offered by the R9 drawbead is greater than the R5 drawbead geometry due to a higher bead depth.
- The draw-in on the longer side of the stamped part is same for both geometries. The draw-in on the drawbead side is higher due to additional wrap over the bead radius.

7.2 Stamping simulation

The stamping simulation of the rectangular pan is in two parts, namely, geometric drawbeads and the equivalent drawbead model.

Geometry and Mesh

A quarter surface model of the actual stamping die was created in SOLIDWORKS™ and then imported into LS-DYNA™. This reduced the number of elements and allowed faster computation of the model. The punch, die and the blankholder were meshed using the automatic mesh refinement tool in LS-DYNA™ in which the intricate features such as the drawbead geometry are meshed with smaller elements and flat surfaces such as the blankholder are meshed using larger elements. It was ensured that all curvatures in the model consist of at least 3 to 5 elements over the profile as recommended by LS-DYNA™ (LS-DYNA Theory Manual, 2014). The blank was modelled using an adaptive mesh refinement feature in which the local mesh experiencing higher deformation is refined to increase the accuracy of the solution. This feature is particularly useful for representing the smaller effective bending radius of the blank when it passes through the drawbead.

Element formulation

The same element formulation was used in both equivalent and geometric models of the drawbead. The parts were modelled with shell element formulation Type-2 in LS-DYNA^{TM} with five through-thickness integration points. Since, the parts were modelled using automatic mesh refinement and the blank with adaptive meshing, the parametric analysis to determine effects of different mesh size on the accuracy of the model was not necessary.

Material model

The punch, die and the blankholder were modelled as steel components with rigid material model MAT_20 in LS-DYNA. The blank was modelled using MAT_36 that is based on a non-quadratic and anisotropic Barlat-89 yield function. Similar to AA5754-O in Section 3.3.3, the Voce hardening law rule was used to obtain the effective flow stress-strain curve for AA6111-T4. The Barlat-89 yield function locus for AA6111-T4, in comparison with AA5754-O, is illustrated in **Figure 7.5** and the material properties in **Table 2.1**.

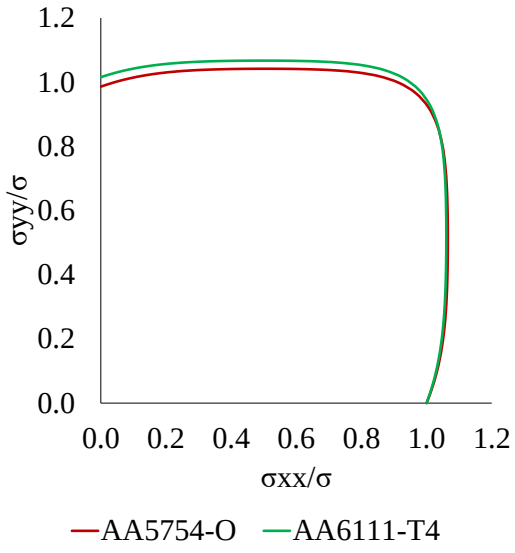

Figure 7.5: Comparison of Barlat-89 yield loci for AA5754-O and AA6111-T4

Contact definition

The contact between the blank and the die parts such as the punch, die and the blankholder was modelled using the FORMING_ONE_WAY_SURFACE_TO_SURFACE_SMOOTH contact card. This contact is especially suitable for sheet metal forming applications as it generates a fitted contact surface from the rigid body mesh and calculates the contact force based on the newly fitted surface. Thus, contact forces over tighter curvatures such as the groove radius and drawbead end geometry can be accurately obtained. A Coulomb friction model with maximum allowable frictional stress was used to limit the frictional shear stress to a value less than the yield stress on the blank material. The coefficient of friction of 0.15, which was obtained from the proposed drawbead design methodology, was used in the simulation.

The coefficient of friction value in the forming simulation represents the contact between the blank and blankholder or die experiences. It has been shown that the coefficient of friction is significantly influenced by parameters such as contact pressure (Xu, 2003). The twist-compression friction test conducted in the research work demonstrated that the coefficient of friction reduces with increase in contact pressure. The detailed explanation for this has been included in Appendix D. Similar findings were identified by Karupannasamy *et al.* (2014) while modelling contact behaviour in deep drawing. Additionally, the friction model provided in AutoForm™, the commercial forming simulation package, uses a contact pressure based friction model (AutoForm, 2013). Thus, contact pressure dependency of the coefficient of friction has been widely acknowledged.

In the stamping simulations in this work, Coulomb friction model was considered appropriate. Spacers were used in the stamping experiments to maintain a fixed

blankholder gap. Having a fixed blankholder gaps results in uniform application of the blankholder force that does not act on the blank in the blankholder; either before or after the drawbeads. The blankholder force only acts over the drawbeads to keep them in a closed position. It has shown by Nine (1982a) that the Coulomb friction model can be successfully used to represent the blank-drawbead contact as the DBRF increases linearly with increase in the real contact area between the blank and the drawbead. Moreover, because of the idealised geometry of the rectangular pan used in used in validation experimentation and simulation, the pressure dependence of friction was of lesser significance. However, a pressure dependent friction model may be necessary where constant pressure on the blank does not exist in the absence of spacers and when the part geometry is complex (Hol *et al.*, 2014).

7.2.1 Geometric drawbead model

In the geometric drawbead model, the drawbead is modelled fully as shown in **Figure 7.6**. The first measure to check the accuracy of prediction of the numerical model is the correlation with the experimental force, as the punch force will increase as it tries to overcome the restraining force, applied by the drawbead, to form the blank. It can be seen in **Figure 7.7** that the punch force predicted by the geometric drawbead model correlated well with the experimental force. The maximum error observed towards the end of the stroke for R5 drawbead was 4.4% and that for R9 drawbead was 3.7%. Thus, the geometric drawbead model accurately predicted the punch force.

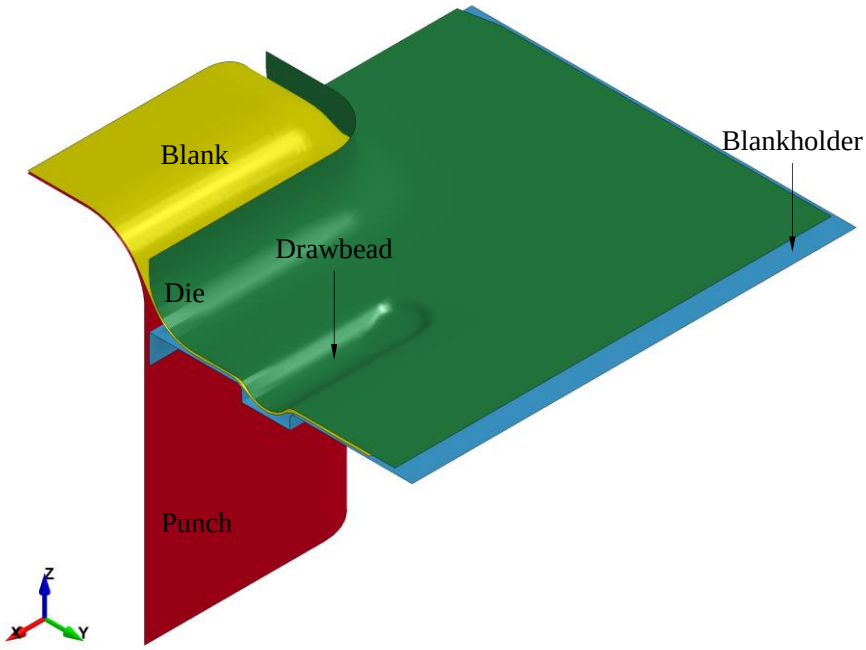

Figure 7.6: Geometric drawbead finite element model

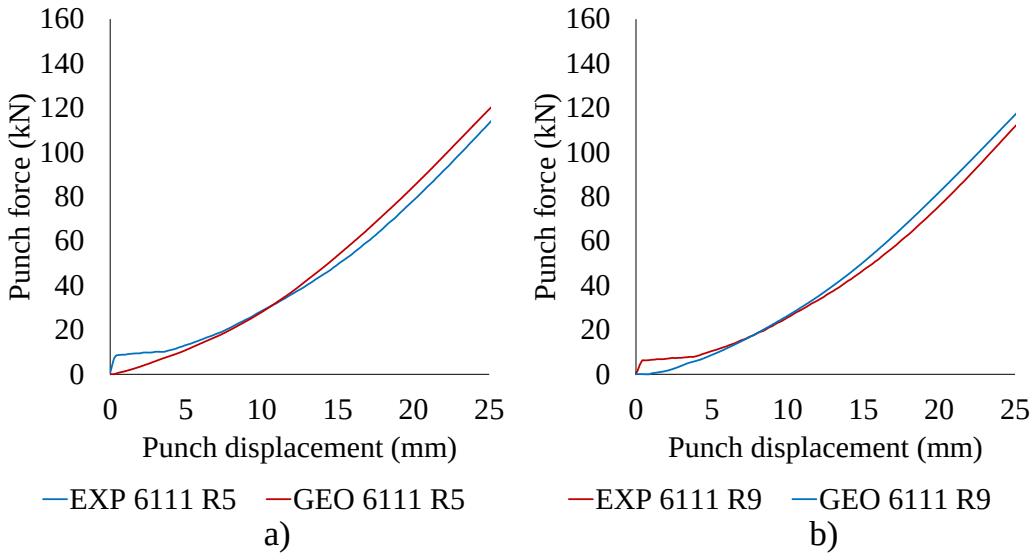

Figure 7.7: Comparison of geometric drawbead experimental and numerical punch force R5 a) and R9 b)

The second and slightly more robust measure is the wall thickness prediction as it directly indicates the accuracy of the sectional (elongation) deformation representation of the blank in the numerical model. **Figure 7.8** shows the locations on the wall of the part for thickness measurement on the physical and numerical parts. The results in the

form of thickness comparison are shown in **Figure 7.9**a) for R5 drawbead and **Figure 7.9**b) for R9 drawbead. The maximum error between the measured wall thickness and the predicted thickness is 1.9% for R5 and that of R9 drawbead is 3.2%. The relatively higher error in the case of the R9 drawbead is possibly due to the reduced clinching of the blank over the drawbead end as seen in **Figure 7.8**a). Although the exact reason is not understood, the maximum error is within the range of 5% and therefore, it can be said that the geometric drawbead model accurately predicts the wall thickness.

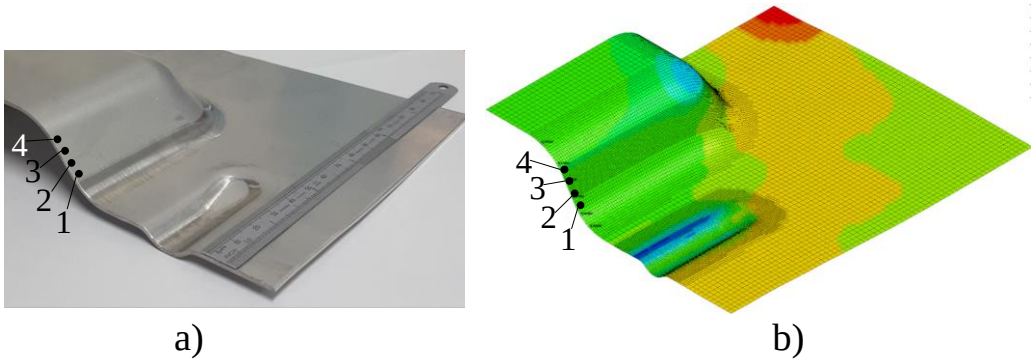

Figure 7.8: Thickness measurement locations on the physical part a) and virtual part b)

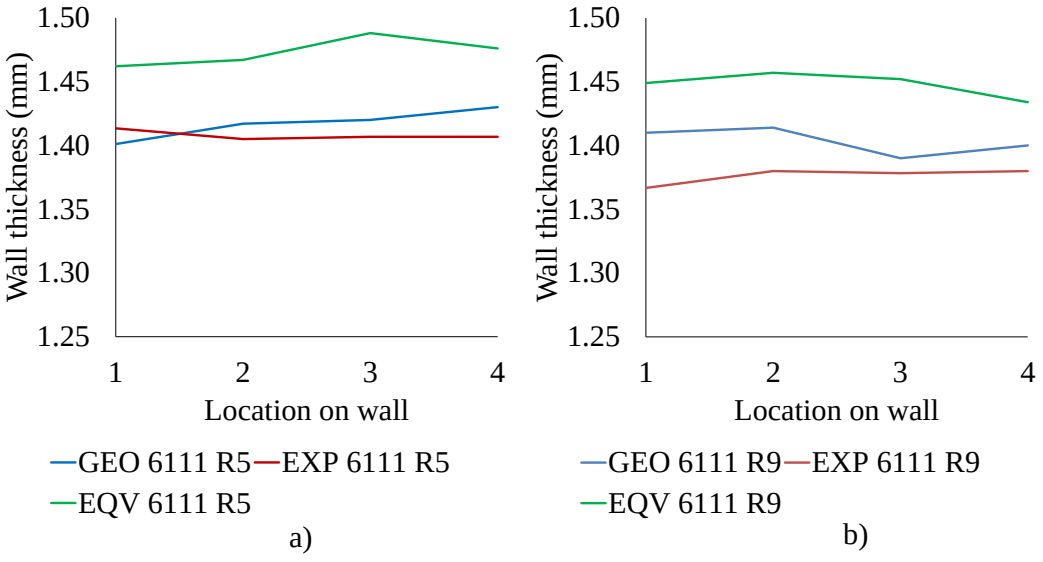

Figure 7.9: Comparison of wall thickness obtained from experiments, geometric drawbead model and equivalent drawbead model for drawbead geometry R5 a) and R9 b)

The third measure to verify the accuracy of the drawbead model is the draw-in prediction as it reflects the nature of the flow of the blank into the die. It is calculated by measuring the difference between the original size of the blank and final size of the blank at the end of the forming stroke. **Table 7.1** shows the comparison of the draw-in for R5 and R9 drawbeads simulated by the numerical model. It can be seen that the draw-in prediction for both the geometries correlated well with a maximum deviation of 20% corresponding to 0.7 mm only. Hence, it can be interpreted that the geometric drawbead model accurately predicts the draw-in.

Table 7.1: Experimental and simulated (geometric drawbead model) draw-in for R5 and R9 drawbeads

Bead radius	Draw-in direction	Experimental draw-in (mm)	Geometric drawbead FE model (mm)	Absolute error (mm)
R5	Length	3.50	4.20	0.7
	Width	5.25	5.70	0.45
R9	Length	3.67	3.90	0.23
	Width	6.25	7.20	0.95

It is established that results from the geometric model are in agreement with the experimental results. Therefore, the next step is to compare the effectiveness of the two geometries in avoiding wrinkling, splits and insufficient stretch. Based on the GEP, the hypothesis is that the R5 drawbead model will result in severe thinning if not splits and hence will not be a suitable choice for the drawbead geometry. This is checked with the help of forming limit diagram and formability plots.

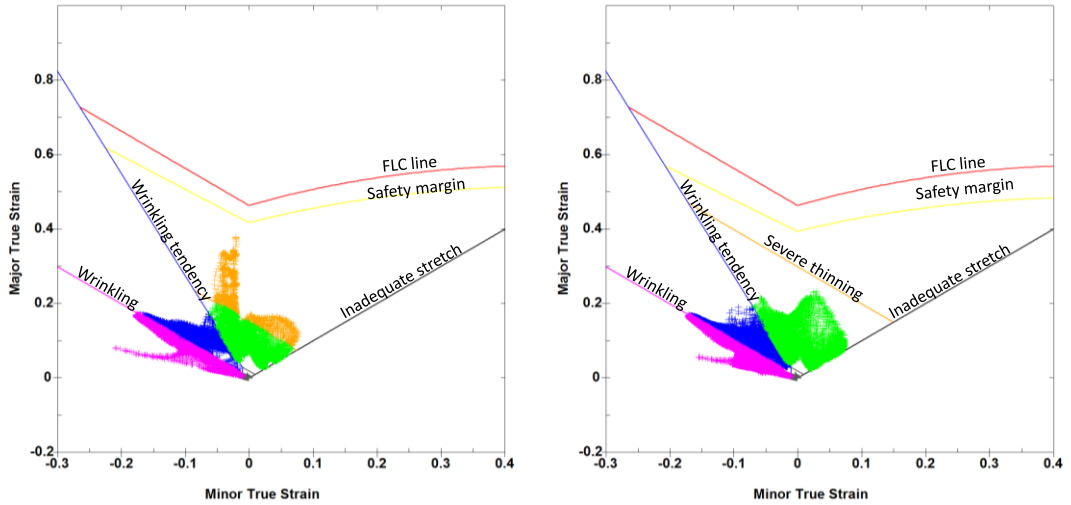

Figure 7.10: Forming limit diagram for geometric beads R5 a) and R9 b)

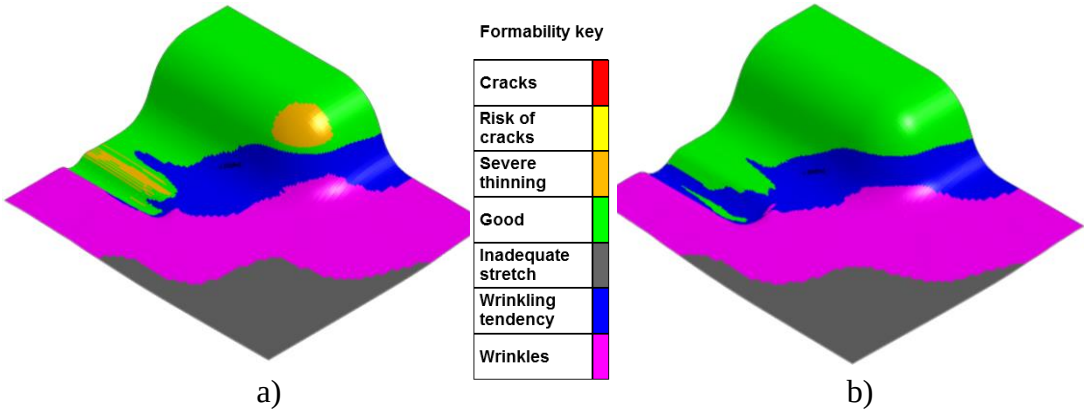

Figure 7.11: Formability key for geometric beads R5 a) and R9 b)

A forming limit diagram is a useful tool for predicting the failure of sheet metal under different deformation modes during the forming operation. The formability key complements the forming limit diagram by identifying areas with different failure modes. A comparison of R5 and R9 drawbead performance through the forming limit diagram is shown in **Figure 7.10**. Severe thinning is observed at the exit of the drawbead and over the punch corner as seen in **Figure 7.11**a). This is because the R5 drawbead imparts a higher restraining action to the blank which experiences severe

thinning close to the safety margin, beyond which there is a risk of cracks, i.e., the part has high chances of splitting during the draw stroke. In addition, because of excessive thinning the part may not be able to offer the required structural strength. Such excessive thinning was not observed when the rectangular pan was formed using the R9 drawbead as seen in **Figure 7.11**b) and **Figure 7.10**b). The R9 drawbead offered sufficient restraining force to bring in the required amount of stretch in the part without excessively thinning the blank at the exit of drawbead and over the punch corner. Hence, it can be concluded that R9 drawbead was appropriate for forming a rectangular pan.

7.2.2 Equivalent drawbead model

Equivalent drawbead models are commonly applied during the forming feasibility studies in industry. Therefore, simulations with equivalent drawbead models were performed to test the application of the proposed drawbead design methodology and to compare the results with experiments and the geometric drawbead model.

In an equivalent drawbead model, a drawbead is represented by a set of nodes (line of force) to which a restraining force, expressed in terms of N mm^{-1}, is manually allocated. If required, the allocated restraining force is adjusted by changing the 'scale factor' until a good agreement between experimental and predicted punch force is observed. The equivalent drawbead model applied to simulate the stamping experiment in this study is shown in **Figure 7.12**. The elements in the drawbead box which cross the line of force experiences a restraint. The restraining force for R5 and R9 drawbeads used in the model was obtained from the respective 2D drawbead models from Section 6.2. The coefficient of friction of 0.15 obtained from Section 6.1 was used in the contact definition.

The comparison of experimental punch force and the predicted punch force for R5 and R9 drawbeads is shown in **Figure 7.13**a) and **Figure 7.13**b) respectively. Ideally, a scale factor of two, which is the default value in LS-DYNA, should give accurate force prediction. However, in this case, the scale factor of four gave excellent correlation with the experimental punch force. The scale factor of three under predicted the punch force. The need to increase the scale factor was because of the fact that the equivalent drawbead model neglects the effect of drawbead end geometry.

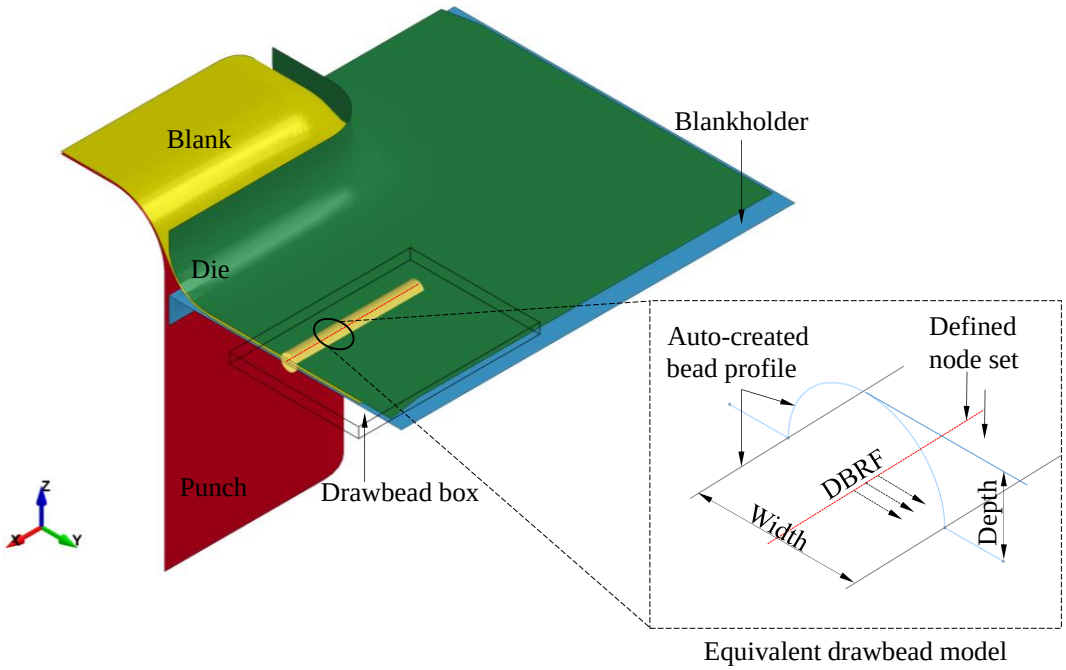

Figure 7.12: Equivalent drawbead model

Similar findings were reported by Chen and Weinmann (2003) while studying the effect of drawbead end geometry on the restraint experienced by the blank. In their experiments and simulations using geometric drawbeads, it was observed that the drawbead end radius must be at least two times larger than the bead radius otherwise severe blank deformation can occur at the end of the drawbeads. However, the drawbead end radius on the drawbead tooling used in this study was equal to the bead

radius and resulted in severe deformation of the blank. This was captured by the geometric bead model but not by the equivalent model. In addition, the increased scaling factor might create the necessity to use a severe drawbead geometry on a physical die, which may cause splits during the tryout stage and significant rectifying efforts.

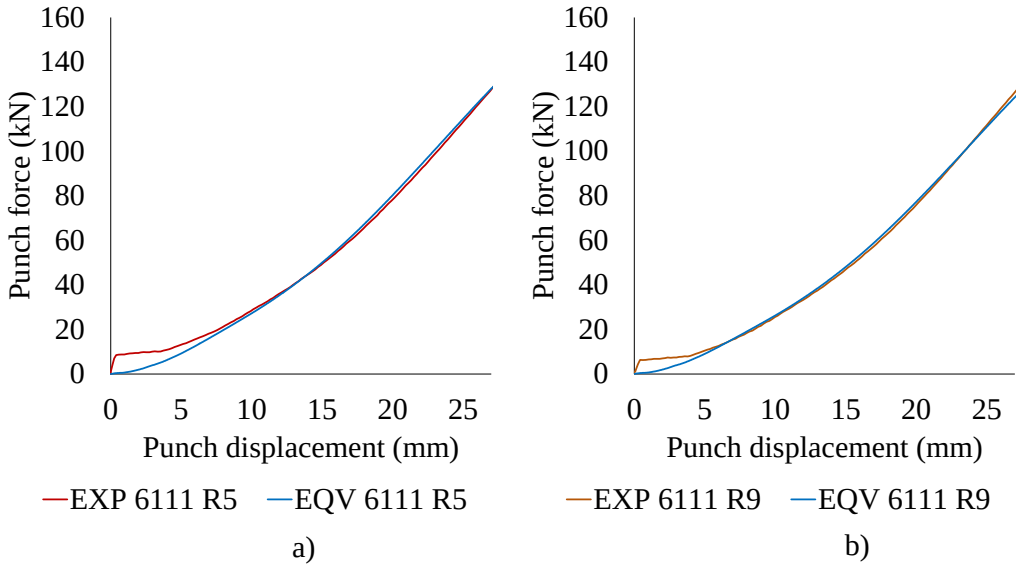

Figure 7.13: Comparison of punch forces obtained from experiments and equivalent drawbead model for R5 a) and R9 b)

The wall thickness predictions from the equivalent drawbead model are shown in **Figure 7.9**a) and **Figure 7.9**b) for R5 and R9 drawbead geometries. It can be seen that the equivalent drawbead model overestimates the wall thickness for both the drawbead geometries by more than 6% whereas the wall thickness predicted by the geometric model has a maximum deviation of 2%. The equivalent drawbead model does not simulate the dynamic change in the plastic strain due to simultaneous stretching and bending/unbending of the blank elements passing over the drawbeads which may lead to underestimation of thinning at the exit of drawbead in the blankholder and subsequently in the wall region.

The comparison of draw-in predicted by the equivalent drawbead models for R5 and R9 drawbead geometries is shown in **Table 7.2**. As expected the equivalent drawbead model overestimated the draw-in, as the wrap of the blank over the drawbead is not considered. The draw-in estimated by the equivalent drawbead model is 1.65 mm more than the experimental value in case of R5 whereas the geometric drawbead model shows a maximum deviation of 0.45 mm only, **Table 7.1** and **Table 7.2** respectively.

Table 7.2: Experimental and simulated (equivalent drawbead model) draw-in for R5 and R9 drawbeads

Bead radius	Draw-in direction	Experimental draw-in (mm)	Equivalent drawbead FE model (mm)	Absolute error (mm)
R5	Length	3.50	4.50	1
	Width	5.25	6.90	1.65
R9	Length	3.67	4.10	0.43
	Width	6.25	7.60	1.35

7.3 Conclusion

The optimum drawbead geometry with R9 bead radius based on GEP analysis was effective in achieving sufficient stretch and mitigating wrinkles in the formed rectangular pan whereas the less preferred drawbead geometry with R5 bead radius caused severe thinning at the exit of the drawbead and over the punch corner. This proves that the drawbead geometry selected based on GEP analysis works effectively on full-scale parts.

The punch force, wall thickness and draw-in predictions from the geometric drawbead model using the coefficient of friction determined from the proposed drawbead design procedure showed excellent correlation with the experimental results and hence it

proved that the proposed methodology to determine the coefficient of friction is correct.

The geometric drawbead model is more accurate than the equivalent drawbead model in predicting the punch force, wall thickness and draw-in. The assigned DBRF in the equivalent drawbead model was scaled to match the experimental punch force. This may lead to a selection of a severe drawbead geometry, which can potentially cause splits in the tryouts.

8 Innovation and industrial benefits

This section highlights the innovation and industrial benefits of this research work that Jaguar Land Rover can use to increase the productivity of their die design process.

8.1 Innovation

This research establishes a hybrid approach (combination of drawbead test and finite element analysis) that is holistic and scientific. The main innovation is in the practice of numerically modelling the drawbeads for stamping of aluminium alloys as seen in **Figure 8.1**. The hybrid method (green dotted line) forms the background of the forming feasibility simulations. Use of an accurate coefficient of friction and drawbead geometry derived from the hybrid method in the forming feasibility simulations provides correct predictions in the first attempt. This eliminates the forming feasibility loop (red dotted line) in the existing industrial die design practice as illustrated in **Figure 2.15**. Consequently, a precise die design can be obtained directly reducing the need for remachining of drawbeads during the tryout stages.

The other innovations are the unique use of the drawbead test and a novel criterion to select optimum drawbead geometry. In previous work, the drawbead test was mainly used to obtain a coefficient of friction at a specific drawbead depth and to evaluate different forming lubricants. In the work conducted here, the drawbead test is innovatively used to calibrate the drawbead FE model to obtain an accurate coefficient of friction. This coefficient of friction is then used in the drawbead simulation of carefully chosen drawbead geometries to obtain corresponding drawbead restraining forces. Another innovation is the unique use of outputs from drawbead simulations to formulate a drawbead selection criterion called the Geometry Effectiveness Parameter

(GEP). This aids in the selection of an optimum drawbead geometry to be directly used in the forming feasibility simulations.

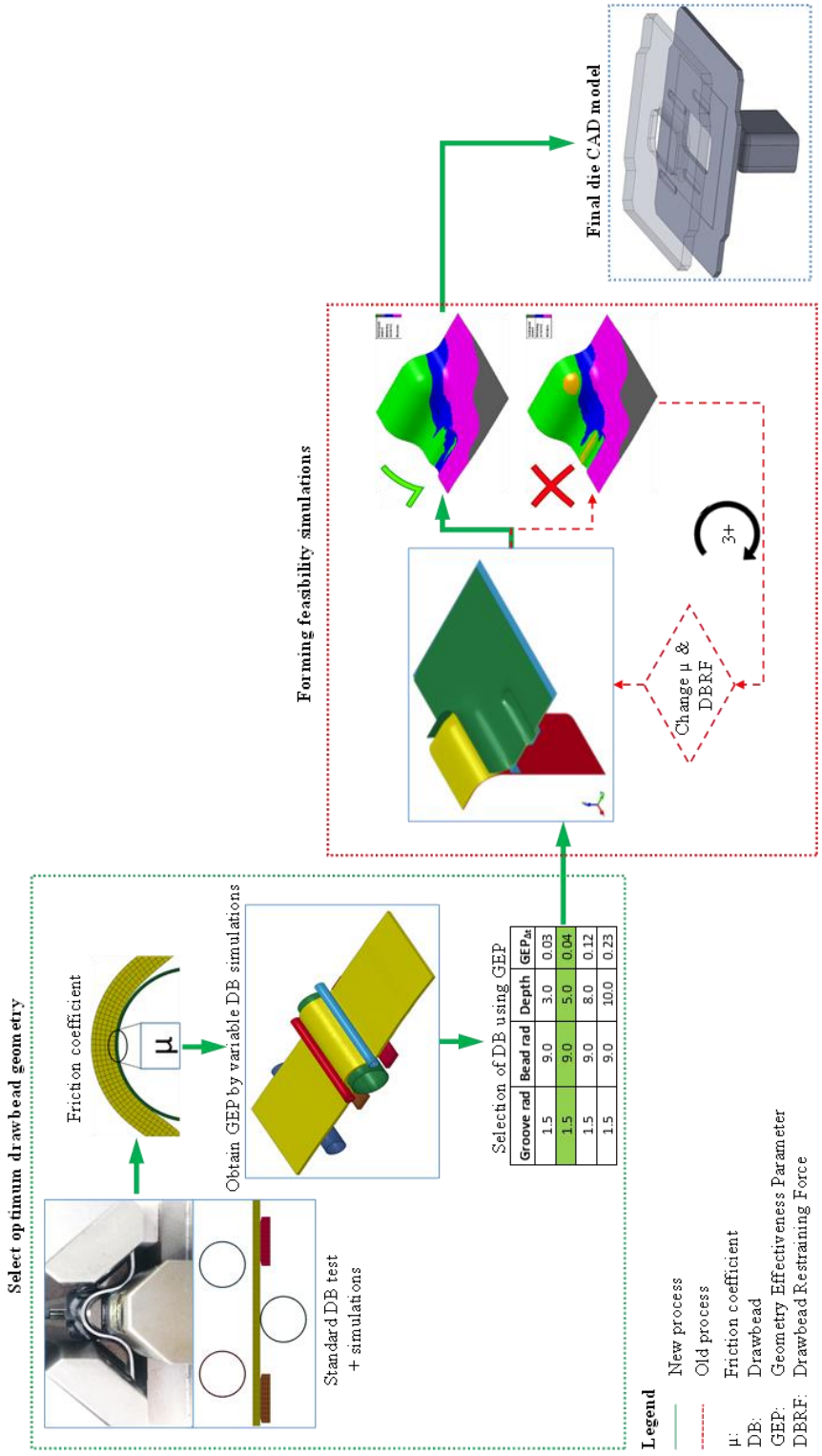

Figure 8.1: Application of the innovative method for numerical modelling of drawbeads for stamping aluminium alloys

8.2 Industrial benefits

8.2.1 Benefits of a formability comparison between aluminium and steel

- The knowledge to assess the formability of the aluminium part designs in the concept planning stage. The implications of curvature or radii requiring material with a small r/t ratio can be assessed quickly without having to conduct simulations.
- Formability comparison can be included in the standards for body engineering for body-in-white engineers to appreciate the design changes required for forming of aluminium alloys. This will reduce the time spent in assessing formability and engineering changes.
- In order to achieve good simulation accuracy, the material cards in AutoForm^{TM} need to be updated regularly to account for the batch-to-batch variation in raw material. The current industrial practice is to seek help from material suppliers, which is time consuming. The MATLAB program created for this project allowed the generation and comparison of yield loci for Von Mises, Hill-48 and Barlat-89 models. This application reduces the dependency on material suppliers for creating and updating the material parameters to be used in forming feasibility.

8.2.2 Benefits from mapping of the die design process

- Recording the die design process created a visual process depiction making it easier to identify breakdowns and problems within the process. It also allowed the relation of inputs and outputs to be seen and for the assignment of ownership of part or the entire process to respective personnel.

- The die-design process map is an aid to both new and experienced stamping engineers, providing them with an overall view of the process.
- The tasks in the process map can be assigned with cost and time factors and can be included in process documentation to benchmark and mark progress of new tooling launch programmes with the older initiatives.

8.2.3 Benefits from the investigation of drawbead design approaches

- The experimentation provided knowledge of how drawbead tests can be used to derive effectively the drawbead forces.
- The significance of taking into account the effect of both drawbead radii and depth on drawbead forces rather than focusing on drawbead depth alone.
- A demonstration of how analytical models assist in improving understanding of the analytical drawbead model used in AUTOFORM^{TM} and the cause of any less understood errors encountered when conducting feasibility simulations.
- The parametric study on the element type, mesh size, number of integration points and contact representation was undertaken (Submission 3) for setting up the drawbead and rectangular pan stamping models can be used to improve the AUTOFORM^{TM} simulation environment; further enhancing the accuracy of the forming feasibility studies.
- A demonstration that simple 2D drawbead models can effectively be used to obtain drawbead forces.

8.2.4. Benefits from the proposed drawbead design approach

- The ability to obtain the coefficient of friction by eliminating not only the trial and error process but also the need for complex non-linear friction modelling.
- The acquisition of DBRF and blankholder force without the need for analytical models and trial and error procedure.
- The development of a geometry effectiveness parameter (GEP) allowing selection of only those drawbead geometries that fit in the existing die and press environment.
- The hybrid approach can be extended to other blank materials to create a database of coefficients of frictions and drawbead geometries for commonly occurring sheet and die material combinations that can be readily used in forming feasibility simulations.

8.2.4 Benefits from the Geometry Effectiveness Parameter (GEP)

- The GEP not only considers the effect of the drawbead geometry on thinning but also takes into account the impact on the press capacity.
- GEP completely eliminates the need for complex optimisation procedures and is, therefore, easy to implement.
- GEP can complement forming simulations by helping in setting up the drawbead reduction strategy in AutoForm^{TM}, saving time in identifying the set of appropriate drawbead geometries.

8.2.5. Potential cost savings through the optimised drawbead selection procedure

The automotive body-in-white consists of both structural and exterior panels. Exterior panels are complex and have tighter dimensional tolerances than the structural panels.

Therefore, in the cost calculations in this section, structural components and associated processes have been assigned lower relative costs than exterior panels. Typically, 26 different die sets are required for a new car, 11 for structural panels and 15 for exterior panels. As per the die design process, **Figure 2.15**, a die-set usually undergoes two tryout stages, one at the toolmaker and the other on the in-house production line. Each tryout on average may consist of three attempts. The drawbead design along with process parameters is altered in these trials to get a part of acceptable quality. Having a drawbead geometry selected and validated in the simulations will save at least one iteration in either of the two tryouts. The cost of tryout consists of two components, the cost of die rework and the cost of tryout itself, which are explained below.

Table 8.1 shows the indicative cost of die rework per iteration in either of the tryout stages. The cost of rework will vary depending on the complexity of the part, tryout location and severity of rework. It was assumed that the forming feasibility software, AutoForm^{TM}, deliberately overestimated the drawbead height and that rework consisted of reducing the severe drawbead height by re-machining and re-grinding operations. Typically, the material and labour costs are higher because of non-standard materials and processes required in a tryout. As a result, it is difficult to allocate an exact cost. For ease of calculation, only labour and material costs are considered. It is assumed that the rework per iteration of a tryout for a structural component is about two weeks or 100 hours. The extent of rework for the die set for exterior panel might be higher because of higher part quality expectations and hence the rework hours and costs required will be doubled.

Table 8.1: Cost of die rework

	Component type	
	Structural	Exterior
Cost of die rework per iteration		
Rework hours (hrs)	100	200
Labour cost per hour (£/hr)	£50	£50
Total labour cost	£5,000	£10,000
Material cost	£5,000	£10,000
Total rework cost per iteration	**£10,000**	**£20,000**

The second cost, the cost per tryout attempt, is shown in **Table 8.2**. This mostly involves the cost of time associated with people involved in a tryout at any stage. Typically, because of the complexity and higher part quality requirements, there are more stakeholders in a tryout of an exterior panel's die-set. There may be internal stakeholders such as those from Stampings Engineering, Manufacturing, and Quality departments. External stakeholders could be engineers from the toolmaker, the material supplier and external technical consultants if any. These stakeholders will have different per hour rates and may include the cost of travel and accommodation depending on the tryout location. However, one standard per hour rate is applied for ease of calculations.

Table 8.2: Cost per tryout attempt

	Component type	
	Structural	Exterior
Cost per iteration of tryout		
Press operator (nos)	2	2
Toolmaker (nos)	2	4
JLR (nos)	1	2
External consultant (nos)	1	2
Total manpower per tryout attempt (nos)	6	10
Hours per tryout iteration (hrs)	12	24
Man cost her hour (£/hr)	£50	£50
Press per hour cost (£/hr)	£100	£100
Total manpower cost	£3,600	£12,000
Cost of press per hour (£/hr)	£1,200	£2,400
Total cost	**£4,800**	**£14,400**

From **Table 8.1** and **Table 8.2**, the total indicative cost saving per tryout attempt per die set is £14,800 for structural and £34,400 for exterior components. Considering 6 out of 26 die sets with drawbead geometries per car need rework, the cost savings from this research could potentially be £28,800 for a structural and £86,400 for an exterior component.

9 Conclusion

This section reviews the research work conducted on the drawbead design for aluminium alloy forming as part of the Engineering Doctorate programme. The conclusions address the original respective objectives set out at the start of the project (Section 1.2). Innovation is demonstrated by addressing the original objectives and knowledge gaps in academic and industrial drawbead design practice raised in Sections 2.3 and 2.4.

1. **Understanding the difference between steel and aluminium in terms of forming behaviour.**

   It is known that the stamping dies, especially drawbeads, designed for forming steel are not appropriate for aluminium alloys. However, the limited work published on drawbeads for aluminium alloys did not clearly explain the difference between the forming behaviour of steels and aluminium. The difference in the formability of steels and aluminium alloys by virtue of basic mechanical properties and yield functions used in the material models has been explained. Due to the absence of strain rate hardening, aluminium alloys have poor bendability as compared to low carbon steel and therefore, needs the higher r/t ratio. In addition, the normal anisotropy is lower than that for steel, which limits the amount of draw-in achieved. However, the initially larger n-value than steels enables aluminium alloys to have slightly better stretchability than low carbon steels. It was understood that the result is that larger drawbead radii and shallow drawbead depths must be employed for aluminium forming and at the same time higher draw depths must be avoided if possible. In addition, it was found that non-quadratic yield functions such as Barlat-89 are

more suitable for representation of aluminium alloys in the forming feasibility simulations than quadratic functions such as Hill-48.

2. **Establish the key steps in automotive die design and tryout process**

   Based on the fact that there is limited documentation on the drawbead configuration aspect, the current die design process was documented. It was necessary to record the current die design process to understand how the drawbead forces and coefficient of friction were determined in forming feasibility simulations. It was established that the drawbead forces and coefficient of friction were determined through a trial and error basis. Furthermore, the drawbead geometry often needed alteration during the tryout stages.

3. **Understanding and comparing the state of the art drawbead design methods and study the actual flow of the material over drawbeads**

   Three key drawbead design approaches have been identified and investigated: experimental (Section 3.1), analytical (Section 3.2) and finite element modelling (Section 3.3). The experimental approach involved testing of different material and gauges to obtain the coefficient of friction and drawbead forces. Extending this to a range of drawbead geometries was an expensive and time-consuming process. Another significant drawback was that the coefficient of friction acquired through this method changed with both drawbead depth and strip thickness. It was demonstrated in finite element simulations of the drawbead test (Section 3.3) that the coefficient of friction remained constant over the entire range of drawbead depths. This demonstrated that Coulomb friction law can be appropriately used in the simulations. Although the roller drawbead test eliminates sliding friction, the effect of friction and work

hardening cannot be uncoupled. The work hardening effect increases with increase in sheet thickness that leads to a lower coefficient of friction making the coefficient of friction more dependent on deformation mechanics than tribology.

Analytical models such as the Stoughton model assumed the sheet material conforms to the bead geometry as it flows through the drawbead. In practice, this is not the case. This assumption led to the prediction of smaller effective bending radius and consequently over prediction of drawbead forces. The Stoughton model, like other analytical models, employed a Power law for obtaining effective flow stress and Hill's quadratic anisotropic yield criteria, Hill-48, which are not suitable for aluminium alloys and may contribute to over prediction of forces. Therefore, analytical models were found to be inappropriate for determining the drawbead forces and subsequently, the drawbead geometry.

4. **Develop and prove a scientific method to derive an optimised drawbead geometry along with a coefficient of friction**

   It has been identified that the industrial drawbead design practice is based on trial and error. In addition, the academic approaches discussed did not offer a holistic drawbead design process. Therefore, using the knowledge gathered from the investigation (Chapter 3), a hybrid approach was designed (Chapter 6), which not only provided the coefficient of friction but also the drawbead restraining and blankholder force. It used a roller and fixed drawbead set-ups in drawbead tests to derive experimental forces. A finite element model calibrated to the roller set-up is then used to determine the coefficient of friction. Later, a drawbead selection criterion, Geometry Effectiveness

Parameter (GEP), as discussed in Chapter 5, was used to select the optimised drawbead geometry. GEP can also directly benefit the forming feasibility simulation process by enabling stamping engineers in setting-up an appropriate range of drawbead geometries in the drawbead optimisation feature in AUTOFORM^{TM}. The coefficient of friction and drawbead geometry selected by this approach was validated using the stamping experiment and simulation of a rectangular pan using 1.5 mm AA6111-T4 aluminium alloy (Chapter 7). It was observed that the experimental and simulation results such as punch force, thinning and draw-in, correlated well. This indicated that the coefficient of friction and drawbead geometry obtained from the proposed drawbead design method could be suitably applied to the forming of a 3D part. This innovative approach involves minimum experiments and eliminates the need for complex friction modelling, mathematical modelling of drawbead forces and use of any optimisation algorithms to select the drawbead geometry. Hence, it is simpler and faster than the industry's current trial and error drawbead design approach.

To conclude, this work has brought together experimental and numerical modelling methods to develop a simple mechanism for designing drawbeads for forming of aluminium alloys. The main innovation is the way in which these concepts have been brought together, overcoming the respective limitations in each domain to deliver a solution with wide practical applicability. Stamping experiments and simulations have confirmed the validity of the model.

10 Limitations and future work

The limitations of the proposed methodology for the selection of optimised drawbead geometries are stated in this chapter. Suggestions for overcoming the limitations are also briefly mentioned.

- **Sheet material and gauge**

  The proposed methodology uses a drawbead test to generate data required for calibration of numerical drawbead models. In Section 3.1, it was observed that the drawbead test results such as the coefficient of friction and drawbead restraining force are dependent on the sheet material and gauge. Therefore, for maintaining consistency in results and to develop an end-to-end drawbead design methodology only 1.5 mm thick strips of AA5754-O and AA6111-T4 were used in the experimentation. To determine optimum drawbead geometry for other sheet material and gauges, tensile tests to capture the material properties to input in the numerical drawbead model and new drawbead test needs to be carried out. The procedure to determine optimum drawbead geometry for other sheet material and gauges will remain same as explained in Section 6.1.

- **Geometry effectiveness parameter (GEP)**

  A parameter to select optimised drawbead geometry was established in Section 5.2 which takes into account the through thickness strain at the exit of the drawbead, as the drawbead test was the basis for developing drawbead design methodology. The drawbead is used to introduce stretch in the part in areas such as the wall. Ideally, the through thickness strain in the wall area should have been used in the formulation of the GEP. However, the formulation of

GEP can be easily extended to include the through thickness strains in the wall area, perhaps from stamping simulation of a rectangular pan.

11 Appendices

Appendix A: Research methodology of investigation of drawbead design approaches

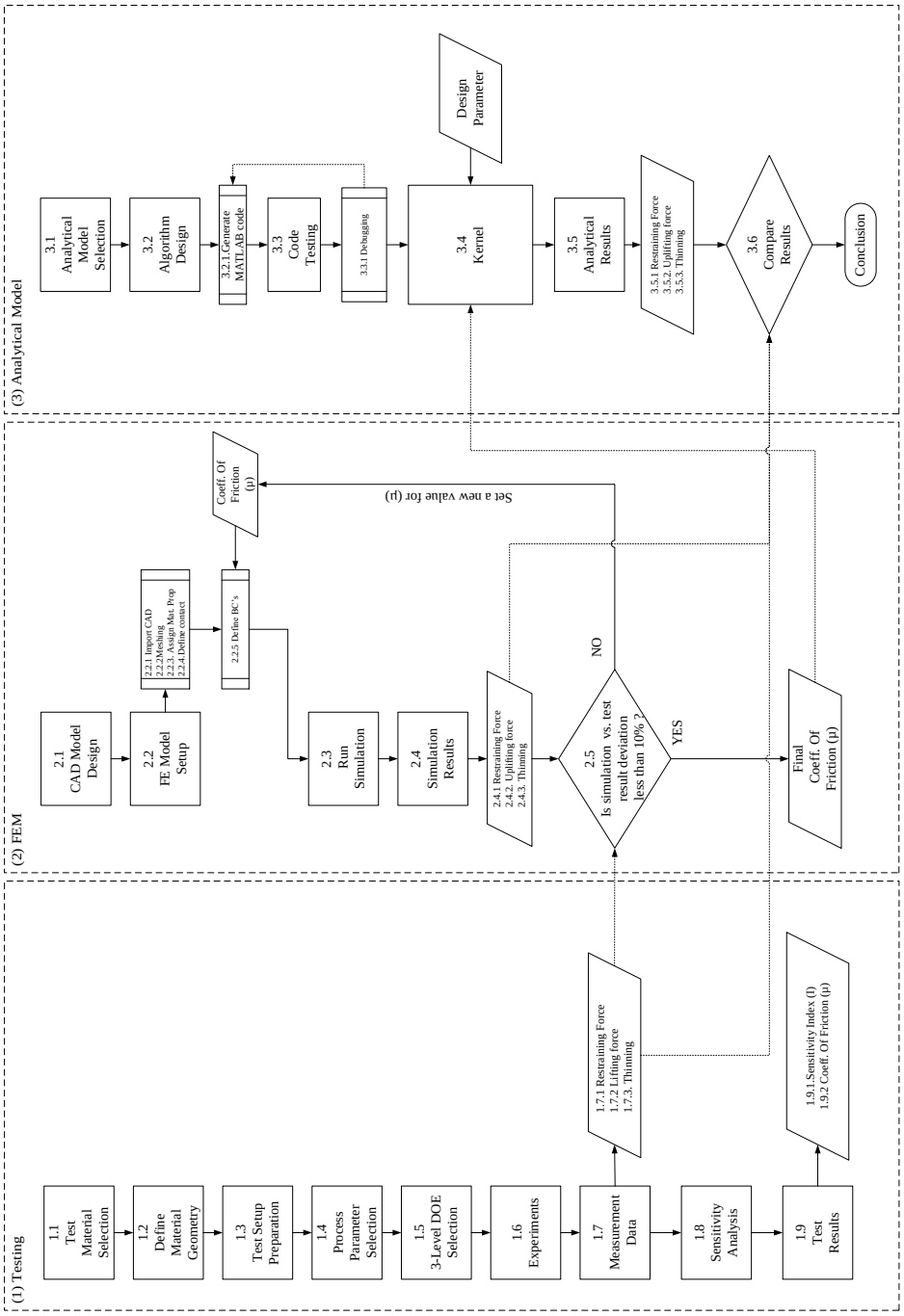

Figure A.1: Flow chart of research methodology applied in the investigation of drawbead design approaches, Chapter 3

Appendix B: Experimental results

Table B.1: Table showing blankholder force and drawbead restraining force from fixed drawbead test at various draw speeds

Draw speed (mm/s)	BHF (kN)	DBRF (kN)
10	4.5	4.8
	4.5	4.9
	4.5	4.9
20	4.4	4.7
	4.3	4.6
	4.3	4.7
30	4.2	4.6
	4.2	4.5
	4.3	4.7
40	4.3	4.6
	4.1	4.4
	4.2	4.5
50	4.2	4.5
	4.2	4.5
	4.3	4.5
60	4.3	4.6
	4.2	4.5
	4.2	4.5
70	4.2	4.4
	4.1	4.4
	4.2	4.4
80	4.1	4.3
	4.1	4.3
	4.1	4.4
90	4	4.2
	4.1	4.3
	4.2	4.4
100	4.1	4.3
	4	4.2
	4	4.3

Table B.2: Table showing experimental results from drawbead tests for different test strip gauges

Thickness	Roller		Fixed		μ
	Bead load(kN)	Draw load(kN)	Bead load(kN)	Draw load(kN)	
0.9	1.7	1.5	1.9	1.9	0.07
	1.6	1.4	1.9	1.9	0.08
	1.7	1.5	1.9	1.9	0.07
1	1.6	1.4	2	2.1	0.11
	1.6	1.4	2	2.1	0.11
	1.6	1.4	2	2.1	0.11
1.2	2.3	2	2.6	2.9	0.11
	2.3	2	2.7	2.9	0.11
	2.3	2	2.6	2.9	0.11
1.5	3.5	2.9	4.4	4.7	0.13
	2.9	2.8	4.3	4.6	0.13
	3.5	2.9	4.4	4.7	0.13
2	10.1	5.9	10.3	9	0.10
	10.1	5.8	9.8	9	0.10
	10.1	5.8	9.8	9	0.10

Appendix C: Formulation of the Stoughton Model

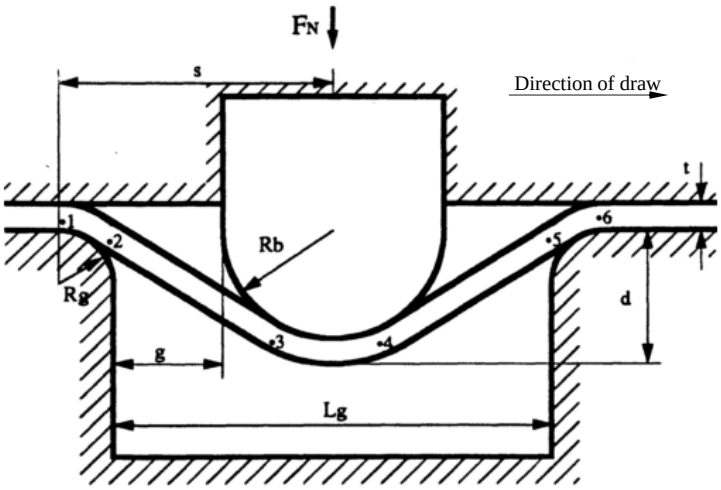

Figure C.1: A drawbead forcing the strip into the groove where it will bend/unbend at points 1 to 6 when drawn

Following are the steps in calculating the drawbead forces:

1. R_g = groove radius
2. R_b= drawbead radius
3. d = drawbead depth
4. g = groove clearance
5. L_g = groove width
6. t = strip thickness

1. Calculate the contact angle θ, or effective bending angle

$$\theta = tan^{-1}\left[q\frac{\sqrt{(1-p)^2+p(2-p)(1-q)^2}-(1-q)}{(1-q)^2}\right]$$

Where, p is the effective bead depth, given by

$$p = \frac{d}{(2R+t)}$$

In addition, q defines the fit of strip over the drawbead, given by

$$q = \frac{(2R + t)}{(2R + g)}$$

Where, R = R_g = R_b. For full drawbead depth, p = 0 and q = 1.

2. Calculate the effective bending radius of the strip, R_{eff}. For full drawbead depth, R_{eff} = R.

$$R_{eff} = \frac{R}{sin(\theta)}$$

3. Calculate the effective surface strain or strain in the outer most fibre of the strip.

$$\varepsilon_{m_i} = \frac{1 + \bar{R}}{\sqrt{1 + 2\bar{R}}} ln\left(\frac{1 + \frac{t_i}{R_{eff}}}{1 + \frac{t_i}{2R_{eff}}}\right)$$

Where the present thickness t_i is given by

$$t_i = t_{i-1} e^{-\gamma \varepsilon_{a-i}}$$

And the average effective strain in the strip after a bend or unbend is given by

$$\varepsilon_{a_i} = \varepsilon_{a_{i-1}} + \gamma \varepsilon_{m_{i-1}}$$

Where, γ is a constant that is between 0 and 1, default of 0.5 is recommended.

4. The bending or unbending force at each bending and unbending point respectively is given by

$$F_i = \frac{wKt_i}{1+n}\left(1+\frac{R_{eff}}{t_i}\right)\left(\frac{1+2\bar{R}}{(1+\bar{R})^2}\right)\left\{\frac{1}{2+n}\left[a_i\frac{1+\bar{R}}{\sqrt{1+2\bar{R}}}\right.\right.$$

$$\left.- b_i\varepsilon_{a_i}\right]\left[\left(\varepsilon_{a_i}+\varepsilon_{m_i}\right)^{2+n}-{\varepsilon_{a_i}}^{2+n}\right]$$

$$+\frac{b_i}{3+n}\left[\left(\varepsilon_{a_i}+\varepsilon_{m_i}\right)^{3+n}-{\varepsilon_{a_i}}^{3+n}\right]$$

$$-\left(\varepsilon_{a_i}{\varepsilon_{m_i}}^{1+n}\right)\left[a_i\frac{1+\bar{R}}{\sqrt{1+2\bar{R}}}\right.$$

$$\left.\left.+\frac{1}{2}b_i\varepsilon_{m_i}\right]\right\}\left[f\left(\varepsilon_{m_i}\frac{v}{t_i}\frac{1+\frac{t_i}{R_{eff}}}{\frac{t_i}{2R_{eff}}},\dot{\varepsilon}_0,m\right)\right]$$

Where i ranges from 1 to 6 for six bending and unbending points, and constants,

$$a_i = 1-\frac{{t_i}^2}{48\,{R_{eff}}^2}\ and\ b_i = 1-\frac{t_i}{4R_{eff}}$$

$$f(\dot{\varepsilon},\dot{\varepsilon}_0,m) = \left(\frac{\dot{\varepsilon}}{\dot{\varepsilon}_0}\right)^m$$

5. Calculate elastic force arising during elastic deformation of the strip when blankholder closes.

$$F_e = \frac{(2Ew\delta t^3)}{(2R+g)^3}$$

The above is derived using a concept of modelling strip as elastic beam whose length L=4R+2g and is only valid when R_b=R_g and the elastic displacement δ is given by

$$\delta = min\left(d, 2(2R+t)\frac{R\sigma_y}{tE}\right)$$

Where σ_y is the yield stress of the strip material.

6. Calculate the drawbead restraining force (DBRF) which is a summation of bending or unbending force at six bending and unbending points along with a frictional contribution and elastic force during blankholder closing with its frictional component.

$$DBRF = e^{\mu\theta}\left[e^{2\mu\theta}\left(F_1 e^{\mu\theta} + \mu F_e + F_2 + F_3\right) + \mu F_e + F_4 + F_5\right] + F_6$$

7. Finally, calculate the blankholder force, BHF, which is necessary to prevent the uplifting the blankholder during drawing motion of the strip. This force is simply the summation of the vertical components of the forces described in step 6.

$$\begin{aligned} BHF = \quad & F_e cos\theta \\ & + \frac{1}{2(1+\mu^2)}\left\{F_1\left[\left(e^{\mu\theta}(2\mu cos\theta + (1-\mu^2)sin\theta)\right) - 2\mu\right]\right. \\ & + \left[\left(e^{2\mu\theta}(\mu cos\theta + sin\theta) + \mu cos\theta + sin\theta\right)\left(F_1 e^{\mu\theta} + \mu F_e\right.\right. \\ & \left.\left. + F_2 + F_3\right)\right] \\ & - \left[\left(e^{-\mu\theta}\left(2\mu cos\theta - sin\theta(1-\mu^2)\right)\right.\right. \\ & \left.\left.\left. - 2\mu\right)\left(e^{2\mu\theta}\left(F_1 e^{\mu\theta} + \mu F_e + F_2 + F_3\right) + \mu F_e + F_4 + F_5\right)\right]\right\} \end{aligned}$$

The drawbead restraining force

```
t_vector = [t1 t2 t3 t4 t5 t6];
a_vector = [a1 a2 a3 a4 a5 a6];
b_vector = [b1 b2 b3 b4 b5 b6];
Epsilon_vector = [Epsilon_1 Epsilon_2 Epsilon_3 Epsilon_4 Epsilon_5 Epsilon_6];
Epsilon_M_vector = [Epsilon_M_1 Epsilon_M_2 Epsilon_M_3 Epsilon_M_4 Epsilon_M_5 Epsilon_M_6];

for i=1:6

    Thickness = t_vector(i);
    a_constant = a_vector(i);
    b_constant = a_vector(i);
    Epsilon_i = Epsilon_vector(i);
    Epsilon_M_i = Epsilon_M_vector(i);

    FA1 = w*Thickness*K_6111/(1+n_6111)*(1+2*Reff/Thickness)*((1+2*R_6111)/(1+R_6111)^2);
    FA2 = 1/(2+n_6111)*(a_constant*(1+R_6111)/sqrt(1+2*R_6111)-b_constant*Epsilon_i);
    FA3 = (Epsilon_i+Epsilon_M_i)^(2+n_6111)-Epsilon_i^(2+n_6111);
    FA4 = 1/(3+n_6111)*b_constant*((Epsilon_i+Epsilon_M_i)^(3+n_6111)-Epsilon_i^(2+n_6111));
    FA5 = (a_constant*(1+R_6111)/sqrt(1+2*R_6111)+1/2*b_constant*Epsilon_M_i)*Epsilon_M_i*Epsilon_i^(1+n_6111);

    F(i) = FA1*FA2*(FA3+FA4-FA5);

end

d2 = 2*(2*Rb+t)*(Rb*Sigma_Y_6111/t/E_6111);
Delta = min([d d2]);

Fe=(2*E_6111*w*Delta*t^3)/((2*Reff+g)^3); % Elastic force exerted by the strip when the drawbead closes at the

DBRF=((F(1)*exp(Mu*Theta_Rad)+(Mu*Fe)+F(2)+F(3))*exp(2*Mu*Theta_Rad)+(Mu*Fe)+F(4)+F(5))*exp(Mu*Theta_Rad)+F(6);
disp('DBRF [kN]')
DBRF*1E-3
```

Figure C.2: An excerpt of MATLAB script of Stoughton Model to obtain the drawbead restraining forcing

Appendix D: Pressure dependency of coefficient of friction

The blankholder pressure is the normal pressure applied on the area of sheet metal located in the blankholder region. It should be high enough to avoid wrinkling and low enough to avoid tearing of sheet metal. The blankholder pressure is simply the ratio of the maximum normal force available at the blankholder and the area of the blank in the blankholder. The blankholder force required is a function of the yield strength of sheet metal and the friction between the sheet and the tool surfaces. Ideally, the blankholder force should be uniformly distributed over the sheet metal allowing controlled flow of the material into the die cavity. However, in practice, the

blankholder pressure differs due to factors such as thickening of the sheet around the corners, deviation in sheet thickness and misalignment of die surfaces due to wear and tear of press components.

As discussed earlier, the coefficient of friction is a ratio of the normal force and frictional force. Thus, blankholder force or force at a given sheet-die contact has a significant influence on the coefficient of friction. In the research field, blankholder pressure is known as the contact pressure. Fundamentally, the contact pressure is shared between the asperities in contact and the lubricant film at the sheet die interface. **Figure D.** illustrates the relation between contact pressure and the coefficient of friction at different lubricant coat weights.

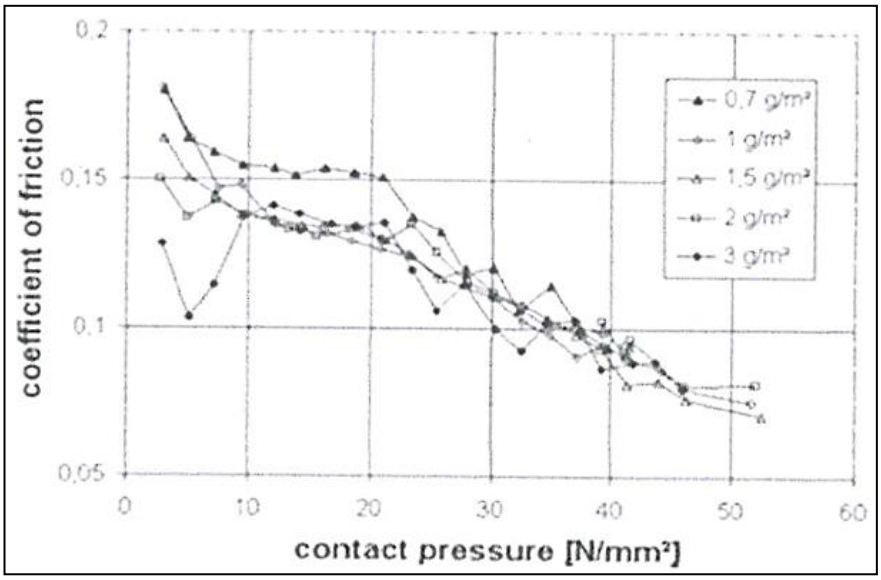

Figure D.1: Relation between contact pressure and coefficient of friction (AutoForm, 2013)

It can be clearly observed that the coefficient of friction reduces with increasing contact pressures. The first law of friction stated that coefficient of friction increases with increasing pressure. This law is true in the case of static and dry friction. However, under the presence of lubricant film and relative motion between the sheet and die, the coefficient of friction reduces with an increase in the contact pressures.

The presence of the lubricant film avoids metal-to-metal contact and reduces the coefficient of friction. In addition, the lubricant viscosity and the relative velocity creates a hydrodynamic effect where the normal force is partly shared by the lubricant in the surface voids. The normal load on the metal-to-metal contacts flattens the surface asperities and increases the real area of contact, which reduces the contact pressure as well.

Further, from the **Figure D.**, it can be observed that the increase in the lubricant coat weight or static lubricant film thickness only reduces static coefficient of friction. The coefficient of friction plots for different lubricant coat weights converges with an increase in the contact pressure. The increase in lubricant coat weight under a given contact pressure range does not have a significant effect on the coefficient of friction.

12 References

Autoform. 2013. *RE: Equivalent drawbead model in AutoForm.* Personal communication with Joshi, Y. K.

Bae, G., Huh, H. & Park, S. 2012. A simulation-based prediction model of the restraining and normal force of draw-beads with a normalization method. *Metals and Materials International,* 18**,** 7-22.

Banabic, D. 2010. Sheet Metal Forming Processes: Constitutive Modelling and Numerical Simulation, Berlin, Springer-Verlag.

Carleer, B. D., Vreede, P. T., Drent, P., Louwes, M. F. M. & Huétink, J. 1994. Modelling drawbeads with finite elements and verification. *Journal of Materials Processing Technology,* 45**,** 63-68.

Ces Edupack 2014. Granta Design Limited. Cambridge, UK.

Chen, C. C. & Weinmann, K. J. 2003. A Finite Element and Experimental Study of Sheet Deformation as Influenced by Drawbead End Geometry. SAE International.

Dalton, G. M. & Schey, J. A. 1991. Effects of Bead Surface Preparation on Friction in the Drawbead Test. SAE International.

Demeri, M. Y. 1993. Drawbeads in sheet metal forming. *Journal of Materials Engineering and Performance,* 2**,** 863-866.

Dierke, H., Krawehl, F., Graff, S., Forest, S., Šachl, J. & Neuhäuser, H. 2007. Portevin–LeChatelier effect in Al–Mg alloys: Influence of obstacles – experiments and modelling. *Computational Materials Science,* 39**,** 106-112.

Duarte, E. & Oliveira, S. The influence of sheet thickness on drawbead restraining force in sheet metal forming. 18th International Congress of Mechanical Engineering, 2005 Ouro Preto, MG. ABCM, 1-6.

Dutton Simulations. 20th June 2014 2014. *RE: DYNAFORM training.* Personal communication with Joshi, Y.

Emblom, W. J. & Weinmann, K. J. 2007. The Correlation Between Punch Forces and Wrinkling for Aluminum Sheet Metal Stamping with Adjustable Drawbeads. SAE International.

Esener, E., Firat, M. & Gürler, B. Predictive Modeling Of Drawbeads Using Regression and Neural Network Techniques. 7th International Conference and Exhibition on Design and Production of Machines and Dies/Molds, Ankara, Türkiye, 2013.

European Aluminium Association. 2013. Aluminium in cars: unlocking the light-weighting potential. Available: http://www.european-aluminium.eu/media/1326/aluminium-in-cars-unlocking-the-lightweighting-potential.pdf.

Figueiredo, L., Ramalho, A., Oliveira, M. C. & Menezes, L. F. 2011. Experimental study of friction in sheet metal forming. *Wear,* 271**,** 1651-1657.

Firat, M. 2008. An analysis of sheet drawing characteristics with drawbead elements. *Computational Materials Science,* 41**,** 266-274.

Firat, M. & Cicek, O. 2011. A FE technique to improve the accuracy of drawbead models and verification with channel drawing experiments of a high-strength steel. *The International Journal of Advanced Manufacturing Technology,* 55**,** 107-119.

Han, L., Li, G., Han, X. & Zhong, Z. 2006. Identification of geometric parameters of drawbead in metal forming processes. *Inverse Problems in Science and Engineering,* 14**,** 233-244.

Hance, B. M. & Walters, G. N. 1999. Effects of Sheet Thickness on the Coefficient of Friction Determined by the Draw Bead Simulator (DBS) Test. SAE International.

Hol, D. I. J., Wiebenga, I. J. H., Dane, I. C., Meinders, D. I. V. T. & Boogaard, D. I. a. H. V. D. 2014. A software solution for advanced friction modeling applied to sheet metal forming. *IDDRG 2014.* Paris.

Hosford, W. F. & Caddell, R. M. 2011. Metal Forming: Mechanics and Metallurgy, Cambridge University Press.

Jaguar Land Rover. Forming Lightweight Materials for High Volume Production: Aluminium Focus. Global Automotive Lightweight Materials, 2013.

Jaguar Land Rover. 2014. *RE: Visit to Halewood and Solihull press shops.* Personal communication with Joshi, Y.

Jaguar Land Rover. 2016. *Jaguar Land Rover corporate website* [Online]. Available: http://www.jaguarlandrover.com/gl/en/ [Accessed October 2016].

Joshi, Y., Christiansen, P., Masters, I., Bay, N. & Dashwood, R. Numerical Modelling of Drawbeads for Forming of Aluminium Alloys. Journal of Physics: Conference Series, 2016. IOP Publishing, 032082.

Karupannasamy, D. K., Hol, J., De Rooij, M. B., Meinders, T. & Schipper, D. J. 2014. A friction model for loading and reloading effects in deep drawing processes. *Wear,* 318**,** 27-39.

Keum, Y. T., Kim, J. H. & Ghoo, B. Y. 2001. Expert drawbead models for finite element analysis of sheet metal forming processes. *International Journal of Solids and Structures,* 38**,** 5335-5353.

Lange, K. 1986. Handbook of Metal Forming, Springer-Verlag.

Lee, M. G., Chung, K., Wagoner, R. H. & Keum, Y. T. 2008. A numerical method for rapid estimation of drawbead restraining force based on non-linear, anisotropic constitutive equations. *International Journal of Solids and Structures,* 45**,** 3375-3391.

Levy, B. S. & Van Tyne, C. J. 2007. Effect of Draw Beads on the Mechanical Properties of Sheel Sheet. SAE International.

Levy, B. S. & Van Tyne, C. J. 2009. Predicting the Radius of a Sheet Bent Around Drawbeads. SAE International.

Li, R., Bohn, M. L., Weinmann, K. J. & Chandra, A. 2000. A Study of the Optimization of Sheet Metal Drawing with Active Drawbeads. *Journal of Manufacturing Processes,* 2**,** 205-216.

Li, R. & Weinmann, K. J. 1999. Formability in Non-Symmetric Aluminium Panel Drawing Using Active Drawbeads. *CIRP Annals - Manufacturing Technology,* 48**,** 209-212.

Ls-Dyna Theory Manual 2014. LS-DYNA Theory Manual, California, USA, Livermore Software Technology Corporation (LSTC).

Maker, B. N. 2000. On Drawbeads in Sheet Metal Forming. SAE International.

Marciniak, Z., Hu, J. & Duncan, J. 2002. Mechanics of sheet metal forming, Butterworth-Heinemann.

Miller, W. S., Zhuang, L., Bottema, J., Wittebrood, A. J., De Smet, P., Haszler, A. & Vieregge, A. 2000. Recent development in aluminium alloys for the automotive industry. *Materials Science and Engineering: A,* 280**,** 37-49.

Naceur, H., Guo, Y. Q., Batoz, J. L. & Knopf-Lenoir, C. 2001. Optimization of drawbead restraining forces and drawbead design in sheet metal forming process. *International Journal of Mechanical Sciences,* 43**,** 2407-2434.

Nanayakkara, K., Kelly, G. L. & Hodgson, P. D. Determination of coefficient of friction in partially penetrated drawbeads. Steel grips Suppl. Metal Forming, 2004.

Nine, H. 1982a. The applicability of Coulomb's friction law to drawbeads in sheet metal forming. *Journal of Applied Metalworking,* 2**,** 200-210.

Nine, H. 1982b. New drawbead concepts for sheet metal forming. *Journal of Applied Metalworking,* 2**,** 185-192.

Nine, H. D. 1978. Drawbead Forces in Sheet Metal Forming. *Mechanics of Sheet Metal Forming.* Springer US.

Personal Communication. 2013. *RE: Introductory meeting with stamping engineering team at Jaguar Land Rover.* Personal communication with Joshi, Y.

Raghavan, K. S., Comstock, R. J. & Hance, B. M. 2014. An Indirect Method to Determine Friction Coefficient in the OSU Punch Stretch Test. SAE International.

Ren, F., Chappuis, L. & Xia, Z. C. 2009. Drawbead Restraining Force Modeling: Nonlinear Friction. *SAE Int. J. Mater. Manuf.,* 2**,** 530-536.

Samuel, M. 2002. Influence of drawbead geometry on sheet metal forming. *Journal of Materials Processing Technology,* 122**,** 94-103.

Sanchez, L. R. & Weinmann, K. J. 1996. An Analytical and Experimental Study of the Flow of Sheet Metal Between Circular Drawbeads. *Journal of Engineering for Industry,* 118**,** 45-54.

Schey, J. 1983. Tribology in metalworking, Ohio, ASM.

Schey, J. A. 1996. Speed effects in drawbead simulation. *Journal of Materials Processing Technology,* 57**,** 146-154.

Sheriff, N. M. & Ismail, M. M. 2008. Numerical design optimisation of drawbead position and experimental validation of cup drawing process. *Journal of Materials Processing Technology,* 206**,** 83-91.

Smith, D. A. 1990. Die design handbook, Society of Manufacturing Engineers.

Stoughton, T. B. Model of drawbead forces in sheet metal forming. 15th IDDRG, 1988 Dearbon, USA. 205.

Taherizadeh, A., Ghaei, A., Green, D. E. & Altenhof, W. J. 2009. Finite element simulation of springback for a channel draw process with drawbead using different hardening models. *International Journal of Mechanical Sciences,* 51**,** 314-325.

Talat 1996. Tribology in cold forming of aluminium sheet, Stuttgart, Euroepan Aluminium Association.

Trzepieciński, T. & Lemu, H. G. 2014. Frictional conditions of AA5251 aluminium alloy sheets using drawbead simulator tests and numerical methods. *Strojniški vestnik-Journal of Mechanical Engineering,* 60**,** 51-60.

Tufekci, S. S., Wang, C.-T., Kinzel, G. L. & Altan, T. 1994. Estimation and Control of Drawbead Forces in Sheet Metal Forming. *SAE International*.

Weidemann, C. The blankholding action of drawbeads. 10th Biennial Congress of IDDRG, 17-21 April 1978 University of Warwick, England. 79-85.

Weinmann, K. J., Michler, J. R., Rao, V. D. & Kashani, A. R. 1994. Development of a Computer-Controlled Drawbead Simulator for Sheet Metal Forming. *CIRP Annals - Manufacturing Technology,* 43**,** 257-261.

Xu, K. 2003. Effects of Contact Pressure on the Coefficient of Friction in Friction Tests. SAE International.

Xu, S. G., Bohn, M. L. & Weinmann, K. J. 1997. Drawbeads in Sheet Metal Stamping - A Review. *SAE International*.

Xu, S. G. & Weinmann, K. J. 1996. A Three-Dimensional FE Study of Sheet Metal Flow Over the Drawbead. SAE International.

You, Y. 1998. Calculation of drawbead restraining forces with the Bauschinger effect. *Proceedings of the Institution of Mechanical Engineers, Part B: Journal of Engineering Manufacture,* 212**,** 549-553.

Zharkov, V. A. 1995. Theory and practice of deep drawing, London, Mechanical Engineering Publications.